Alma Mater Studiorum - University of Bologna

Facolty of Mathematics, Physics and Natural Sciences

Research Doctorate in Geophysics, ciclo XXII

Settore scientifico disciplinare: GEO/10

Preliminary studies for the establishment of a Tsunami Early Detection Algorithm to be used in the frame of a tsunami warning system

PhD thesis of Lidia Bressan

Coordinatore di dottorato
Prof. Michele Dragoni

Tutore:
Prof. Stefano Tinti

Referente:
Prof. Maurizio Bonafede

Final exam year 2009

Contents

Chapter 1

Introduction

1.1 Purpose of the thesis

The aim of this thesis is to present and discuss TEDA, an algorithm for the automatic detection of tsunamis and large amplitude waves on sea level records. TEDA has been developed in the frame of the Tsunami Research Team of the University of Bologna for coastal tide gauges and it has been calibrated and tested for the tide gauge station of Adak Island, in Alaska. A preliminary study to apply TEDA to offshore buoys in the Pacific Ocean is also presented. The test of TEDA to sea level records has been possible thanks to a collaboration with NCTR/PMEL/NOAA (NOAA Center for Tsunami Research/Pacific and Marine Environmental Laboratory/National Oceanic and Atmospheric Administration) that made available such data.

1.2 Tsunamis

Tsunamis are a series of surface waves in the sea that can be generated by various sources, which are most frequently earthquakes and landslides, but also, even if much more rarely, submarine volcanic explosions or meteoric impacts. Their most evident characteristic is that, despite the very limited height of the waves when they propagate in the open sea (of the order of centimeters to a few meters in extreme cases), the level of the waves increases to heights of a meters to tens of meters in the worst cases when the tsunami reaches the coast. At the coast, tsunamis can be very dangerous, causing inundation and lot of losses in human lives and properties, while offshore they may remain unnoticed.

The source event causes a tsunami because it displaces a big quantity of water over a big surface. Since gravity tends to restore the water level to the equilibrium, waves are generated and propagate in the water. They are characterized by long period (from a few minutes to an hour) and long wavelength, of the order of kilometers, according to the initial surface of displaced water. Because of the long period and the long wavelength, in most cases the linear shallow water approximation of gravity waves is adequate to describe tsunami propagation. This approximation implies that the propagating waves are non-dissipative, i.e. they do not lose energy while propagating and therefore they can hit coasts very far from their generation, on the other sides of oceans. In the reality, for long distances, dispersion is present, even if is not a dominant term. With this approximation, the propagation velocity depends only on the depth of the sea, $c = \sqrt{gd}$, with g the acceleration of gravity and d the depth of the sea, and in the open ocean it can reach values of hundreds of km/h. As a consequence, a tsunami generated on the coasts of Chile, for example, will reach Japan in less than 24 hours. When tsunami waves approach the coast, and the depth of the sea decreases, the linear theory ceases to be valid, and their behavior can be explained by non-linear theory of surface waves, with shallow water approximation. In general, near the coast, the propagation velocity decreases with the depth, compriming the waves and increasing their height. In addition, tsunami waves are subjected, as all surface waves, to diffraction, reflection, refraction, superposition and so on. On a complex shape coast, with basins and complex bathymetry, the tsunami behaves in a very complicated way.

Tsunamis can be of a wide range of magnitudes, from very low magnitude, which can be only seen in the sea level records, to very high amplitudes. It is important to stress that tsunamis can be dangerous even if they are not very big. In some low coastal areas, or in harbours, even waves of amplitudes of less than one meter can provoke a lot of damage, causing partial flooding in very low areas and strong currents in harbour and canals (see Whitmore et al., 2008).

It is important to study tsunami records, not only for scientific purposes but also in order to estimate the tsunami impact at the coast, for tsunami hazard mitigation.

1.3 Tsunami Warning Systems

Tsunami warning systems are complex structures with the goal to give warnings that a tsunami has been generated to places that might be affected. In order to do so, they monitor seismic and sea level stations, collect data, estimate the possible tsunami threat and, in case, issue warnings. To prevent damage from tsunamis, warnings are not enough: it is important to stress the fact that it is necessary to have well planned emergency operations, and education and hazard mitigation programs. The local emergency measures, which can be very complicated to organize, are in the hand of local authorities (see Bernard et al., 2006; *Developing tsunami-resilient communities: the National Tsunami Hazard Mitigation Program* 2005).

In the past 50 years tsunami warning centers started to develop, in general after that a major tsunami stroke: for example, in the U.S.A. tsunami warnings began in 1949 as a response to the 1946 tsunami generated in the Aleutian Islands that hit the Hawaii. The West Coast and Alaska Tsunami Warning Center (WC/ATWC) started after the 1964 Alaskan tsunami. The Chilean national tsunami warning system and the Pacific tsunami warning center were established respectively in 1966 and in 1968 after the 1960 Chilean tsunami, which devastated Chile and caused losses of lives and properties in Hawaii and Japan. The Indonesian Tsunami Warning Center, and those of all countries facing the Indian Ocean, started after the 2004 Sumatra tsunami. The Pacific tsunami warning system PTWC is the oldest international Tsunami Warning System and has its center (the PTWC) in Hawaii. Today the PTWC collects seismic and sea level data, and releases international tsunami alerts to national authorities for events occurring in the Pacific Ocean. Almost all countries along the Pacific coast are part of the PTWS and some have additional national tsunami warning system. National TWSs contribute to data collections for the PTWS and are responsible of local emergency measures.

After the 2004 Sumatra tsunami, it become evident to all coastal communities that tsunami warning systems are necessary, together with the need of inter-statal communications and coordination (see Synolakis and Bernard, 2006). Since the Sumatra 2004 event, tsunamis have got the attention of the people and the scientific community, with the consequence of a fast developing of new technologies, and new attempts in building up tsunami warning systems, as testified by recent publications, as Bellotti, Di Risio, and De

Girolamo, 2009; Leonard et al., 2008; Liu, Wang, and Salisbury, 2009; Reymond et al., 1996; Šepić, Denis, and Vilibić, 2009; Zhang, Yip, and Ng, 2009. The main example is the Indonesian Tsunami Warning System, born and developed in a very short time (Schroeter et al., 2006; Taguchi et al., 2006).

The goal of a tsunami warning system is to know when and where a tsunami has been generated, and to give estimations of when, where and with which strength the tsunami will hit. The system is based on the collection and processing of seismic and sea level data from various instruments: from seismometers to coastal tide gauges and offshore buoys. Recently also new kind of instruments have been proposed and introduced, as for example the use of GPS associated with buoys in the GITEWS system (Kato et al., 2001, "A new tsunami monitoring system using RTK-GPS").

Nowadays, tsunami warnings are issued by tsunami warning centers on the basis of seismic data. The most critical part for a tsunami warning center is to know if a tsunami has been generated or not. With the actual knowledge, it is impossible to distinguish between tsunamigenic and not tsunamigenic earthquakes, even if many study concern this topic, as for example Chew and Kuenza, 2009. An earthquake, the most common source of tsunamis, might trigger a tsunami or not depending on the seismic magnitude, the fault mechanism, the rupture slip and geometry. Very large earthquakes might trigger very small tsunamis, and at the same time, dangerous tsunami waves might be generated by not so big earthquakes. In addition, a tsunami might be very strong in near locations, but it might dissipate very quickly and not affect places further from the source. At the same time, tsunamis can be generated by landslides and volcanic eruptions. These tsunamis are usually not transoceanic, and do not propagate and hit very far from the generation site, but they can strike very hard in the near coasts. In addition, they are not preceded by a clear precursor, as a seismic signal. A recent example is the Stromboli 2002 tsunami, generated by a landslide, that hit the island of Stromboli and with much less intensity the islands nearby, and even less the coasts of Sicily (Tinti et al., 2005).

In case of tsunamis not generated by earthquakes, and to confirm the tsunami generation in case of seismic generated tsunamis, it is therefore necessary to measure a tsunami wave. Only the measurement of a tsunami wave gives the certainty of a tsunami generation, together with many other useful information, as time of arrival, size, period. Of course, to use the

measurement of a tsunami wave for a warning system, it is important to have this information as soon as possible. Therefore real time automatic tsunami detection, i.e. the identification of a tsunami wave in real time, can play an important role in tsunami warning systems. Confirmation of tsunami generation comes usually from offshore buoys or from tide gauges.

In order to better explain the difficulties and the question for tsunami detection, the characteristics of the sea level signal are described.

1.4 Sea level recorders: coastal tide gauges and offshore buoys

After an initial warning based on seismic data, the other main component of the monitoring system of a tsunami warning system is the sea level network: tsunamis can be recorded at the coast by tide gauges, or offshore, by BPRs, bottom pressure recorders (offshore buoys). Nowadays, many new-technology instruments are being developed to measure tsunami waves, with the use of satellites and GPS. Nevertheless, tide gauges are still the most common and spread instruments, followed by offshore buoys.

A sea level network is a system of instruments, as tide gauges and offshore buoys, that collects data from many strategic places and that covers the area of interest. The network should be carefully planned, in order to choose the best disposition and location of tide gauges and offshore buoys. It is important not to have blind areas, and on the opposite side, it is desirable to have a redundancy of stations, which assures that the information about the propagation of the tsunami will be transmitted in case of losses of data or breakdowns. The array of tide gauge stations and offshore buoys should be set accordingly to the potential tsunamigenic sources (Schindelé, Loevenbruck, and Hébert, 2008). An important aspect is also the implementation of national and international policies of inter-communication, which allows the sharing of sea level data that refer to different institutions (Komen and Smith, 1999).

It is important to take into account that tide gauges are nowadays present in very many harbour, even if with improper sampling rate, and their upgrading is easier and cheaper than offshore BPR deployment. With the exclusion of the Pacific Ocean, where an offshore buoys network is in operation for years and the buoys are almost all around the coasts, in the other sea

and oceans the planning of offshore buoys network can be quite complicated and implies very high costs.

Coastal tide gauges are born towards the end of the 19^{th} century, to measure tides, in order to help navigation, and to prevent floodings due to storm surges. They are usually installed inside harbours, in sheltered locations. Nowadays sea level data are used for many purposes, from tidal analysis and prediction, to oceanographic research, sea level change, coastal defense and storm surge warning systems.

In general, every country has its own network, characterized by different instruments, sensitivity, precision and sampling interval. The latter is very important because, in order to measure a tsunami, tide gauges need to have an adequate sampling interval, which do not filter tsunami waves. Since tide gauges are born with the purpose of measuring tides, it is still common to have tide gauges with sampling intervals from 6 min to 1 h, which ensures that a tsunami signal cannot be properly recorded. In order to measure tsunamis, tide gauges need to have at most 1 min sampling interval: depending from the source, the size of the tsunami and the location of the tide gauge, the tsunami main period varies, in the range from 1 or 2 min, for example in case of small tsunamis caused by landslides, to one hour.

Only recently, and especially after the 2004 Sumatra tsunami, it became evident that tide gauge networks with a suitable sampling rate could be very useful for measuring tsunamis, not only for scientific purposes, but also for tsunami warnings (see for the Mediterranean Sahal et al., 2009). A general renewal of tide gauge networks started, or it was strengthened if already planned, which consisted mainly in the updating of tide gauge stations to shorter sampling intervals, in order to measure tsunamis and long period waves. This process has started some years ago and it is still continuing, both along the Mediterranean coasts and on the Ocean coasts. In the Mediterranean, the implementation of a tsunami warning system is still at its first steps, and proposals of sea level networks have been published, as Schindelé, Loevenbruck, and Hébert, 2008. In Italy, the awareness of a tsunami warning system is testified by publications, as Maramai and Tinti, 1996, and by the TSUNET Project, which aims to set up a network of stations placed in different locations in southern Italy for sea level and other meteorological measurements (Tinti, Bressan, and Zaniboni, 2009). In Spain, the REDMAR sea level network (Spanish Harbours Authorities Tide

Gauge Network) has installed new stations and has been updating since 2006 all tide gauge stations to 1 min sampling interval. Together with the tide gauge network updating, a tool for real time automatic detection of sudden oscillations of sea level has been developed and implemented in Puertos del Estado web site, with the goal of detection of tsunamis and meteotsunamis, i.e. atmospherically generated seiches of large amplitude (see Omira et al., 2009). Recently also in the Caribbean Sea, tsunami awareness has started, as testified by Henson et al., 2006. In the Pacific coast, and in particular in the USA and in Canada, this process started much before, because of the more frequent occurrences of strong tsunamis in the Pacific. In Canada, a tide gauge network to measure tsunamis (see Rabinovich and Stephenson, 2004) has been started with the purpose of improving the national tsunami warning system.

In order to be able to detect a tsunami wave, it is important to know the signal of the sea level recorder. In a sea level record, the tsunami signal is superimposed to the usual sea level oscillations that will be from here indicated with background. There are various kind and models of both offshore and coastal tide gauge, but their background signals have some distinctive characteristics. An important signal in both offshore and coastal sea level is the tide, which might be of prevalent diurnal, semi-diurnal or mixed component. The tide level varies from location to location. In general, sea level records at the coast or offshore, in the middle of an Ocean, have some important differences.

Sea level series at the coast, according to the recording sampling interval, shows a wide range of waves. The short period waves are wind waves, of the order of a second. In case of a strong storm at the coast, wind waves can have longer periods; in case of a storm or rough sea offshore, storm waves that propagates till the coast are long waves, and can have periods till to 20 seconds. These waves are usually filtered in tide gauges with a long sampling interval.

Longer period waves and the dynamics of tides and of the sea in general, are strongly influenced by the morphology of the coast and by the bathymetry of the location of the tide gauge. The local influence is very strong because gulfs, river's mouths, basins, the shape of the coast and the surrounding landscape act as a filter and can amplify some waves with certain periods and directivity and damp others with other characteristics.

In basins of complex shape and bathymetry, the dynamic of the waves is complicated. There are places where local topography and bathymetry is favorable for the development of standing waves oscillations, called seiches. This phenomenon is due to the resonance of waves in closed or semi-closed basins: waves of specific periods depending mostly on the shape and size of the basins are trapped and might persist with large amplitudes for days. Areas where seiches develop embrace very different scales, starting from small pools, harbors and lakes to gulfs and bays and in general any closed or semi-enclosed basins. The main characteristic of seiches is that they are standing waves, therefore their period is regulated by the physical dimensions, shape and depth of the basin and coincide with the natural periods of the water system. Their period is therefore characteristic of the oscillating basin, and might vary from a few minutes to hours, in the long wave range. Seiches phenomena of large amplitude are usually caused by atmospheric forcing, as strong winds, atmospheric pressure changes, or by forcing of incoming waves, as tsunami waves or strong storm waves, or even by long period seismic waves. For extreme cases, seiches phenomena are also called meteotsunamis. The nature of the standing wave allows the oscillations not to dissipate and to ring in the basin for a long time, of the order of hours or days, even if the cause that triggered them vanished. Even in places where seiches are not strong, coastal tide gauges always present a typical spectrum due to the location, easily recognizable because constant and with periods from few minutes to the tidal periods. The background sea level signal of coastal tide gauges is the combination of all waves types, such as wind waves, typical oscillation periods, seiches, storm waves, tides.

Coastal tide gauges present some disadvantage for early warnings: they measure the tsunami wave right at the coast, leaving very little time for emergency operations. In addition, the tsunami signal is distorted by the local effects. On the other hand, exposed locations with limited local influence might have too noisy background, especially in case of storms and heavy sea conditions, so that sheltered locations are still preferable in recording tsunamis (Rabinovich and Stephenson, 2004). For this reason, systems of offshore buoys that can measure sea level in the open sea have been developed, with the goal of measuring the tsunami wave before it reaches the coast and right after its generation. They are based on sea level records by BPRs, bottom pressure recorders located offshore in the open sea, at the

ocean floor, which measure the water load pressure, convert it to sea level data and transmit it to warning centers. The first system of this sort to be developed is the DART buoy system of NOAA, started in 1986, that is in operation in the Pacific Ocean (González et al., 2005; Kulikov, Rabinovich, and Spirin, 1983; Titov et al., 2005).

Offshore sea level records are dominated by tides. Opposite to coastal tide gauges, they have the additional advantage that short waves, such as wind waves, are naturally filtered out, while long waves, as tsunami waves, are recorded unfiltered. For this reason, BPR sea level measurements have been chosen for real-time tsunami reporting for the PTWC and WC/ATWC tsunami warning centers (Titov et al., 2005).

The sea level serie of a BPR presents a wide range spectrum, recording from oceanic tides to meteorological forcing events, long surface gravity waves, seismic signals, tsunamis. All offshore buoys signal appear characterized by noise, which increases in case of atmospheric disturbances. The level of the noise depends on the location of the buoy, and in general if a buoy is set in the open ocean or near a continental shelf, where the noise has usually a higher level(Kulikov, Rabinovich, and Spirin, 1983).

1.5 Tsunami detection algorithms

A real time automatic detection algorithm is a useful tool to implement within a tsunami warning system, because it can provide the proof of tsunami generation and very useful information for warnings and for the evaluation of the tsunami threat. Tsunami Warning Systems in operation in the Pacific (PTWS) and in the Indian (IOTWS) oceans or in development, like the NEAMTWS in the Euro-Mediterranean region, include real-time detection algorithms.

At present, U.S. NOAA system is provided by a real-time algorithm for offshore buoys to discriminate an anomalous wave, based on tide prediction and on the deviation of the signal from the expected tide (see Mofjeld, "Tsunami detection algorithm"), while for coastal tide gauges, a real-time detection algorithm was in operation till the DART buoy system was developed (Mero, "NOAA/National Ocean Service Application of Real-Time Water Levels"). In British Columbia, Canada, tide gauges installed for tsunami recording are provided with a real-time algorithm, whose detec-

tions are used to warn responsible personnel in order to further investigate the tsunami event (Rabinovich and Stephenson, 2004). GITEWS, German-Indonesian Tsunami Early Warning System, uses an automatic tsunami detection algorithm installed in tide gauges that is based on rapid changes of sea level (Falck et al., 2010; Illigner and Schöne, 2009).

The importance of detection algorithms is also testified by the interest devoted to them by the scientific community: see for example recent contributions by Beltrami, 2008; Kato et al., 2000; Vela and Pérez, 2009; Wijeratne and Woodworth, 2009, Martin-Neira and Buck, 2005, "Tsunami detection using the PARIS concept".

The goal of a real time automatic detection algorithm is to indicate the presence of a tsunami wave, when the latter is recorded.

In this work, a tsunami early detection algorithm has been developed, with the goal of giving an automatic warning if the instrument records a tsunami wave or large amplitude long period waves. Tsunamis can be recorded, and therefore detected, both in the open sea, by offshore buoys, and at the coast, by coastal tide gauges. These instruments are the most commonly used to measure tsunami waves and the algorithm here presented, TEDA, can be tested in both cases.

Both methods, coastal and open sea detection, present advantages and disadvantages. On one hand, tsunami detection offshore gives a lot of time for tsunami threat estimations, warnings and emergency measures, while detection at the coast might give very little time to emergency operations, since the tsunami is already at the coast. Detection at the coast can be useful, if the wave is detected before its maximum, also taking into account that the first wave might not be the highest and the most dangerous one. In addition, coastal tide gauge records can give a very useful estimation of the amplitude of the tsunami waves for places further away from the source. In case of landslide generated tsunamis, detection at the coast remains the only possibility to give warnings to the population. In case of tsunamis generated by an earthquake very close to the shore, the tsunami might hit the coast before that offshore buoys, generally located far from the coast, might record the tsunami wave. This is one of the reasons, for example, why Japanese and Chilean tsunami warning systems base their warnings exclusively on seismic data for near field events. Seismic based systems assure the fastest warning, but they are subject to warnings that need to be fast confirmed or

canceled, and to mistakes of evaluation. A redundant system, with coastal and offshore detection, is desirable, mostly for places that might be hit by landslide generated tsunamis or that are very near to possible tsunamigenic trenches.

From an operational point of view, tsunami detection is not an easy task. For coastal tide gauges installed in places affected by seiches, and with strong resonant characteristics, the tsunami can excite typical background oscillations, masking its source spectral signature (Honda et al., 1908; Miller, 1972; Miller and Snodgrass, 1962; Munger and Cheung, 2008; Rabinovich, 1997; Rabinovich, Thomson, and Stephenson, 2006; Sanchez and Farreras, 1983; Van Dorn, 1984, 1987). The wave to detect is therefore very similar to usual background oscillations, with the same period. The only criterion to distinguish seiches to tsunami waves is therefore the wave amplitude. In case of simultaneously atmospheric phenomena that rise seiches level, the detection of similar amplitude tsunami is impossible since the signal cannot be distinguished from seiches (Thomson, Rabinovich, and Krassovski, 2007).

For offshore buoys, despite the fact that long waves are measured unfiltered, the small tsunamis are characterized by waves in the open ocean of very small amplitudes, of less than one centimeter. In addition, if the offshore buoy is located near the source, even the seismic waves are recorded: the vertical acceleration of the seismic waves is recorded as variations in pressure, then converted to water load of amplitudes as large as meters. The seismic signal might therefore mask the tsunami signal, making detection complicated.

The major difficulty of tsunami detection is to avoid false detections and to ensure the efficiency and the reliability of the detection algorithm. This implies not to miss any tsunami detection and at the same time to avoid false detections. False detections are difficult to avoid and they introduce serious problems: on one hand, people that experienced false warnings might as a consequence underestimate the tsunami threat in case of real tsunami detection. This is also valid for the authorities responsible to give warnings, with obvious disastrous consequences. At the same time, while emergency measures are necessary in case of real threat, and might include evacuation, stops of all business activities and works, in case of a false warning they imply big financial costs (Cox, 1979; Johnston et al., 2007; Schwartz, 2004).

Chapter 2

TEDA algorithm description and principles

2.1 TEDA principles and goals

TEDA, which is the acronym of Tsunami Early Detection Algorithm, is the name of a real-time algorithm for tsunami and sudden large waves detection for tide gauges. The real-time feature refers to the fact that it has been developed to work at a station level and that, at every new data acquisition, TEDA variables are updated and checked in view of a possible tsunami detection. It is worth to stress again that TEDA is based only on a single station sea level data. TEDA is composed of two part: an algorithm that aims to detect tsunami waves, and a tool for the identification of long period large amplitude waves. The principle on which TEDA aims to identify the tsunami is based on the hypothesis that the incoming tsunami waves are somehow different from the previous waves, either because they introduce new frequencies in the background spectrum and/or because they increase amplitudes of the typical spectral frequencies. Hence TEDA tsunami detection is based on the comparison between the latest signal, which might include a tsunami wave, and the previous background signal. These two signals are characterized by proper functions and compared to each other, and under specific conditions a detection is triggered. TEDA has been tested for the coastal tide gauge of Adak Island, USA. The strategy of TEDA is valid independently from the location of the station, along the coast or offshore, therefore a preliminary analysis for the application of TEDA to offshore

buoys in the Pacific Ocean has been performed.

A modern Tsunami Warning System should be equipped by different tools to estimate a possible tsunami threat, in order to assure redundant methods to back up procedures that might fail in some situations. At present, after a tsunami warning, tsunami threat confirmation (or cancellation) is usually given by reading the sea level records of sensors located offshore or at the coast. One could believe that coastal tide gauges cannot provide useful data, since any information based on them would come too late. This is not always true, since tsunami may travel very long distances and be damaging very far from their source, and therefore coastal tide gauge records of closer stations can be used for warning for more remote coasts. Moreover, detection at the coastline is important because, in some cases, it might be the fastest way to issue warnings to the population, since offshore buoys might be too far to record the tsunami waves before the tsunami hits the coast. This can happen for tsunamis generated by faults located really close to the shore or partially offshore and partially inland, and, in particular, for landslide generated tsunamis, which are almost always not announced by a precursor as clear as a strong earthquake.

The idea of an algorithm like TEDA that is independent from every kind of external information was born to work on coastal tide gauge stations, where detection has to be fast in order to give the population as much time as possible to react to the tsunami threat. Fast detection is possible since only one tide gauge record is analyzed, which cuts all the time needed for collecting and processing other data, such as seismic, GPS, etc. A detection algorithm based at station-level assures the possibility to use functions updated at every new data acquisition, without the need for waiting for a great load of data such as the whole first tsunami wave to make a decision on a tsunami alert. Of course, the advantage of being fast has the cost of increasing the possibility of error and increasing the detection uncertainties, as will be discussed later. The goal of TEDA is to signal a tsunami detection in the location where the instrument is installed.

In this chapter, the working scheme and structure of TEDA are explained, which means the definition of all the variables used in TEDA, the illustration of the criteria used for tsunami detection and for the declaration of a TEDA tsunami state. The method to indicate long period large amplitude waves, and the seismic signal detection, both part of TEDA, are also

described.

2.2 Working scheme

2.2.1 Method

From the hypothesis that the incoming tsunami waves are different from the previous waves, it descends that one needs to characterize both the instantaneous (most recent) and the previous sea level signals, which is accomplished by introducing two time functions: the instantaneous signal function IS and the background signal function BS. Both functions IS and BS, as well as all other time functions forming the structure of TEDA, are updated at every new data acquisition, which is a condition for TEDA to be real-time. The choice made is to base TEDA on the average slope of the sea level data corrected for the tide. The instantaneous signal function IS is calculated over a short time interval, denoted by IST, from the average slope of the sea level IS_T, then corrected for the tide by means of the tidal function TF. The background signal function BS is computed over a time interval, indicated with BST, longer than and preceding IST. The instantaneous signal function IS and the background signal function BS are compared through the control function CF, which, together with the instantaneous signal IS, is used to examine the presence of an incoming tsunami wave in the most recent signal, in which case a detection is triggered. When a detection is triggered, a tsunami state condition starts, during which tsunami detection is suspended. During a tsunami, the function BS is contaminated by the tsunami signal and usually assumes larger values than before the tsunami. Once it is declared, the TEDA tsunami state lasts till the function BS decreases back to the value it had at detection time.

TEDA functions depend on a number of parameters that have to be set according to the characteristics of the background signal and of the expected tsunami. The research of the optimal configuration of the TEDA parameters that is the most appropriate for a specific site is here indicated as TEDA calibration. The TEDA configuration is therefore site-dependent.

TEDA is implemented by means of the scientific language GNU Octave, and makes use of predefined functions.

2.2.2 Notations

Sea level data are hereafter denoted by the time series $m(t)$, $m(t_i)$ or m_i. Nowadays, all modern instruments make use of digital technology. In modern instruments, to avoid aliases problems, one distinguishes between the sensor sampling interval and the measurement sampling interval, say dt, the latter being a multiple of the former: any sea level data point is usually the average over the measurement sampling interval of the sea level taken by the sensor at the smaller sampling interval. In the following, we will consider only the measurement sampling interval and refer to it simply as the sampling interval. According to different instruments, the times associated with the acquired data are either the end or the center of the sampling interval. Here it was assumed that the time associated with a data point is the end of the time interval considered, i.e. the i^{th} data point m_i refers to the time interval $[t_{i-1}, t_i] \equiv [t - dt, t]$, which starts at the time of the release of the previous data point and ends at the time when the data point is acquired and stored by the station and made available for analysis.

The actual recording time, i.e. the time of the last data point, is indicated hereafter with t or t_i, with i the actual recording index. If we consider the n data points $m_1, m_2, \ldots, m_n$ corresponding to the instants $t_1, t_2, \ldots, t_n$ separated by the sampling time dt, it is worth pointing out that the duration of the time interval covered by the set of n data results to be ndt, while the length of the time interval $[t_1, t_n]$ is $(n-1)dt$.

2.2.3 The function IS_T

Let us name $IS_T(t)$ the average slope of sea level data, calculated by means of the least-squares method, over the short time interval $IST = [t - t_S, t]$, going back from the actual recording time t till time $t - t_S$. IS_T is calculated in the data domain, therefore its unit is $[cm/n]$, with n the number of data points. From a computational point of view, IS_T is calculated over the interval

$$IST = [t_{i-N_S+1}, t_i] \equiv [t - t_S, t], \tag{2.1}$$

where N_S is :

$$N_S = \lceil t_S/dt \rceil, \tag{2.2}$$

where the notation $\lceil x \rceil$ indicates the smallest integer not bigger than x and dt indicates the recording sampling interval. The time t_S is taken here in the order of ten minutes. Since the time will be measured in unit of dt in the following, and the sea level elevation will be given in cm, the function IS, which has the dimension of a velocity, will be expressed cm/dt.

2.2.4 The tidal correction

The influence of the tide in the average sea level slope IS_T can be quite strong, therefore a tidal correction is needed. Since it is very difficult to separate in real-time the tidal components from waves of other origin, like wind waves, tsunami or long waves, the computation of the tidal function $TF(t)$ was based directly on IS_T, according to the procedure illustrated here below.

At every time step, the function $TF(t)$ is estimated through a polynomial fitting of the average sea level slope IS_T over a proper "past" time interval and then by extrapolating the value to the actual time t. The fitting is calculated over a time interval, denoted by TFT, of length t_T of the order of few hours, going from the time $t - t_T - t_{G_{TF}}$ to the time $t - t_{G_{TF}}$ (see also Table 2.1):

$$TFT = [t_{i-N_{G_{TF}}-N_T+1}, t_{i-N_{G_{TF}}}] \equiv [t - t_{G_{TF}} - t_T, t - t_{G_{TF}}], \tag{2.3}$$

with

$$N_T = \lceil t_T/dt \rceil, \tag{2.4}$$

$$N_G = \lceil t_G/dt \rceil, \tag{2.5}$$

$$N_{G_{TF}} = 2 + N_G, \tag{2.6}$$

$$t_{G_{TF}} = t_G + 2dt. \tag{2.7}$$

The time t_G (and therefore $t_{G_{TF}}$) is a time interval introduced in TEDA in order to keep the function TF independent from the most recent signal IS. For this reason, t_G was chosen so that $t_S \leq t_G < t_{G_{TF}}$, which implies $N_S < N_{G_{TF}}$. From (2.1) and (2.3), with IST starting from t_{i-N_S+1} and TFT ending at $t_{i-N_{G_{TF}}}$, it follows that $t_{i-N_{G_{TF}}} < t_{i-N_S+1}$ and therefore the calculation of $TF(t)$ does not involve any data used for the computation of $IS_T(t)$. The separation of the intervals of time used to compute $TF(t)$

Table 2.1: Time intervals

	time domain	data interval index	length	
IST	$= [t - t_S, t]$	$\equiv [i - N_S + 1, i]$	t_S	N_S
TFT	$= [t - t_{G_{TF}} - t_T, t - t_{G_{TF}}]$	$\equiv [i - N_{G_{TF}} - N_T + 1, i - N_{G_{TF}}]$	t_T	N_T
BST	$= [t - t_{G_{BS}} - t_{BS}, t - t_{G_{BS}}]$	$\equiv [i - N_{G_{BS}} - N_{BS} + 1, i - N_{G_{BS}}]$	t_{BS}	N_{BS}

t_S	length of the time interval IST	N_S	$= \lceil t_S/dt \rceil$
t_T	length of the time interval TFT	N_T	$= \lceil t_T/dt \rceil$
t_{BS}	length of the time interval BST	N_{BS}	$= \lceil t_{BS}/dt \rceil$
t_G	time gap used to make TFT and BST independent from IST	N_G	$= \lceil t_G/dt \rceil$
$t_{G_{TF}}$	$= t_G + 2dt$	$N_{G_{TF}}$	$= N_G + 2$
$t_{G_{BS}}$	$= t_G + dt$	$N_{G_{BS}}$	$= N_G + 1$

and $IS_T(t)$ assures that, when anomalous waves like tsunami start to affect the instantaneous signal, the tidal correction will be not affected at least for a time as long as $t_{G_{TF}} = t_G + 2dt$. Indeed, anomalous waves contribution would be taken into account only starting from time $t - t_G + dt = t - t_{G_{TF}} + 3dt$, one data point at the time, for every new data acquisition.

The estimation of the tidal slope has been calculated in two different ways depending whether the instrument is installed in a coastal tide gauge station or in an offshore buoy. The reason is that usually tsunami wave height is much smaller offshore than at the coast, while tides are equivalent and sometimes larger offshore. Hence detiding requires much higher precision for signals of offshore buoys than of coastal stations. For offshore buoys, high precision tidal correction has been computed through a second order polynomial fitting, while for coastal tide gauges a zero-degree polynomial fitting (mean) has been used. The time interval TFT and its length t_T have been adapted according to the two different cases.

Low precision tidal correction

In case of coastal tide gauges, the estimation is simply the mean of $IS_T(t')$, indicated with $\langle IS_T \rangle$, with $t' \in TFT$, then further smoothed in a 5-min time interval starting from the actual time t and going backwards. The smoothing consists in averaging TF over its previous 5 min values. The

function TF is therefore computed according to the following steps:

$$TF(t_i) = \langle IS_T(t') \rangle \qquad \text{with } t' \in TFT, \tag{2.8}$$

$$TF(t_i) = \langle TF(t'') \rangle \qquad \text{with } t'' \in [t_{i-N_A}, t_i], \tag{2.9}$$

indicating with $N_A = \lceil 5min/dt \rceil$.

High precision tidal correction

In case of offshore buoys, the estimation of the tidal slope is accomplished by first least-squares fitting the sea level data with a parabola in the time interval TFT, and then by extrapolating the parabola to the actual time t. The parabola has been computed in a local reference frame, i.e. as a function of a local time, defined by means of the following expression:

$$\begin{cases} t'_j = t_j - t_i + t_{G_{TF}} + t_T, \\ j' = j - i + N_{G_{TF}} + N_T. \end{cases} \tag{2.10}$$

where t_i is the actual recording time. In this way, TFT can be written as $TFT = [0, t_T] \equiv [1, N_T]$ and the actual time t_i becomes $t' = t_{G_{TF}} + t_T$ in the new variable. Indicating with $p_1(t)$, $p_2(t)$ and $p_3(t)$ the coefficients of the parabola that fits IS_T in TFT, the tidal correction at the actual time t' becomes

$$TF(t) = TF(t') = p_1 t'^2 + p_2 t' + p_3. \tag{2.11}$$

2.2.5 The function IS

The function IS, the average detided sea level slope, is equal to the average sea level slope IS_T with the tidal function TF subtracted:

$$IS(t_i) = IS_T(t_i) - TF(t_i). \tag{2.12}$$

The functions IS, IS_T and TF are shown in Figure 2.1.

2.2.6 The function BS

The background function BS is meant to characterize some significant feature of the previous background signal, without the influence of the tide, and

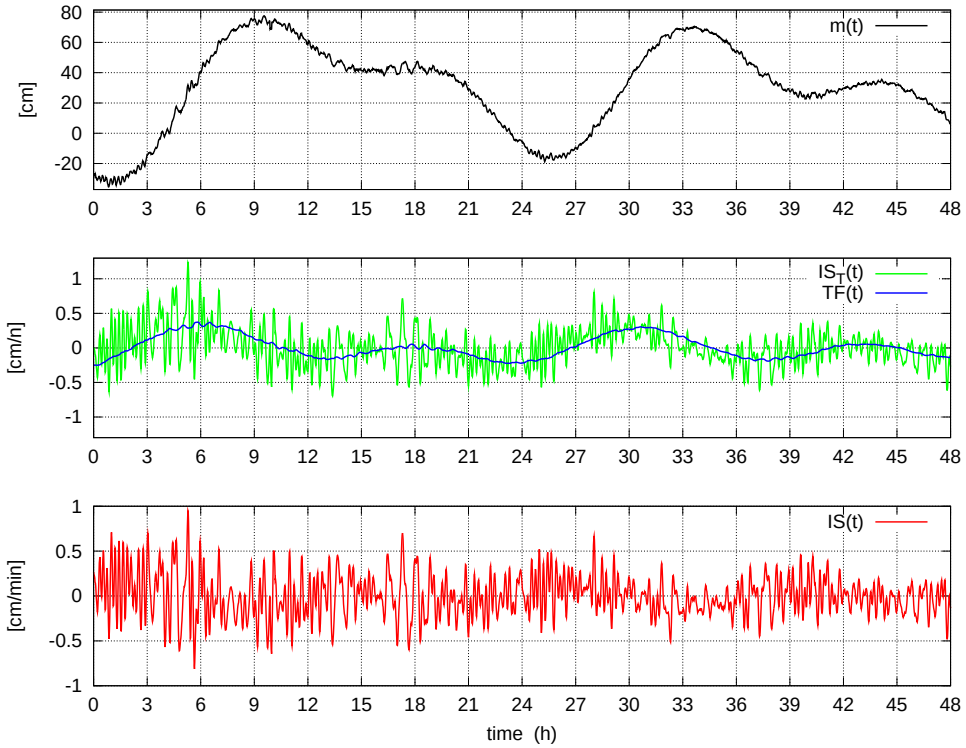

Figure 2.1: The TEDA function $IS(t)$ is computed by subtracting the tidal function $TF(t)$ from $IS_T(t)$. Here the original sea level $m(t)$ is shown in the top panel, the average sea level slope function IS_T with the tidal function TF are given in the central panel, and the instantaneous function IS, corresponding to the detided average sea level slope, is plotted in the bottom panel. The sea level data are from the tide gauge of Adak Island, in Alaska, USA. Low precision tidal correction has been used here.

it should be easily compared to IS. The consequent conclusion is to base it on the previous detided sea level slope IS. The BS estimation should take into account a time interval, indicated with BST, longer than and independent from IST:

$$BST = [t_{i-N_{G_{BS}}-N_{BS}+1}, t_{i-N_{G_{BS}}}] \equiv [t - t_{G_{BS}} - t_{BS}, t - t_{G_{BS}}], \quad (2.13)$$

starting from time $t-t_{G_{BS}}-t_{BS}$, with $t_{BS} \gg t_S$. As usual, $N_{BS} = \lceil t_{BS}/dt \rceil$. The delay time $t_{G_{BS}}$ (see Table 2.1) is a gap introduced to avoid or minimize the correlation between the quantities $IS(t)$ and $BS(t)$. Three possible ways of computing BS have been tried for the TEDA, which correspond to three methods designated hereafter as A1, A2 and A3. All such methods make use of the values of the instantaneous function $IS(t')$ with t' belonging to the interval BST. The corresponding values of $BS(t)$ are denoted by BS_1,

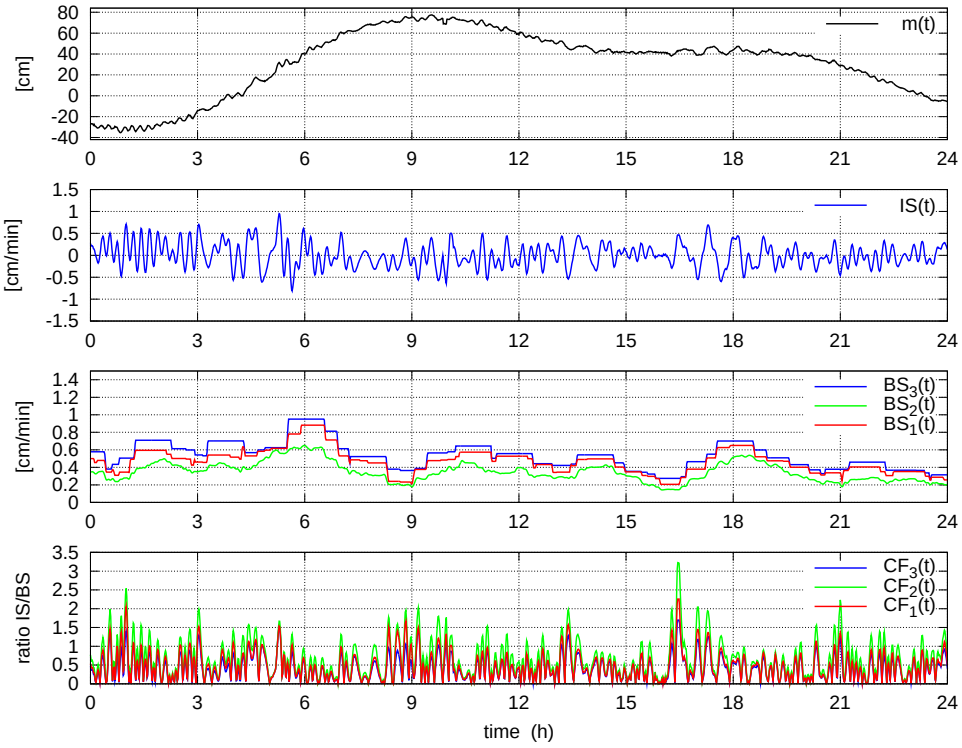

Figure 2.2: TEDA working scheme is here shown. From top to bottom, sea level data $m(t)$ are shown (top panel), the function IS (second top panel), the functions BS of the three methods A1, A2 and A3 (third top panel) and the function CF (bottom panel).

BS_2 and BS_3 and are defined as follows:

$$BS_1(t) = \left(max\left(IS\left(t'\right)\right) - min\left(IS\left(t'\right)\right)\right) \cdot \frac{1}{2}; \qquad t' \in BST \tag{2.14}$$

$$BS_2(t) = \sigma\left(IS\left(t'\right)\right) \cdot \sqrt{2}; \qquad t' \in BST \tag{2.15}$$

$$BS_3(t) = max\left(\left|IS\left(t'\right)\right|\right); \qquad t' \in BST \tag{2.16}$$

Notice that the function BS is always positive.

2.2.7 The function CF

The comparison between the instantaneous and the background signals is performed by means of the control function CF, which is simply the positive ratio between the two:

$$CF(t) = \frac{|IS(t)|}{BS(t)}. \tag{2.17}$$

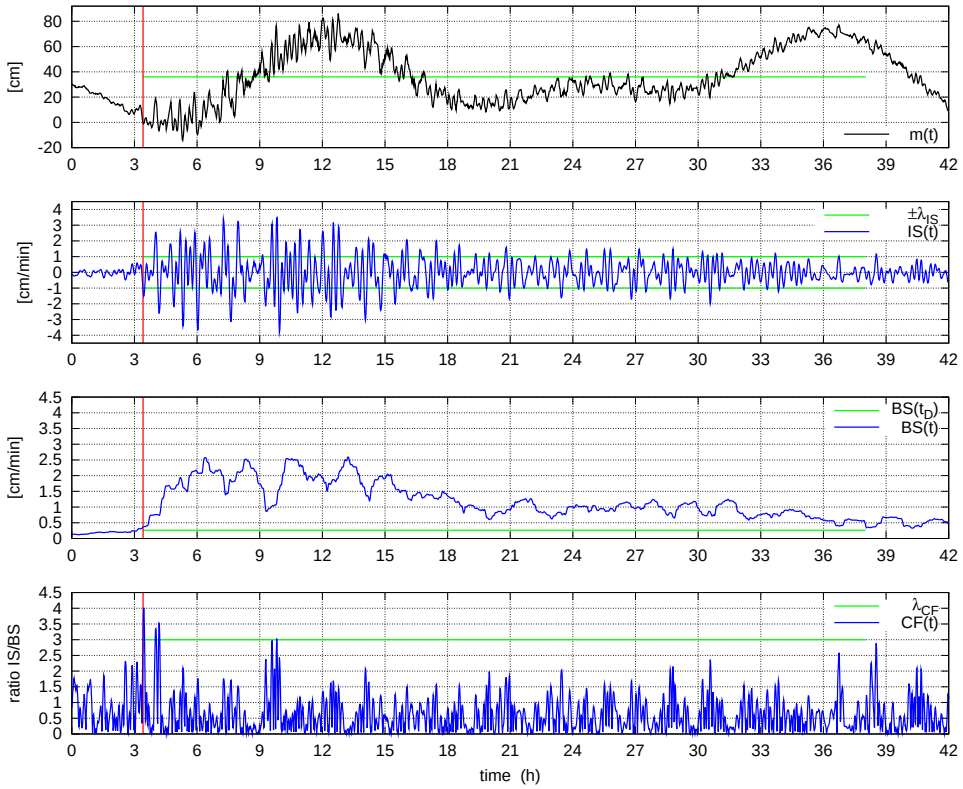

Figure 2.3: TEDA detection working scheme. From top to bottom: sea level data $m(t)$ are shown (top panel), the function IS (second top panel), the function BS (third bottom panel) and the function CF (bottom panel), calculated with method A2. Red vertical lines indicate the moment when a detection is triggered, while horizontal green lines indicates that the tsunami state is on. When $CF(t) > \lambda_{CF}$ and $|IS(t)| > \lambda_{IS}$ as in (2.19), a detection is triggered. In the central top panel, the tsunami state line has the values of IS thresholds λ_{IS}. In the central bottom panel, the tsunami state line is evidencing the value of $BS(t)$ at the detection time, which determines the duration of the tsunami state itself. In the bottom panel, the tsunami state line has the value λ_{CF} value. Notice that during the tsunami state the detection is suspended (notice for example an other detection condition between $t = 3$ h and $t = 6$ h).

The control functions corresponding to the methods A1, A2 and A3 are here denoted as CF_1, CF_2 and CF_3.

2.2.8 TEDA detection criteria and the tsunami state

TEDA assumes that a detection occurs at the actual recording time t when both $CF(t)$ and $|IS(t)|$ surpass a given threshold. Indicating with t_D the time when a detection is triggered, and with λ_{CF} and λ_{IS} the CF and IS

thresholds respectively, the detection condition is the following:

$$\begin{cases} CF(t_D) > \lambda_{CF} \\ |IS(t_D)| > \lambda_{IS} \end{cases} \tag{2.18}$$

or, in an equivalent way:

$$\begin{cases} CF(t_D) > \lambda_{CF} \\ IS(t_D) > \lambda_{IS} \quad \vee \quad IS(t_D) < -\lambda_{IS}. \end{cases} \tag{2.19}$$

An example of the functions, by which TEDA is structured, is shown in Figure 2.2.

A tsunami state starts whenever a detection is triggered. TEDA tsunami state is a condition during which tsunami detection is suspended, i.e. the function $CF(t)$ is calculated, but not checked for detection. The duration of a tsunami state is ruled by the BS function: during the tsunami, the background function $BS(t)$ is expected to grow to values higher than normal, owing to large amplitude tsunami oscillations being incorporated in the computation interval of $BS(t)$. When BS decreases below its value at the detection time, the tsunami state ends since it is assumed that the anomalous oscillations have definitely damped down to the usual background level. In other words, the tsunami state lasts during the entire interval, after a detection, when the function $BS(t)$ is above its value at the detection time, and it ends at t_{end} as soon as $BS(t) < BS(t_D)$. The condition for the tsunami state is therefore $BS(t') \geq BS(t_D)$, with $t' \in [t_D, t_{end}]$.

2.3 Determination of the TEDA parameters

The determination of the values of temporal parameters t_S, t_G, t_T, and of thresholds λ_{CF} and λ_{IS}, is to be carefully set. According to the typical background waves of the location where the instrument is installed, and of the possible expected tsunami waves, the suitable combinations of temporal parameters and threshold values might differ. These have to be carefully searched and established, which is a process we refer to here as TEDA calibration. The method for testing TEDA that has been used, which is explained in detail in the next chapter, allows one at the same time to choose the best combination of thresholds and parameters and to evaluate

TEDA performance, which further has permitted us to determine the best performing method between A1, A2 and A3.

2.4 TEDA security detection for tide gauges

Tsunamis approaching the coast varies in period, waveform, amplitude. At the shore, tsunami waveforms are not predictable (nor their characteristics, as amplitude, period and shape) without carefully simulating source and propagation till the interested point. In general, there are tsunamis that approach with positive or negative leading wave, which might be the highest or not. In addition, a tsunami record might visually presents itself with an ordinated pattern of waves, like a regular wave train, or without any apparent structure.

The principle by which TEDA works, i.e. that tsunami waves should introduce an abrupt change in the sea level record, implies that a slowly increasing signal, typical of phenomena of atmospheric origin, is not supposed to trigger a detection. Indeed in this case, the functions IS and BS are expected to increase simultaneously, and therefore their ratio CF is not expected to exceed the threshold. In other terms storm waves and oscillations induced by the increasing seiches would not trigger a tsunami detection.

In case of a tsunami with leading wave of very small amplitude and arriving as a wavetrain of progressively larger waves, the algorithm explain in previous sections fails the detection, even if later waves might be high and dangerous. Tsunami waves are dangerous not only because of their amplitudes, but also because long period waves induce strong currents even if the wave amplitude is not too large. For example, a tsunami wave at low tide smaller than the tidal range would not inundate anywhere, but the currents induced might cause a lot of damage to harbours and beaches, attacking moored vessels and producing erosion. For this reason, it is necessary to introduce in TEDA a 'secure' detection, based on wave amplitude, in order not to miss important waves that would not trigger a detection in the situations just explained.

Since $IS(t)$ is the detided sea level slope, it can be considered as

$$IS(t_j) = \frac{m_j^* - m_{j-N_S+1}^*}{t_S} = \frac{m_j^* - m_{j-N_S+1}^*}{N_S\, dt}, \tag{2.20}$$

where m_j^* represents an approximation of the detided sea level at time t_j. The quantity $(m_j^* - m_{j-N_S+1}^*)/N_S$ is an approximation of the average detided sea level change dM_j after each data acquisition dt, as in the following approximation:

$$dM_j = (m_j^* - m_{j-1}^*) \simeq \frac{m_j^* - m_{j-N_S+1}^*}{N_S} = dt \cdot IS(t_j). \tag{2.21}$$

The total sea level change $M(t_i)$ in $t_{sec} = dt\, N_{sec}$ time, from time $t_i - t_{sec}$ to time t_i, is calculated as follows:

$$M(t_i) = \sum_{j=i-N_{sec}+1}^{i} dM_j = dt \sum_{j=i-N_{sec}+1}^{i} IS(t_j). \tag{2.22}$$

The sum of the detided sea level slope $IS(t_j)$ from a specific time t_0 to the actual time t brings back to the residual tidal waves, not completely filtered out by the tidal correction. In order to focus on tsunamis and potentially dangerous long waves, the time t_{sec} has to be carefully determined: the main elevation change of a wave occurs from its minimum to its maximum, or viceversa, i.e. in a time equal to half the period of the wave. The determination of t_{sec} means to stress the amplitude of such waves with period $P = 2 \cdot t_{sec}$. To evidence the amplitudes of waves with periods of tsunamis or of long waves that might cause strong currents, the optimal value of t_{sec} has to be selected taking into account the different values of their periods.

A secure detection is triggered every time $M(t)$ passes the threshold λ_M. Once a detection is triggered, a warning is issued, with a duration of an hour. If the oscillations do not reach again the value λ_M within an hour, the warning ceases, otherwise it lasts till an hour after the last warning issue.

The way of computing the amplitude of waves $M(t)$ is an approximation that depends on the value of t_S used to calculate the function IS. Higher t_S values might damp or evidence the maxima and the minima of the amplitude of the waves $M(t)$ so calculated, respect to lower values of t_S. In setting the threshold λ_M, it is necessary to take into account the value of and the effect that this causes.

A possible criterion to determine the threshold λ_M for $M(t)$ is to fix a level of potentially dangerous current velocity v_{max}, and from there to draw λ_M. Shortly, the period of a standing wave in an open basin with a narrow rectangular shape (an harbour), of length L and constant depth d, is given

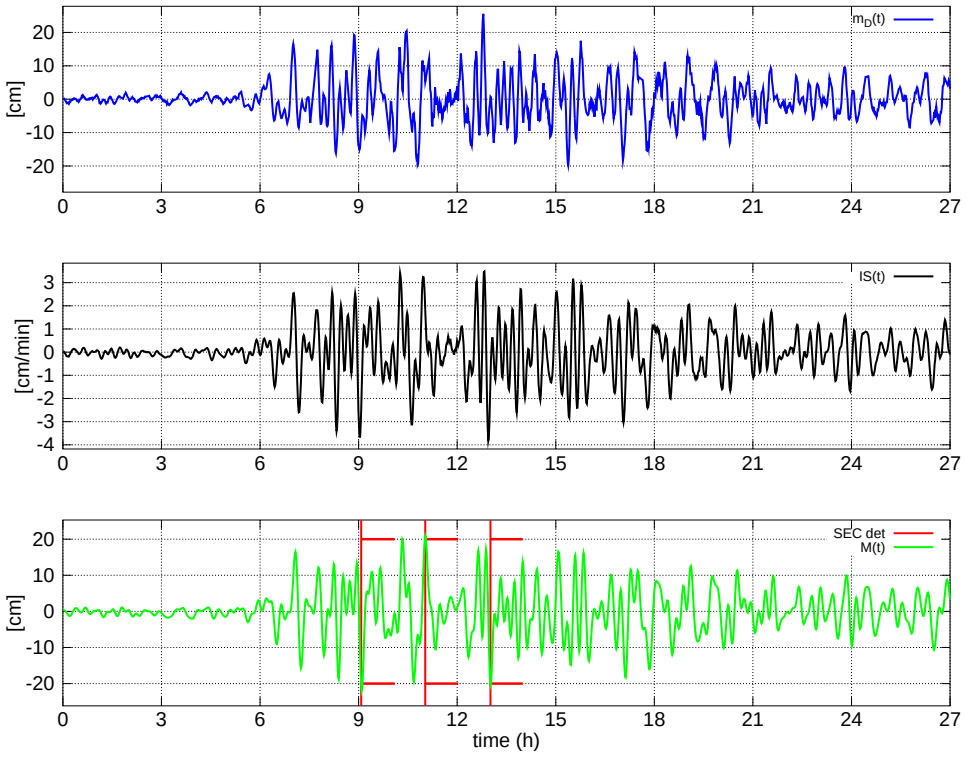

Figure 2.4: Secure detection. Example of Adak tide gauge record, in Alaska, for the Kuril Island 2006 event, for the following setting: $t_S = 12$ min, $t_{sec} = 8$ min, $\lambda_M = 20cm$. From top to bottom: detided sea level data $m_D(t)$ are shown (top panel), the function IS (second top panel), and the function $M(t)$. The secure detection triggers a warning when $M(t) > \lambda_M$.

by Merian's formula:

$$P_n = \frac{4L}{(1+2n)\sqrt{gd}}, \tag{2.23}$$

with n the number of the nodes of the wave and g the gravitational acceleration. The fundamental mode can be found with $n = 0$. The maximum and average horizontal velocity of a particle at the nodes are:

$$\begin{cases} v_{max} = \dfrac{H}{2}\sqrt{\dfrac{g}{d}}, \\ \overline{v} = \dfrac{H\,L}{\pi\,d\,P_n}, \end{cases} \tag{2.24}$$

with H the wave height. Setting $\lambda_M = H/2$, the relative wave amplitude is obtained.

2.5 TEDA seismic waves detection for offshore BPRs

BPR means bottom pressure recorder, an instrument that measures the water load pressure at the ocean floor, and converts it to sea level data. In case of earthquake, BPR records also the seismic signal, and in particular surface waves. Seismic oscillations are characterized by very high frequencies and, if the instrument is near the source, by very large amplitude, similar or even larger than the tidal amplitude. In case of BPR near the source, the seismic signal might mask the tsunami because of its amplitude, which can be by more than one order of magnitude bigger than the tsunami signal. In addition, a noise as strong as the seismic signal triggers easily a detection. In order to make sure that a tsunami has been generated or not, seismic signal detection and tsunami detection have to be distinguished. This is easily made by means of an algorithm based on the unexplained variance. Variance of a data interval is calculated as follows:

$$\sigma^2(x) = \frac{\sum_{i=1}^{N}(x_i - \overline{x})^2}{N}, \tag{2.25}$$

with $\overline{x}$ the average of x_i. The explained variance is the component of the variance explained by a model used to describe x. Let us call f the model for x, such that $x' = f(y)$ and $x = f(y) + \varepsilon = x' + \varepsilon$. The explained variance is therefore

$$\sigma^2_{exp}(x) = \sigma^2(x') = \frac{\sum_{i=1}^{N}(x'_i - \overline{x'})^2}{N}, \tag{2.26}$$

while the unexplained variance is

$$\sigma^2_{unexp}(x) = \sigma^2(x) - \sigma^2_{exp}(x) = \sigma^2(x) - \sigma^2(x'). \tag{2.27}$$

To focus on high frequency variations, it is useful to use a linear regression to model the data. The explained variance is in this case the variance due to the trend of data, while the unexplained variance takes into account what remains, which is mainly the high frequency variations. The unexplained variance is therefore a very useful tool to identify seismic signals, because it is very sensitive to high frequency signal. The following step is to model the sea level data m_i with a line for a short time interval, and then the calculation of the unexplained variance is used to identify high frequency

signals.

Since $IS_T(t)$ is the average sea level slope for the time interval IST, this also is used to calculate the unexplained variance. The model is therefore a linear regression that fits the data m, so that $m_j = m'_j + \varepsilon_j$ and $m'_j = f(t_j)$, indicating with m_j the sea level data of time t_j and $t_j \in IST$. With an appropriate variable change in data domain, which allows to write $IST \equiv [1, N_S]$, it follows:

$$m'_j = f(t_j) = IS_{T0} \cdot j + C, \tag{2.28}$$

with $j = 1, \ldots, N_S, \in IST$, $IS_{T0} = IS_T(t)$ and C the zero-degree coefficient of the least-squares fit of sea level m.

From the definition of the explained variance, it follows:

$$\sigma^2_{exp}(m) = \sigma^2(m') = \frac{\sum_{j=1}^{N_S}(m'_j - \overline{m'})^2}{N_S} = f(IS_{T0}, N_S), \tag{2.29}$$

which is only a function of IS_{T0} and N_S, because of the regularity of the time step and of its construction. The unexplained variance is therefore:

$$\sigma^2_{unexp}(m) = \sigma^2(m) - \sigma^2_{exp}(m). \tag{2.30}$$

When the unexplained variance passes a threshold λ_σ, TEDA assumes that there is the condition of a seismic signal and therefore TEDA detections are disactivated. The seismic signal lasts till the unexplained variance $\sigma^2_{unexp}(m)$ decreases below the threshold λ_σ.

Chapter 3

Test of TEDA

3.1 Aim and test procedure

Testing TEDA has two main objectives: it fixes the limits and conditions for which the algorithm works or not, and it allows a correct interpretation of the algorithm behavior through the estimation of the algorithm response. It is relevant to stress that the goodness and validity of a test procedure depends, among others, on the specification of how and for which cases a method has been tested. Ideally, a detection algorithm should be tested on every possible situation; in practice, the infinite number of the potential cases to test is impossible to handle, and conclusions with good confidence about the limits, the validity conditions and the response behavior of the algorithm can be drown from a limited set of tests data, selected by taking care to consider all the main situations that the algorithm could meet. In case of TEDA, it is important to test the algorithm on situations that differ in regard with the main characteristics, i.e. the background signal and the expected tsunami signal.

In this chapter it is described the method used to test and to calibrate TEDA for coastal tide gauges, while in the following chapter, the application and test of TEDA to the tide gauge of Adak Island is presented, specifying the considered cases, background conditions and tsunamis. The method applied in case of offshore sea level signal is slightly different, but based on the method here described, and it is explained in chapter 5 together with the analysis carried out for offshore buoys. TEDA has been applied on data from the Adak Island tide gauge, in Alaska, and on data from BPRs (DART buoys) located in the Pacific Ocean concerning real tsunami events.

Sea level data present very different characteristics depending on the location where the instrument is installed (see the Introduction 1). It is possible to separate two different categories of sea level background and of expected tsunami: on one hand, coastal tide gauge records exhibit typical background signal and tsunami response that are site-dependent, since both are influenced by the morphology of the coastal basin where the gauge station is installed. On the other hand, offshore records are mostly not site-dependent and share many common characteristics, the most relevant one being that the signal is dominated by the tide, with white noise superimposed and with unfiltered long wave spectrum (Titov et al., 2005). For this reason, TEDA has to be calibrated for every coastal tide gauge location, but the calibration for buoys in the open sea can be shared between more offshore locations, since the most evident variations are related to the different mixing of diurnal and semi-diurnal components of the tide and to the noise level.

The procedure illustrated here aims at testing the algorithm for a specific coastal site, evaluating its performance, by determining the most efficient method to characterize the background signal BS among the methods A_1, A_2 and A_3. At the same time the procedure permits the calibration of TEDA, which consists in setting the thresholds λ_{CF} and λ_{IS} for the functions IS and CF and the time parameters t_S, t_{BS}, t_G and t_T that determine the duration and the temporal position of the time intervals used by TEDA. The calibration for TEDA is site-dependent, and the detection ability of TEDA might vary significantly from location to location. TEDA should therefore be tested for every site where the algorithm is going to be introduced.

In a coastal site that is not affected by frequent and strong seiches, i.e. with a bathymetry not favorable to the excitation of natural eigenmodes, tsunami spectrum might be identified and separated by the background spectrum. In this case, the values of the temporal parameters should be chosen on the basis of the typical periods of the expected tsunami and to the characteristic periods of the background waves to filter out. The goal is to make the algorithm sensitive to waves with periods in the tsunami range and less sensitive to background wave periods.

In many cases, however, when the tsunami reaches the coast, it excites coastal resonance oscillations, loosing its proper signature: its spec-

trum is modified and distorted by the local morphology, in a way that the tsunami spectrum overlaps partially or totally the typical background spectrum (Honda et al., 1908; Miller, 1972; Miller and Snodgrass, 1962; Rabinovich, 1997; Sanchez and Farreras, 1983; Satake, Okada, and Abe, 1988; Van Dorn, 1984, 1987).

When this happens, the determination of temporal parameters is problematic, since to be sensitive to tsunami, TEDA turns out to be sensitive also to background waves and to seiches, and this has some negative consequences. Indeed, if some tsunami detection threshold is set low, false detection may results; if, on the contrary, it is set too high, it can lead to missing detections. Unfortunately, there is no theoretical solution, and hence different calibrations are tested in order to identify the most suitable one. The strategy adopted here for coastal tide gauge is to avoid false detection and to accept missing detection, i.e. to renounce to detecting small tsunamis, and to focus on bigger and more dangerous tsunami, in view of applying TEDA to Tsunami Warning Systems. The ground of this decision is that false detections and alarms might heavily compromise the usefulness of the algorithm itself, since people might undervalue a real tsunami threat because of previous experienced false alarm; in addition, false alarms implies big costs and loss of money (Bernard, 2005; Bernard et al., 2006; Cox, 1979; *Developing tsunami-resilient communities: the National Tsunami Hazard Mitigation Program* 2005; González et al., 2005; Johnston et al., 2007; Schwartz, 2004).

In this study, TEDA calibration is carried out empirically: TEDA is applied with some specific values of thresholds and of temporal parameters on the records used for the test. The test consists on two steps: the first consists in testing each temporal parameter combination varying the value of thresholds, in order to identify the best threshold range to work with. The second step consists in comparing the performance of all these configurations, in order to identify the most appropriate thresholds and parameters combination. A preliminary analysis is used to narrow the initial choice of thresholds and parameters values, and to provide a set of possible combinations to test. The test of TEDA is then performed for every configuration and thresholds values.

The test of TEDA consists in running the algorithm on sea level records, not in real time, and to assess its results. For a specific site, TEDA should

be tested on records with different background conditions and with different tsunami signals. Either real event data, when available, or synthetic tsunami signals can be used to test TEDA tsunami detection ability. In the test, TEDA might succeed or fail a tsunami detection, and might trigger false detections, depending both on the tsunami characteristics, like amplitude and spectrum, and on the properties of the background. The performance evaluation consists in discerning the tsunami and background characteristics favorable and disadvantageous for TEDA performance, estimating in this way the limits and the validity domain of the algorithm itself.

To estimate the goodness of detection, it is important to establish, independently from TEDA, how to distinguish real and false detections. This is accomplished by means of the definition of an interval corresponding to a tsunami signal: detections falling within this interval are due to tsunami oscillations and are therefore accepted, while detections falling outside are considered false. Real detections are then evaluated from their characteristics, considering the time of detection and the length of the associated tsunami state: these results, in the form of performance indicators, can be easily compared between the different configurations. For every combinations, the test is carried out on the records available for the site. Different records present different situations, as different tsunamis and different sea state conditions. The probability to meet different sea state conditions increases with the number of event records tested. A first criterion to evaluate the best performing setting is the number of events detected, evaluated by a gain function G. This allows to narrow the choice of cases, discarding the worst performing ones. As second criterion, performance indicators are taken into account. This procedure is explained more in detail in the following sections, and allows the calibration of TEDA to the application considered.

3.2 Preliminary analysis: choice of possible values for parameters and thresholds

The preliminary analysis is a very important step for the algorithm calibration and has the goal to select a small choice of the most likely suitable parameters and thresholds combinations for the site in exam. The preliminary choice of parameters has been carried out with a rough visualization

of the main TEDA functions IS_T, TF, IS, BS and CF, from which it is possible to get an idea of the values of the temporal parameters that should be used.

Some preliminary considerations have to be taken into account. It is important to consider the sampling rate of the record: a higher sampling rate allows to set lower values of temporal parameters. For example, a time of just a few minutes can be too short if the sampling rate of the record is of the order of a minute or so: too few data points might not carry enough significative information.

The level of the thresholds to set depends on the relative IS and CF usual background values, which depend in turn on the respective definition. The value of λ_{IS} depends therefore on the choice of the temporal parameters t_S, t_T and t_G used in computing IS, which in turn depends on the tidal function TF. The same reasoning works for λ_{CF}, which depends on the choice of all temporal parameters t_S, t_T, t_G and t_{BS} since CF involves both IS and BS in its definition. The estimation of possible thresholds is therefore subordinated to the choice of temporal parameters, with which it is better to start.

The way to proceed is to choose the range of the temporal parameters first, starting with the ones of the independent functions and going forward with the ones of the functions derived from others. Every temporal parameters combination forms a TEDA configuration, and will be indicated with C_n. For every configuration C_n, thresholds are then evaluated and set.

The first parameters to calibrate are t_T, t_G and t_S, taking into account that $t_{G_{TF}}$ and t_S are bound since $t_S \leq t_G < t_G + 2dt = t_{G_{TF}}$. The time gap t_G should be short enough not to add a time delay to the tidal function TF, but should be long enough not to constrain the value t_S to too small values. From practical tests, a time gap of about half an hour introduces a noticeable delay and it is therefore desiderable that t_G should be shorter.

The time length t_S, which determines the length of the interval IST, should evidence a tsunami wave slope in the function IS. It cannot be shorter than a few minutes, because it would be strongly influenced by high frequency waves and wind waves, with periods till to 20 seconds, which would add noise to IS masking the tsunami slope. On the other hand, it cannot be too longer than the main tsunami periods, because the average slope IS would not evidence the passage of a tsunami wave. Some theoretical

considerations suggest to pick $t_S < P/4$, where P is the main tsunami period, in order to evidence and catch the first rising or decreasing of the leading tsunami wave. If, in some cases, the detection of the first part of the leading wave is a too difficult achievement, the other possible choice is to set $t_S < P/2$, in order to evidence the slope between maxima and minima. Depending on situations and in particular in case of a location affected by seiches, or with noisy background, and with a short expected tsunami period, such a small value of t_S risks to make IS too sensitive to usual background oscillations. It is therefore advisable to check with higher values of t_S. At the same time, it is important also to limit the value of t_S, in order not to allow t_G to exceed a certain length. With this considerations, more values of t_S are checked, ranging in general from a few minutes to a couple of tens of minutes, to choose a set of possible values.

An important step is the determination of temporal parameter t_T. The length t_T of the time interval TFT has to be chosen so that the function TF fits well the IS_T tidal variations: tidal maxima and minima should not be underestimated, and the function TF should be smooth enough not to follow oscillations of periods shorter than the semi-diurnal tidal period. The value of t_T depends also on the level of precision (high or low) of the TF computation used. The low precision computation requires a time interval t_T enough short not to have a too high sea level change because of the tide, while for the high precision computation it is sufficient to be able to fit the tide change with a parabola, for which purpose it is in general convenient to take t_T shorter than a quarter of the semi-diurnal tidal period. From practical tests, it is evident that small variations of t_G and t_S do not affect the goodness of the tidal approximation for an acceptable choice of t_T. With some visual estimations, it is possible to choose the most suitable t_T value that fulfills the above requirements.

The last step consists in finding a reasonable value for the temporal parameter t_{BS}, by means of a qualitative evaluation of the function BS. The function BS should reflect the characteristics of the previous background noise, following the level of the waves, also in case of a quite fast atmospheric or sea state change. At the same time, the function BS should be stable and not influenced by single waves. The time t_{BS} should fulfill all these characteristics and satisfy the condition $t_{BS} \gg t_S$.

In general, it is easier to narrow the choice of t_{BS} and t_T to very few

values or even only one: TEDA performance is less sensible to them than to changes in t_G or t_{IS}; the latter in particular is the temporal parameter that most affects TEDA functions and performance. It is advisable therefore to test TEDA configurations, keeping t_{BS} and t_T constant and varying the parameters t_G and t_{IS}.

After fixing t_{BS} and t_T and determining a range of t_G and t_{IS} values, thresholds have to be investigated. The level of the threshold λ_{IS} should be around the level of the maximum of the function IS, in order to evidence waves bigger than the background. Since small changes in t_G or t_{IS} do not vary greatly the average value of the function IS, it is possible to estimate a maximum usual level of the function IS for background oscillations and to set in this way an acceptable value of the threshold λ_{IS} for the range of t_S chosen.

The threshold for the function CF is more difficult to set because a small change in its value varies significantly the number of detections and of false detections. An interval of possible λ_{CF} is chosen, from a minimum value $\lambda_{CF\,\min}$, which is assumed as $\lambda_{CF\,\min} = 1$ in this work, to a maximum value $\lambda_{CF\,\max}$. Every configuration is tested with λ_{CF} taking values ranging from the minimum to the maximum in small steps, i.e. falling in the interval $[\lambda_{CF\,\min}, \lambda_{CF\,\max}]$. For every configuration, test results are evaluated as a function of λ_{CF}. Once the most suitable values of λ_{CF} are identified for every configuration, the configurations can be compared between each other.

The preliminary analysis allows to fix values of parameters t_T and t_{BS} and of threshold λ_{IS}; to determine a set of values for t_{IS} and t_G to try, and to select an interval for possible values of λ_{CF}.

3.3 Tsunami signal definition

In order to evaluate TEDA performance, it is important to define a priori which detections are real and which are false, or, in other words, if the detection is due to tsunami waves or not. This is equivalent to define a *tsunami signal interval* TSI, i.e. an interval in the record where the oscillations are due to tsunamis. The temporal limits of tsunami beginning and end are assigned for every tsunami records. The estimation of the beginning of the tsunami signal is equivalent to determine the arrival time of the tsunami. This is an important step for the testing procedure of TEDA: a different

choice of tsunami signal TSI gives different performance results.

Tsunami signal identification is straightforward for synthetic tsunami signals added to a background record: the tsunami signal corresponds to the length and position of the synthetic tsunami signal added to the record. For real events, the tsunami signal identification is not always easy. The estimation of the tsunami signal has been accomplished manually, with the visual identification of tsunami oscillations. To better estimate the limits of the tsunami signal, sea level spectral analysis with periodograms has been performed and taken into account. When available, also tsunami arrival time estimations (ETA) from tsunami numeric simulations are considered. The length and therefore the end of the tsunami signal have been estimated observing in the record when the tsunami oscillations damp to approximately the pre-tsunami background level. In some cases, the continuous presence of waves or noise in the record might mask the arrival of the first tsunami wave, especially when the tsunami leading wave has a similar amplitude as the background waves. In case of no clear tsunami signal, with not identifiable arrival time and tsunami oscillations, a time interval of three hours around the estimated arrival time (ETA) has been used, starting from 30 min before. The anticipation of 30 min aims to account for the uncertainties of the tsunami arrival time estimation ETA. This interval is indicated as *tsunami window*. The tsunami signal TSI will be denoted with $TsuI$ in case of clear tsunami signal identification, while in case of tsunami window it will be indicated by $TsuW$.

Not all detections occurring in the tsunami signal can be considered acceptable detections: the goal of TEDA is to detect a tsunami when its first waves reach the coast, and not when the biggest tsunami waves have already hit the coast. For this reason, an interval TDI for acceptable tsunami detections is defined, and it is equal to the first 3 h of the tsunami signal TSI. In case of not identified tsunami signal, the tsunami detection interval TDI is equivalent to $TDI \equiv TSI = TsuW$.

3.4 Performance indicators

Various indicators are used to evaluate TEDA performance for all combinations of methods, parameters and thresholds. Performance indicators refer to each configuration, and can be grouped in three categories: a first cate-

Table 3.1: Tsunami intervals

	interval	number of detections
TSI	tsunami signal interval	NITD
TDI	tsunami detection interval, first 3 h of TSI	NAD
relations:	$TDI \subseteq TSI$,	NAD $\leq$ NITD

gory of *individual* indicators, is used to evaluate a configuration on a single event record. The second category is of *global* performance indicators, which takes into account all event records for the evaluation of the performance of a configuration. The third category is of *mixed* performance indicators, which are defined for every event record, on the basis of global and individual indicators.

3.4.1 Individual performance indicators

The individual indicators are defined for every configuration and for every event record. The individual indicators are the number of detections, which are counted for every record individually accordingly to different competence intervals, the time of the event detections and the length of the tsunami state of the corresponding event detections. For every configuration and event record, the number of tsunami detections, the delay time of detection and the duration of the tsunami state are computed for every values of the threshold λ_{CF}, and they are therefore evaluated as a function of λ_{CF}. All individual indicators are listed in Table 3.2 and an example of their evaluation can be seen in Figure 3.3.

The number of detections: NT, NITD, NAD, $\mathbf{NF}_E$

For every setting and for every record, the total number of tsunami detections NT is counted, together with the number of detections NITD falling within the interval TSI of the estimated tsunami signal. For records with no clearly identifiable tsunami oscillations, the tsunami signal TSI corresponds to the tsunami window $TsuW$ instead of the interval $TsuI$, and all results of the performance analysis are relative to this window.

In order to detect a tsunami, the detection has to be fast: the number of acceptable detections NAD is defined as the number of detections falling

Table 3.2: Individual performance indicators: for every method, configuration and threshold values, performance indicators are evaluated and used to compare different methods and configurations. In the table, the time interval where the indicators are computed is indicated; the whole record of an event is indicated with WR.

performance indicators		time interval	category
NT	number of total detections	WR	individual
NITD	number of tsunami detections	TSI	individual
NAD	number of acceptable tsunami detections	TDI	individual
NF_E	number of false detections	$\mathrm{WR} - TSI$	individual
TD	time of tsunami detection	TDI	individual
TSP	tsunami state length	TSI	individual

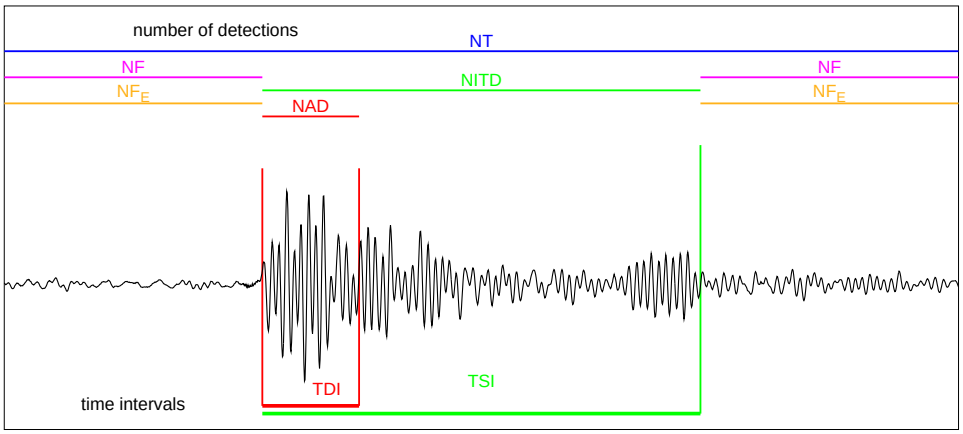

Figure 3.1: Number of detections: Example of tsunami state interval TSI (in green) and tsunami detection interval TDI (in red). Number of detections indicators that counts detections are indicated over the time intervals. This example is taken from the application of Adak Island, and refers to the Andreanov 1996 event (see chapter 4).

within the first three hours window from the beginning of the tsunami signal interval TSI, indicated with TDI. There can be cases of missed detections, when no acceptable tsunami detections occur and NAD= 0.

The number of false detections NF_E is simply the number of detection that occur outside the tsunami signal interval TSI, and it is equal to NF_E=NT-NITD. Particular attention has been focused on the number of false detections. For every method, parameter and threshold setting, the corresponding global indicator has been computed, i.e. the sum NF of all false detections NF_E was calculated for all records, $\mathrm{NF} = \sum_E \mathrm{NF}_E$. A scheme of the number of detections and of the counting interval can be seen

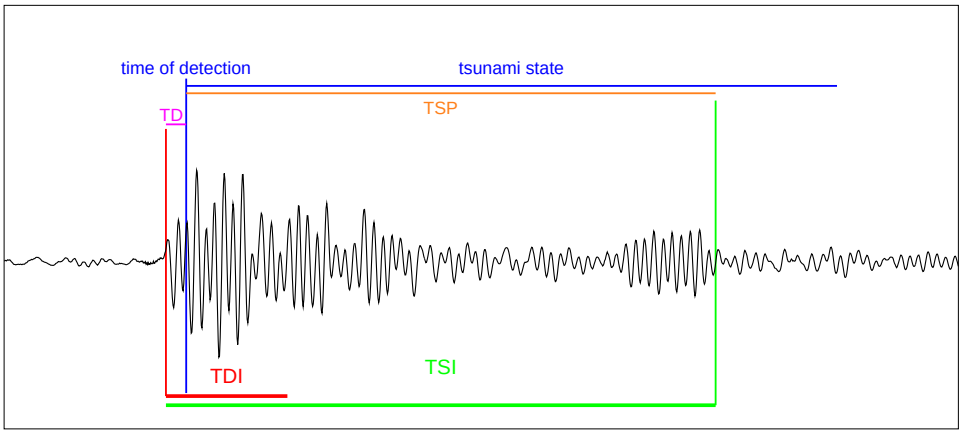

Figure 3.2: Detection time TD and tsunami state length TSP: in the figure is shown how the detection time TD and the tsunami state length TSP are calculated. For the latter, only the part evidenced in orange is used for the computation of the tsunami state duration TSP, which is measured in percentage of the tsunami signal interval TSI. The sea level in the figure is taken from the application of Adak Island, and is the detided record of the Andreanov 1996 event. The detection time and relative tsunami state are just an example.

in Figure 3.1.

3.4.2 The detection time TD

The detection time TD is equal to the delay time of tsunami detection calculated from the beginning of the tsunami signal interval TSI. The delay time of tsunami detection refers only to detections that occur within TDI, i.e. within the first three hours of the tsunami signal. The detection time is therefore calculated only for the detections counted in NAD. A scheme of the detection time TD can be seen in Figure 3.2.

3.4.3 The tsunami state length TSP

The tsunami state length is evaluated in two different ways, according to the kind of tsunami signal, if tsunami oscillations are identifiable or not ($TSI \equiv TsuI$ or $TSI \equiv TsuW$).

In case of tsunami signal identification, TSP is equal to the percentage of the tsunami signal covered by any of the tsunami states triggered by detections. With this definition, it is possible that a detection, occurring before the starting of the tsunami signal, generates a tsunami state active during the tsunami oscillations, which contributes to the determination of

TSP. However, in such cases, the detection is considered false. Tsunami states or their parts outside the tsunami signal TSI are not considered. A scheme of the tsunami state length TSP can be seen in Figure 3.2, together with the detection time TD.

For tsunami signal not identified $TsuW$, the length of the tsunami state loses its meaning and therefore it is simply the length of the tsunami state in minutes.

3.4.4 Global and mixed performance indicators

Table 3.3: Global and mixed performance indicators.

performance indicators		interval	category
NF	number of false detections	WR$-TSI$	global
$\lambda_{CF,m}$	minimum acceptable threshold value		global
DTI	detection threshold range		mixed
DTR	detection threshold range		global
G_E	partial gain function		mixed
G	gain function		global

The global indicators take into account all event records. The mixed value indicators are built for every event record in a complex way, taking into account both global results and individual ones.

The number of false detections NF and the minimum acceptable threshold value $\lambda_{CF,m}$

An important global indicator is the number of false detections NF for all event records, which takes into consideration all the different background signals of all records. In order to stress the importance of avoiding false detections, the choice made was to discard, for every configuration, those thresholds settings that give one or more false detections in any of the record ($NF > 0$). According to the principle of avoiding false detections for the configuration in use, a minimum acceptable threshold $\lambda_{CF,m}$ that prevents false detections is searched for every configuration. The minimum threshold $\lambda_{CF,m}$ is set globally for a configuration, in order not to have false detection

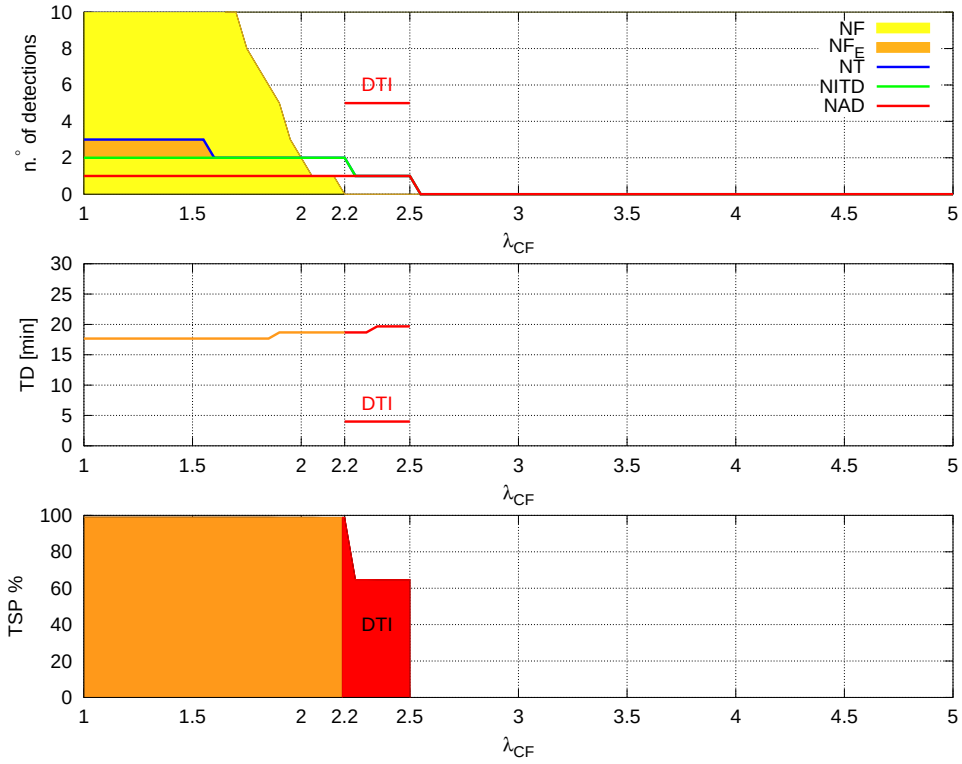

Figure 3.3: Test evaluation: Example of evaluation of a test of TEDA. All individual performance indicators are shown. In the top panel, the number of detections NT (in blue), NITD (in green) and NAD (in red), referring to the record in consideration, are shown. The number of false detections of the record NF_E is the difference between the total number of detection NT and the number of tsunami detections NITD, $NF_E = NT - NITD$, and therefore it is $NF_E = 0$ if the NT = NITD. When $NF_E \neq 0$, NT and NITD lines do not overlap and the presence of false detections in the record is indicated with the orange area between these two lines. The global number of false detections is also indicated in yellow. The threshold range DTI depends on the number of global false detections NF and on the number of acceptable tsunami detections NAD, and it is the threshold range for which NF = 0 and NAD ≥ 1. In the central panel, the detection time TD for acceptable detections is indicated, while in the bottom panel the tsunami state length TSP of the NAD detections is shown. This example is relative to the event record of Kuril island 2006 tsunami in Adak island, with method $A3C_5$, see chapter 4.

in any event records. TEDA performance is very sensitive to variations in the threshold λ_{CF}, which is indeed a key parameter of TEDA calibration.

The detection threshold range DTI and DTR

In the usual functioning of the algorithm, it is expected that for very low threshold values λ_{CF} some false detections are triggered. Rising the threshold, the number of false detections decreases and eventually goes to zero.

The same happens even for tsunami detections, i.e. after a certain threshold TEDA is not able to detect tsunami events any more. Since all configurations and thresholds combinations with false detections are not considered valid, the algorithm works only in a limited interval of CF threshold, indicated as the detection threshold range DTI, which corresponds to the range of λ_{CF} with at least one acceptable tsunami detection (NAD$>$ 1) but no false detections for all events considered (NF$=$ 0).

This allows to set the upper limit of the acceptable values of λ_{CF}, which is indicated with $\lambda_{CF,M}$. The upper limit $\lambda_{CF,M}$ is set individually for each event record, and consists in the maximum threshold value with the detection of the event considered. For values of $\lambda_{CF} > \lambda_{CF,M}$, the event is missed. The interval of acceptable λ_{CF} values is defined for every event and it is indicated with $DTI \equiv [\lambda_{CF,m}, \lambda_{CF,M}]$. To stress that the minimum acceptable value $\lambda_{CF,m}$ is set globally on the base of the global indicator NF, while the upper limit $\lambda_{CF,M}$ is set individually for each event record. The performance indicator DTI shares its minimum value with all event records.

If an event is not detected, DTI $\equiv \varnothing$, otherwise DTI $\equiv [\lambda_{CF,m}, \lambda_{CF,M}]$. An example of all individual performance indicators and interval DTI can be seen in Figure 3.3.

The global threshold range DTR is the intersection of all events DTI.

3.4.5 The gain functions G_E and G

For every configuration and threshold value, a gain function G is introduced in order to take into account the information of DTI for all events, and it is used as an indicator of the detection ability of the configuration in use. The gain function G gives the number of events detected under no false detections condition for each threshold λ_{CF}, and it is indicated with G(A,C,λ_{CF}), because it is defined for every method A and for every configuration C as a function of the threshold λ_{CF}. For every event record, the partial gain function G_E(A,C,E,λ_{CF}) is defined, attributing a value of 1 for such thresholds for which acceptable detection occurs and 0 otherwise:

$$\mathrm{G}_E(\mathrm{A}, \mathrm{C}, E, \lambda_{CF}) = \begin{cases} 1, & \text{if } \lambda_{CF} \in \mathrm{DTI} \\ 0, & \text{if } \lambda_{CF} \notin \mathrm{DTI}. \end{cases} \tag{3.1}$$

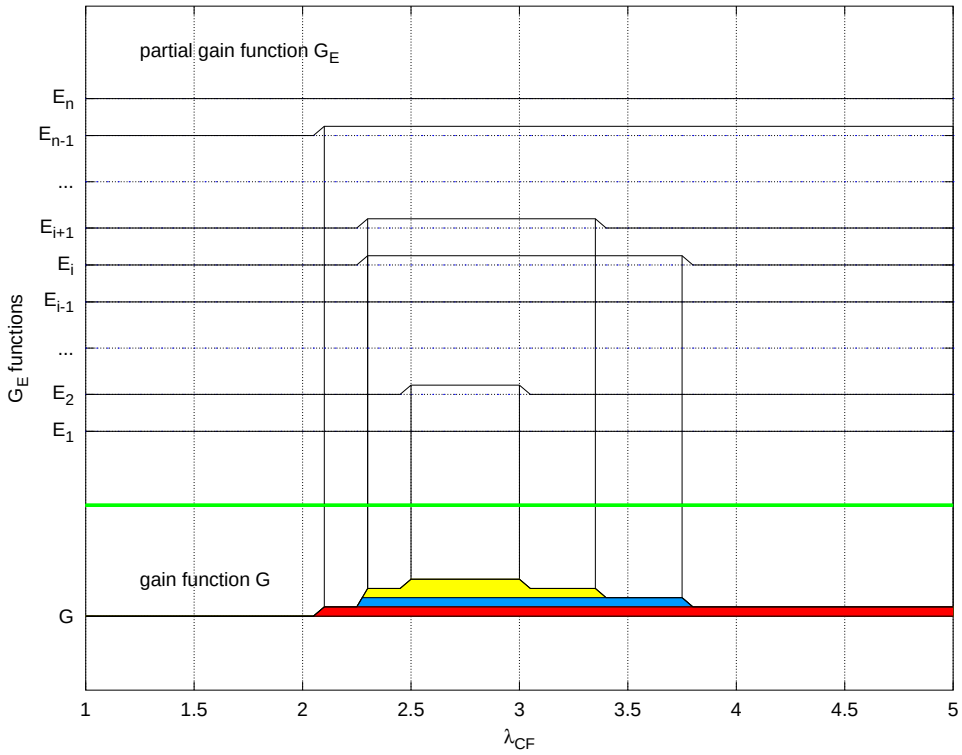

Figure 3.4: Gain function and partial gain functions: for a configuration C of method A, a partial gain function G_E(A,C,E,λ_{CF}) is equal to 1 if $\lambda_{CF} \in TDI$, when the event E is detected without false detections (NF=0). The gain function includes all events and is equal to the sum of all event G_E.

If DTI $\equiv \varnothing$, the event in consideration is missed by the configuration in use and G_E(A,C,E,λ_{CF}) = 0 for all λ_{CF} values. The gain function G is defined as the sum of G_E(A,C,E,λ_{CF}) for all events, as follows:

$$G(A, C, \lambda_{CF}) = \sum_{E} G_E(A, C, E, \lambda_{CF}). \tag{3.2}$$

A scheme of the gain function G construction can be seen in Figure 3.4.

Chapter 4

Application to Adak island tide gauge

4.1 Adak island tide gauge

Adak island is a volcanic island located in the middle of the Aleutian archipelago, in the group of Andreanov islands, in Alaska, USA. The Aleutian islands are a chain of islands parallel to the Alaska-Aleutian subduction zone, on the tectonic margin between the Pacific plate and the North American plate, that continues towards east on the Kuril-Kamchatka subduction zone (Ruppert, Lees, and Kozyreva, 2007). Both the Alaska-Aleutian and the Kuril-Kamchatka subduction zones are characterized by the subduction of the Pacific plate under the north American continental plate, with rates from about 6 cm/yr in southern Alaska to about 8-9 cm/yr in the Kuriles and Kamchatka (DeMets, 1992; DeMets et al., 1994). It is a very active area, both from a seismic and from a volcanic point of view. The fault mechanism varies along the margin because of the curvature of the Aleutian arc, from normal in the east to transform in the western part. Some of the earthquakes occurring along this trench are tsunamigenic, and it is an historical fact that some of them generated destructive Pacific-wide tsunamis, as the 1964 Alaska tsunami.

Studies of past and historical tsunamis and sea level records prove that Adak is often hit by tsunamis. Adak island can be hit not only by tsunamis generated along all the Alaska-Aleutian and Kuril-Kamchatka subduction zones, but also by far field tsunamis, generated all along the subduction

zones on the Pacific plate boundaries.

The town of Adak is situated on Kuluk Bay on the north-east side of the island. During the second World War, in 1943, an important military base of the Navy was built in the island, which was one of the most populated of the Aleutian at the time. A tide gauge was also installed in the harbour in 1943. After the end of the cold war, in the late 1990s, the base was closed and the harbour and airport were converted to civil use. The main harbour, where the tide gauge is located, is the harbour of Sweeper Cove, now part of the Aleut Corporation. The present tide gauge has been installed in 1991, and it is operated by NOS/NOAA (see *Adak tide gauge home page, NOS/NOAA:* http://tidesandcurrents.noaa.gov/geo.shtml?location=9461380).

The tide gauge of Adak island was chosen in this work because it provides important data for tsunami study, since it has been in operation and recording events for almost 60 years. In addition, the events recorded are generated both in near, intermediate and far field, assuring in this way a wide range of tsunamis with different characteristics.

The harbour of Sweeper Cove is open to the ocean through a complex system of bays and basins. It is in a bay of nearly rectangular shape, about 1700 m long and 900 m large, which is connected with Kuluk Bay with a mouth of about 600 m wide (see Figure 4.1). The basin of the harbour has an average depth of less than 20 m (see Figure 4.2). Kuluk Bay opens up in Sitkin Sound, an area of the sea limited by Adak island, Kagalaska island, Little Tanaga island and the Great Sitkin island. Both Sitkin Sound, Kuluk Bay and the basin of Sweeper Cove can be favorable of the rising of resonance waves and the trapping of waves. The site is frequently windy, which is a factor favorable to the onset of strong local seiches that are amplified by a resonant effect of the harbor (Rabinovich, Thomson, and Stephenson, 2006). The local tide has a maximum range of about 2 m.

4.2 Event records and the tsunami signal

The test for Adak tide gauge has been carried out with the use of eight real event records (Andreanov 1996, Kamchatka 1997, Vanuatu 1999, Peru 2001, Hokkaido 2003, Rat Island 2003, Tonga 2006 and Kuril Island 2006 events), numbered and denoted with E_n, as in Table 4.1. In Figure 4.3 all source earthquake locations are given.

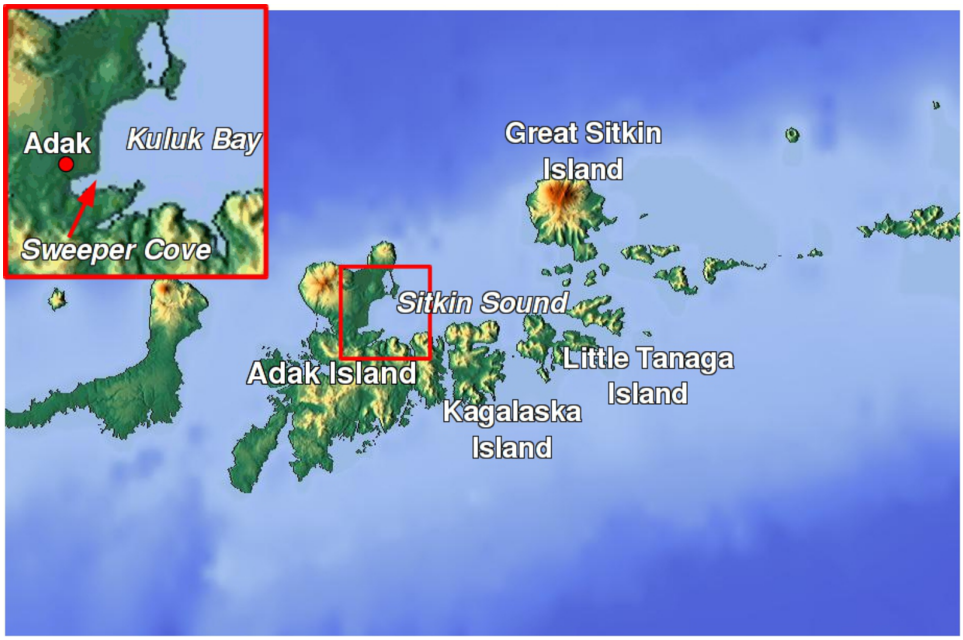

Figure 4.1: Map of Adak Island, Alaska.

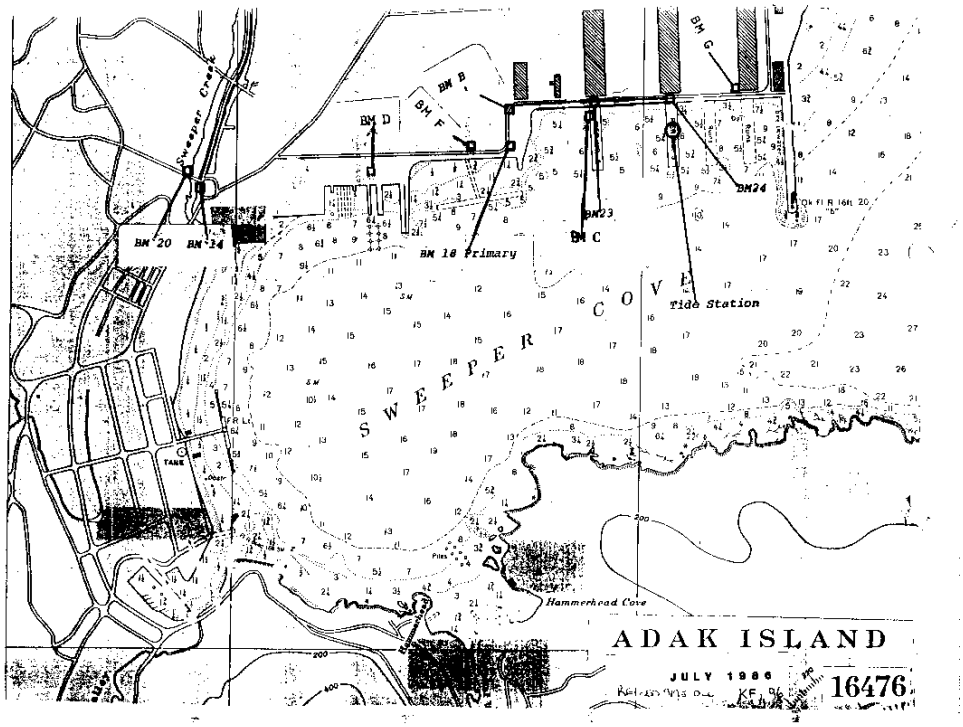

Figure 4.2: Map with bathymetry of Sweeper Cove,July 1986

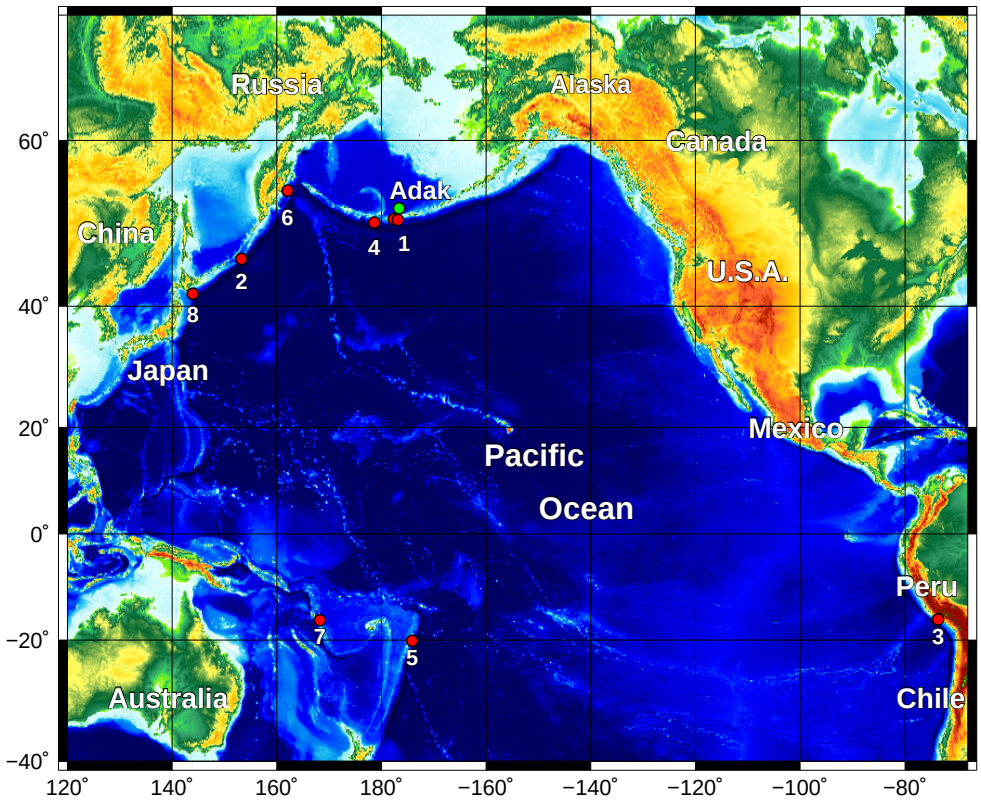

Figure 4.3: Map of the Pacific Ocean with the epicenters of the tsunamigenic earthquakes considered in this work. Adak island is indicated in green, in the Aleutian islands chain. The events are numbered from 1-8: 1) E_1 Andreanov 1996, 2) E_2 Kuril Island 2006, 3) E_3 Peru 2001, 4) E_4 Rat Island 2003, 5) E_5 Tonga 2006, 6) E_6 Kamchatka 1997, 7) E_7 Vanuatu 1999, 8) E_8 Hokkaido 2003.

The number of the events is indicative of their magnitude in Adak, which has been established on the basis of the maximum and minimum wave heights recorded in Adak. The most significative tsunami event between the ones analyzed is Andreanov 1996, which is denoted with E_1; the second tsunami for wave height is Kuril island 2006, which is denoted with E_2, and so on. The E_1 Andreanov 1996 and the E_4 Rat Island 2003 events, which were generated in the Aleutian subduction zone, are considered near field, while all the others are intermediate or far field. All events records can be seen in Figure 4.4, and they have been provided by NCTR/PMEL/NOAA

(NOAA Center for Tsunami Research/Pacific and Marine Environmental Laboratory/National Oceanographic and Atmospheric Administration) with a sampling interval of 1 minute.

All records have been analyzed in order to identify the tsunami signal TSI and to study the typical background and tsunami spectrum. Both the spectral analysis and the identification of the tsunami signal have been carried out on detided records. It is important to stress that the detided signal has not been used as input for TEDA, since TEDA makes use of raw sea level data.

To set the beginning of the tsunami signal, literature or event simulations have been taken into account, in particular Eble et al., 1997 for E_1 Andreanov 1996 event, Wang and Liu, 2006 for the E_2 Kuril Island 2006 event, and tsunami propagation maps obtained by means of WebSIFT for all events (Gica et al., 2008).

The tsunami signal has been identified by inspection for five events, E_1, E_2, E_3, E_4 and E_5, for which a proper tsunami signal interval TSI was recognized. For the remaining three events, E_6 Kamchatka 1997, E_7 Vanuatu 1999 and E_8 Hokkaido 2003, it was not possible to identify the tsunami in the records and a tsunami window $TsuW$ was used to identify the tsunami oscillation, i.e. $TSI \equiv TsuW$. The windows $TsuW$ have been set on the basis of the estimated arrival time ETA derived from the propagation maps calculated via the code WebSIFT. The Figure 4.5 shows the detided event records with the corresponding tsunami signal interval TSI.

The records are quite different in terms of the tsunami signal and of the existing background. The fact that these events occurred in different months of the year (May, June, September, November and December) assures that different climate conditions are taken into account in the test of the algorithm, which is reflected in the different magnitude of the background signal. In order to give a simple estimation of tsunami magnitude and background level, the range of background waves R_b and of tsunami waves R_{TSI} has been given in Table 4.1. The range is the difference between the maximum level and the minimum level reached by tsunami or background oscillations in the detided marigram, i.e. $R = max(m^*) - min(m^*)$, with m^* the detided sea level signal. The tsunami signal interval TSI was used to distinguish between tsunami oscillations and background. Since the goal of TEDA is to detect the first tsunami wave, it is convenient also to know the first tsunami

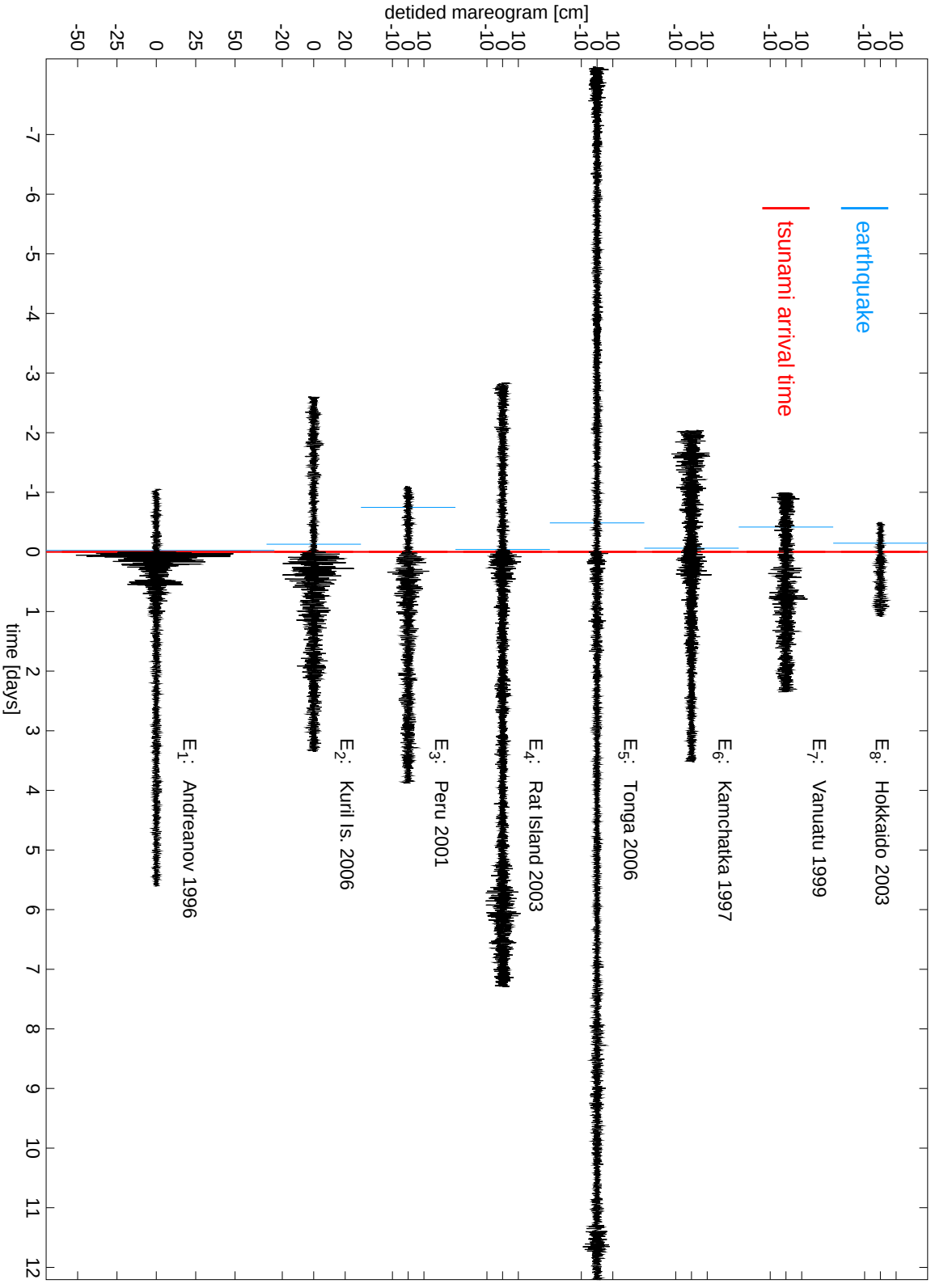

Figure 4.4: Event records.

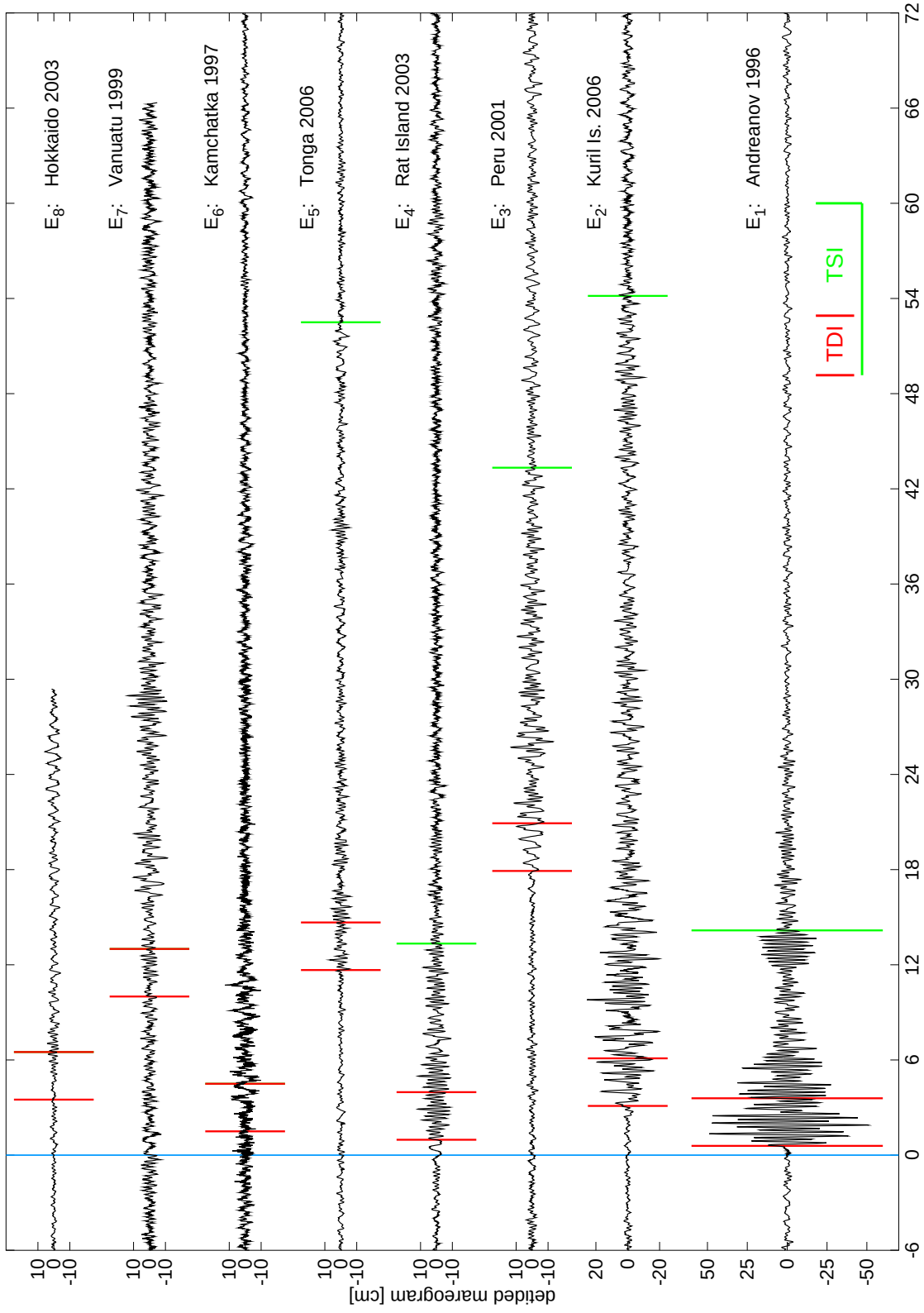

Figure 4.5: Event records with the relative tsunami signal interval TSI and tsunami detection interval TDI.

Table 4.1: Tsunami events: name and date of the event, magnitude of the generating earthquake, height of the first tsunami wave, range of the tsunami oscillations, range of background oscillations in the record and type of the time interval including the tsunami signals. The heights of the first wave and the range of the tsunami and background waves have been estimated on the detided records.

	event	date			M	H_1 $[cm]$	R_{TSI} $[cm]$	R_b $[cm]$	TSI
E_1	Andreanov	10	Jun	1996	7.9	36	100	16	$TsuI$
E_2	Kuril	15	Nov	2006	8.3	15	45	11	$TsuI$
E_3	Peru	23	Jun	2001	8.4	9	27	13	$TsuI$
E_4	Rat island	17	Nov	2003	7.8	9	21	22	$TsuI$
E_5	Tonga	3	May	2006	7.9	8	14	17	$TsuI$
E_6	Kamchatka	5	Dec	1997	7.8	10	18	25	$TsuW$
E_7	Vanuatu	26	Nov	1999	7.3	8	10	25	$TsuW$
E_8	Hokkaido	25	Sep	2003	8.3	4	6	10	$TsuW$

wave height H_1, given together with the range of tsunami waves in Table 4.1. For events with no tsunami signal identified, the height of the first wave is just indicative of the most likely first tsunami wave of the record.

Most of tsunami events here used present moderate tsunami amplitudes. With the exception of E_1 Andreanov 1996 event, with a range of about 1 m and a first wave height H_1 equal to $H_1 = 36$ cm, all the remaining events do not reach 50 cm range and present a first wave height H_1 smaller than $H_1 \leq$ 15 cm. Since Adak is a place affected by seiches, it is interesting to compare the range of background oscillation R_b with the tsunami range R_{TSI}. In Table 4.1 it is evident that the background range R_b can be both smaller and bigger than the tsunami range R_{TSI} of the events considered. This fact is also visible in the detided records of Figure 4.4 and 4.5: some seiches events are evident in the records, especially at the end of the record E_4, Rat island 2003, of E_5, Tonga 2006 and at the beginning of E_6, Kamchatka 1997 event. The highest oscillations in the E_7 Vanuatu 1999 record compare about 6 h after the expected tsunami arrival time ETA. In this case, the cause of the rising of waves amplitude is uncertain, but because of the long delay from ETA, it can not be attributed to the tsunami.

This allows us to evaluate TEDA performance also in cases of seiches phenomena. It is evident that seiches can have significative amplitudes, even bigger than moderate tsunami amplitudes. It seems that seiches phenomena of about 20 cm range R_b are not an infrequent event, taking into account the limited length of the sea level records considered.

The goal of TEDA tsunami detection is to detect tsunamis but not se-

iches. Detection triggered by seiches falling outside the tsunami signal interval are considered false. However, when sea oscillations are very large (i.e. when a given threshold is exceeded) an alert is set by TEDA secure detection independently from the fact that the origin is a tsunami or a seiche.

In case of missing data in the record, data were replaced with linear interpolation. The linear interpolation does not reproduce the missing data, but assures the continuity of TEDA without the risk to add a detection due to the artificial corrections of data.

4.3 Spectral analysis

The spectral analysis has been performed on all event records with FFT, on a mobile window of 10 h and 30 min, with relative shifting of 30 min, on the detided records. The spectra have been then averaged in order to decrease the noise level. The spectra of the tsunami are the spectra computed when the mobile window overlaps significantly the tsunami signal interval TSI, and "significant superposition" here has been taken according to the criterion that at least 50% per cent of the window falls in such interval.

The average spectra of all events and of the background signal is shown in Figure 4.6. Since all spectra are very similar, it is immediately clear that all tsunamis mostly excite the typical resonance periods of the Adak basins, losing their offshore signature. The main typical oscillation periods of Adak turn out to be around 3, 4, 10, 13, 17, 21, 24, 35, 42 and 48-52 minutes. The only exceptions are the E_1 Andreanov 1996 tsunami, which has a distinctive peak around 30 min, and the E_4 Rat island 2003 event, which shows an additional peak with period of 63 min.

Since the period and the spectral characteristics of seiches and tsunamis are almost the same, and for moderate tsunamis also their amplitude is comparable, it is difficult to distinguish tsunami waves and seiches, usually caused by direct atmospheric forcing or from incoming storm waves trains. The main difference in the record is that, unlike tsunamis, seiches often rise slowly in time, following the approaching of the atmospheric perturbation or of storm waves fronts. A tsunami instead can start with a wave of large amplitude. This distinction is exploited by TEDA to discriminate tsunamis from background signals. As it can be seen in the record, moderate seiches might also rise quite fast, as in the beginning of the record E_6, of Kam-

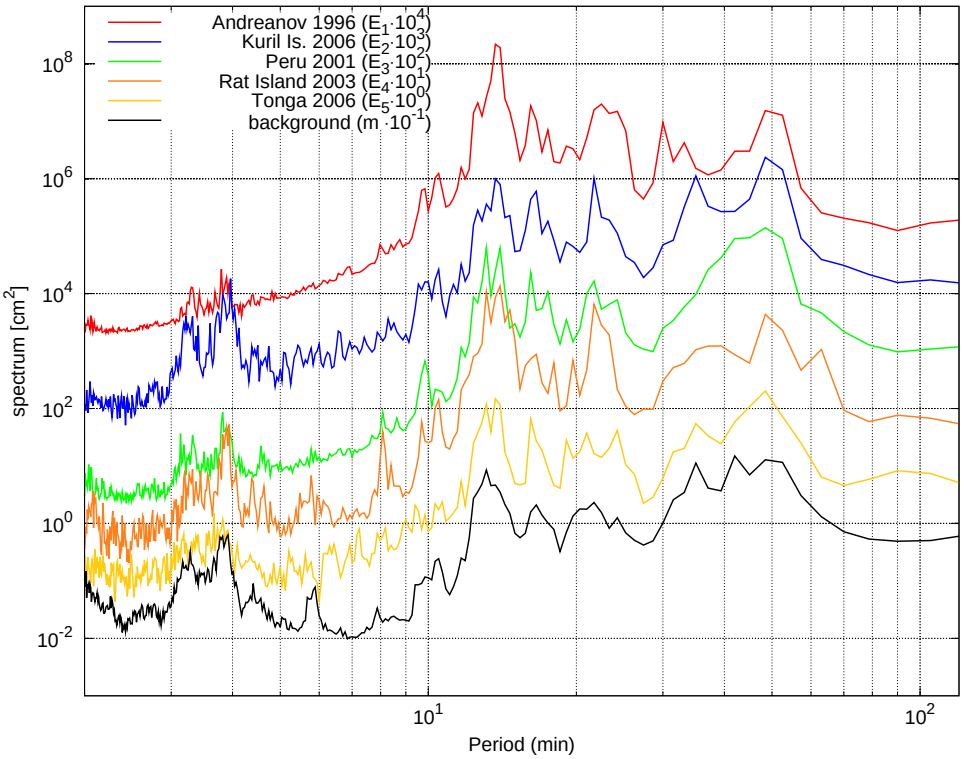

Figure 4.6: Spectral analysis of the tsunami and the background signals. The bottom spectrum is the averaged background spectrum (with no tsunami), while the others are average spectra computed for the E_1 Andreanov 1996, E_2 Kuril Islands 2006, E_3 Peru 2001, E_4 Rat Island 2003 and E_5 Tonga 2006 events. Spectra are shifted vertically to permit a better reading. Notice that all are quite similar, indicating that local eigenmodes are the dominant factor. The main typical oscillation periods are around 3, 4, 10, 13, 17, 21, 24, 35, 42 and 48-52 minutes.

chatka 1997, and this means that TEDA cannot discriminate such seiches from tsunamis. They would be taken as tsunamis and would triggered false detection. The choice however to avoid false detections leads to the direct consequence that tsunamis of moderate amplitude can be missed.

4.4 Preliminary analysis

A preliminary analysis has been performed for Adak island tide gauge, allowing us to select some specific values of temporal parameters and thresholds.

The test has been performed with the parameters configurations listed in Table 4.2: the possible values of temporal parameters are $t_T = 60$ min, $t_{BS} = 60$ min, $t_S = 6, 8, 10$ min with $t_G = 10, 15$ min and $t_S = 12$ min with

Table 4.2: TEDA configuration: a configuration C_n consists in a specific combination of temporal parameters and thresholds that are used to test TEDA.

C_n	t_S $[min]$	t_T $[min]$	t_G $[min]$	t_BS $[min]$
C_1	6	60	10	60
C_2	6	60	15	60
C_3	8	60	10	60
C_4	8	60	15	60
C_5	10	60	10	60
C_6	10	60	15	60
C_7	12	60	15	60
λ_{IS}		1 $[cm/min]$		
λ_{CF}		$1.00, 1.05, 1.10, \ldots, 5.00$		

$t_G = 15$ min. Each parameters configuration has been denoted with C_i, with i in the range $1-7$ increasing with t_S. Each record has been analyzed with all three methods A1, A2 and A3 and all parameter combinations C_{1-7}.

The threshold for the function IS has been set to $\lambda_{IS} = 1$ cm/min, while the threshold λ_{CF} assumes all values, from 1 to 5, with steps of 0.05.

4.5 Test results

For every configuration and event, specific indicators have been introduced to evaluate the performance of the algorithm. The first step in analyzing the results of the test is to take into consideration all configurations that detect at least one tsunami (i.e. start at least one tsunami alarm) under the condition of zero false detection, i.e. $NF = 0$ and $DTI \neq \varnothing$, which implies for the partial gain function that $G_E = 1$ for some values of λ_{CF}.

The partial gain function G_E, which is by definition depending on the threshold parameter λ_{CF}, is given in Figure 4.7 for the events E_1, E_2 and E_5, E_6. Considering all configurations tested, of all events only three are detected by TEDA: E_1 Andreanov 1996, E_2 Kuril Island 2006 and E_5 Tonga 2006 events. The first two are the most relevant tsunamis of the group, with larger wave heights. The last event, E_5 Tonga 2006, is a very small event, with first wave height H_1 of 8 cm and maximum tsunami range of about 15 cm. All other events are not detected. In addition, not all methods and configurations detect the three tsunamis. The E_1 Andreanov 1996 tsunami is detected by most methods and configurations, followed by the E_2 Kuril Island 2006 and by the E_5 Tonga 2006 event. The E_1 Andreanov 1996

tsunami is detected by almost all configurations, except A1C_2 and A2C_{1-6}, and because of its amplitude, the detection range DTI starts at a certain threshold $\lambda_{CF,m}$ and ends at a threshold $\lambda_{CF,M} > 5.0$. The other two events are detected for a much smaller threshold range DTI, usually shorter than 1. The E_2 Kuril Island 2006 tsunamis is detected only by A1C_7, A3$C_{3,5-7}$, while the E_5 Tonga 2006 event is detected by A1C_{5-6} and A3C_{5-6}. Table 4.3 summarizes all the events detected by all the configurations. The detection range can be seen with the partial gain functions G_E, given in the Figure 4.7.

The partial gain functions G_E, grouped per configuration C_i, are given for four configurations in Figure 4.8. All methods A1, A2 and A3, detect at least one tsunami event with at least one parameter combination. Method A2 has the smaller number of detections, and there is no combinations detecting more than one event: only A2C_7 detects the E_1 Andreanov 1996 event. This is due to the high sensitivity of this method, which implies a high number of false detections for background waves.

Methods A1 and A3 work better, with almost all parameter combinations detecting at least one tsunami event, with the exception of A1C_2 that fails all tsunami detection.

All these information, carried by the partial gain functions G_E, are summarized in the gain function G, which can be seen in Figure 4.9 and it is used to select the best performing method and configuration. The only configurations able to detect three events are A1C_5 and A1C_6. These two methods will be further compared in order to choose the best setting for Adak, which will imply the detection of the three events E_1, E_2 and E_5. A comparison of all individual performance indicators is made in Figure 4.10. The comparison is limited to the interval where all three events are detected.

The two configurations A3C_5 and A3C_6 are characterized by almost the same minimum λ_{CF} threshold that implies zero false detections (NF=0),

Table 4.3: TEDA event detection: For every method Ai and configuration C_j the events are given.

	C_1	C_2	C_3	C_4	C_5	C_6	C_7
A1	E_1	-	E_1	E_1	E_1, E_5	E_1, E_5	E_1
A2	-	-	-	-	-	-	E_1
A3	E_1	E_1	E_1, E_2	E_1	E_1, E_2, E_5	E_1, E_2, E_5	E_1, E_2

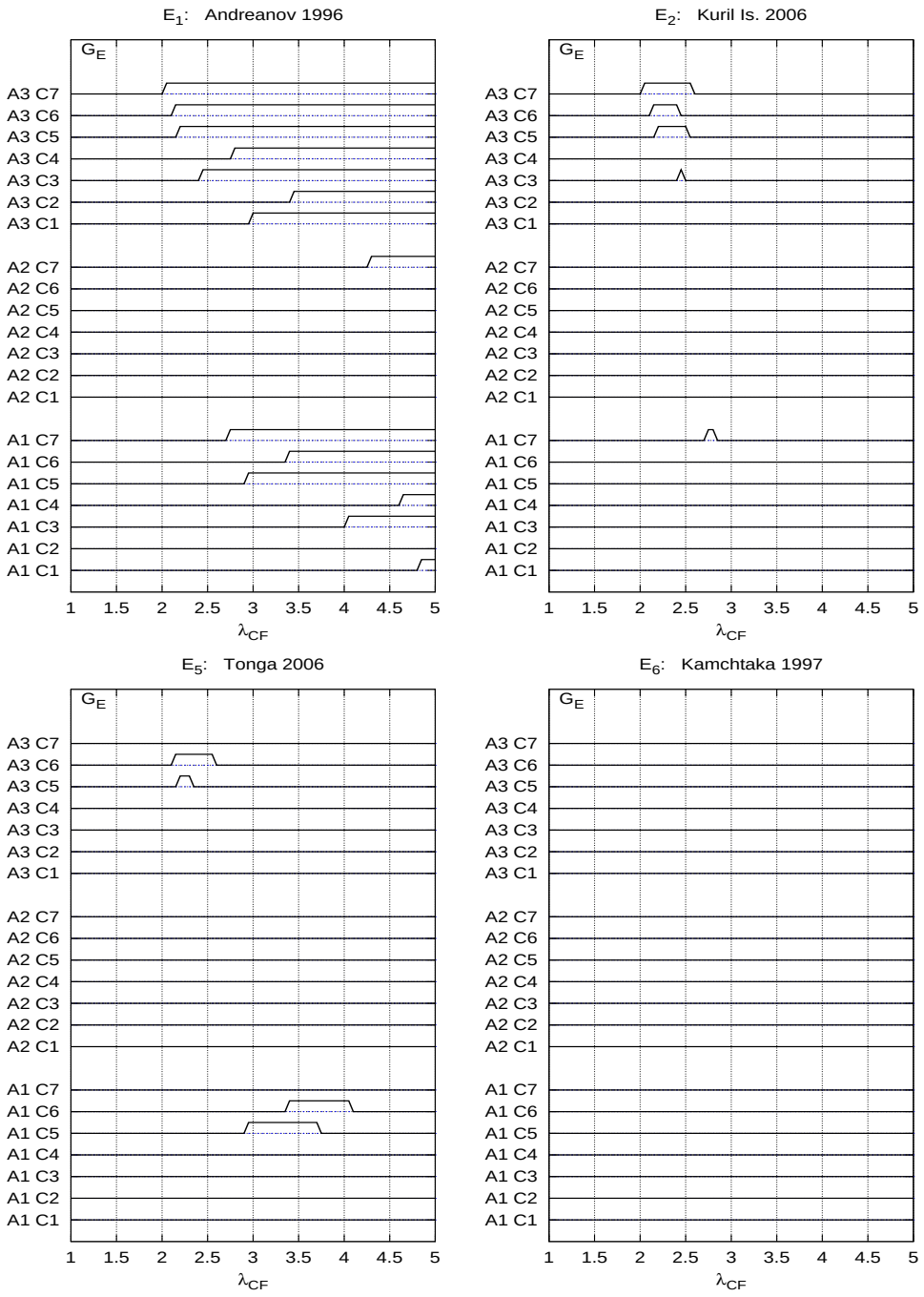

Figure 4.7: Partial gain function G_E for E_1 Andreanov 1996, E_2 Kuril island 2006, E_5 Tonga 2006 and E_7 Kamchatka 1997 events. The function G_E that depends on the threshold value λ_{CF} indicates if the configuration detects the tsunami event ($G_E = 1$) or it does not ($G_E = 0$).

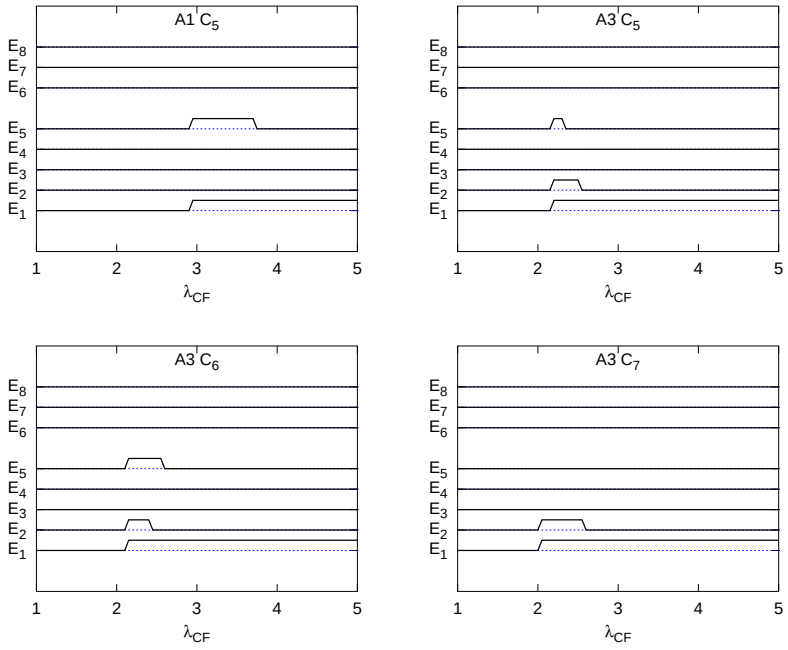

Figure 4.8: Partial gain function G_E for methods A1 C_5, A3 C_5, A3 C_6, A3 C_7.

with $\lambda_{CF,m}(\text{A3C}_5) = 2.20$ and $\lambda_{CF,m}(\text{A3C}_6) = 2.15$. To keep in mind that all detections considered occur only under the condition NF=0, which implies that all detections occur in the tsunami signal TSI, i.e. NITD=NT. In order to detect all three events, the λ_{CF} detection range is limited to $\text{DTR} \equiv [2.20, 2.30]$ for method A1C_5, while for method A1C_6 the threshold detection range is equal to $\text{DTR} \equiv [2.15, 2.40]$. The detection range DTR of method A1C_5 is shorter than that of method A1C_6: their length are respectively 0.1 and 0.25. This first difference is important: a longer DTR suggests that a tsunami can trigger a detection for a wider range of threshold values, and therefore that, once a threshold is fixed, the possibility to detect an event is bigger.

The performance of A3C_5 and A3C_6 is very similar, at least for the cases analyzed here, as they detect the same events at the same time and with the same tsunami state length. The results for the E_1 Andreanov 1996 event are the same for all detection range, with only one detection (NITD=NT=NAD=1) at a time TD=3 min, whose tsunami state covers the entire length of the tsunami signal TSI (TSP $\simeq$ 100%). The results

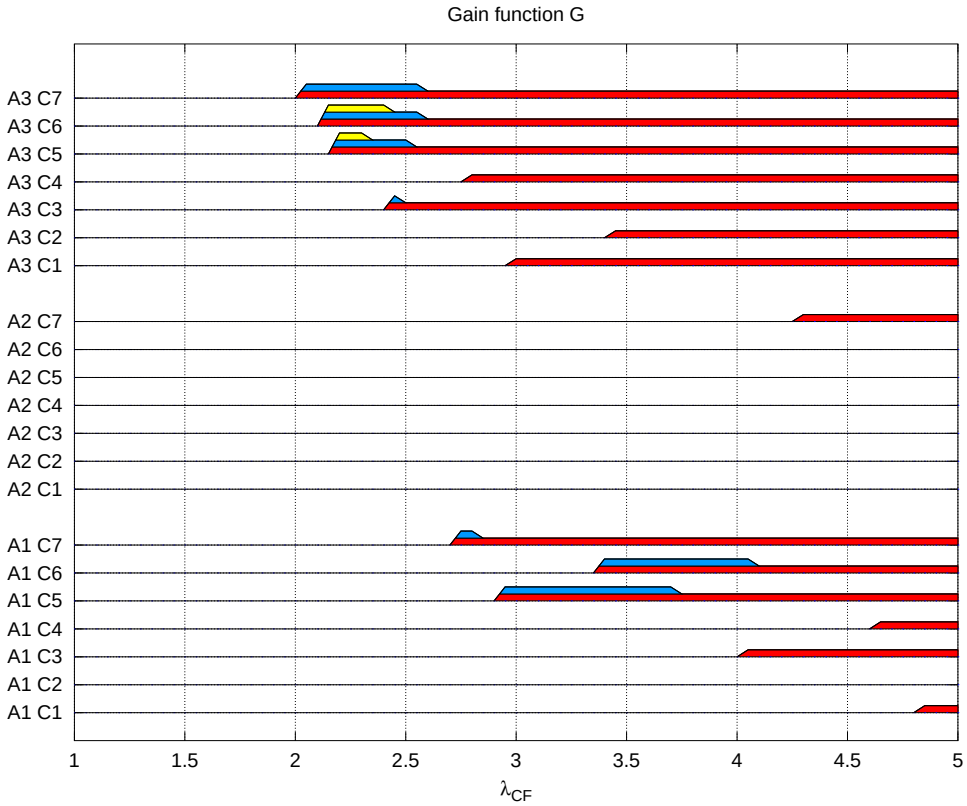

Figure 4.9: Gain function G

for the E_2 Kuril Island 2006 event are also similar. TEDA counts two fast tsunami detection (NAD=NTDI=2) for A1C$_5$, or three fast tsunami detections (NAD=NTDI=3) for A1C$_6$ at the minimum acceptable threshold $\lambda_{CF,m}$. This has a direct consequence on the tsunami state length TSP because of the contributions of additional tsunami detections: for the minimum acceptable $\lambda_{CF,m}$, the tsunami state length is about TSP = 99%, while for higher values of λ_{CF}, it drops to TSP = 65%.

The time of the fastest acceptable detection is of TD=19 min for A1C$_5$ and for lower thresholds λ_{CF} of A1C$_6$. Rising the threshold λ_{CF} the detection time increases to TD=20 min. The results for E_5 Tonga 2006 event are the same for both configurations, with TD= 12 min, two fast tsunami detections (NAD=NTDI=2) at the lowest acceptable threshold $\lambda_{CF,m}$, which contribute to the tsunami state length of the TSP=22%, while for higher values of λ_{CF}, NAD=NTDI=1 and the tsunami state length drops to TSP = 15%.

The main difference is therefore the length of the λ_{CF} detection range

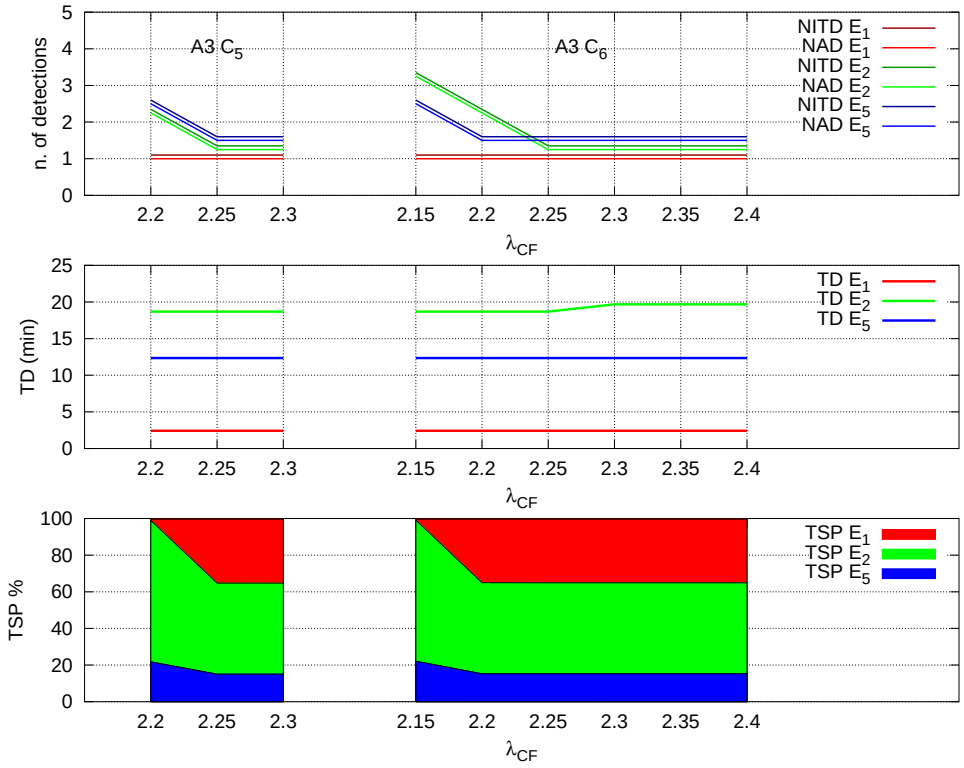

Figure 4.10: Comparison between the configurations A3C$_5$ (left) and A3C$_6$ (right). From top to bottom, the number of detections NITD and NAD (top panel), the detection time TD (middle panel) and the tsunami state length TSP (bottom panel) are shown. In the top panel, number of detections are slightly shifted to make all lines visible. The results referring to each event are distinguished by the color: red for E_1 Andreanov, green for E_2 Kuril Island and blue for E_5 Tonga.

common to the three events. For this reason, the method A3C$_6$ has been chosen as the best one, setting the threshold λ_{CF} to the minimum acceptable value, $\lambda_{CF} = \lambda_{CF,m}$. It corresponds to the following setting: method A3, i.e. $BS(t) = BS_3(t) = max\left(|IS\left(t'\right)|\right)$, $t' \in BST$; $t_S = 10$ min, $t_G = 15$ min, $t_{BS} = 60$ min and $t_T = 60$ min. The threshold λ_{IS} is equal to $\lambda_{IS} = 1$ cm/min and the threshold λ_{CF} is equal to $\lambda_{CF} = 2.15$, which is the minimum threshold to avoid false detections. With this setting, the E_1 Andreanov 1996, E_2 Kuril Island 2006 and E_5 Tonga 2006 events are detected, respectively with delay time of $TD = 3$ min, $TD = 19$ min and $TD = 12$ min from the beginning of the tsunami signal TSI. The length of the tsunami state TSP is nearly TSP=100% for E_1 Andreanov 1996, while for E_2 Kuril Island 2006 TSP=99%, and for E_5 Tonga 2006 event, TSP=22%.

The time of detection can be seen in Figure 4.11. All events are detected

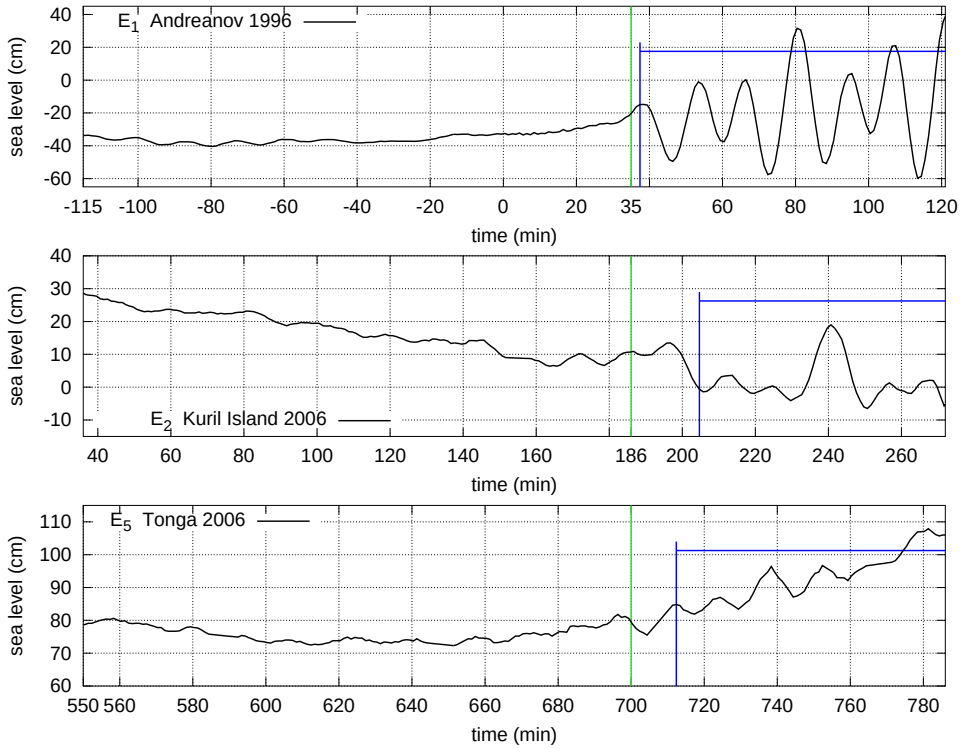

Figure 4.11: Tsunami event detection. From top to bottom, E_1 Andreanov 1996 tsunami, E_2 Kuril Island 2006 and E_5 Tonga 2006 event. The beginning of the tsunami signal interval TSI is indicated in green, while TEDA detection time is marked in blue.

at the first wave. The E_1 Andreanov 1996 event is detected on the increasing sea level of the leading wave (first positive wave). The E_2 Kuril Island 2006 is detected at the first minimum (which is the trough of the first positive wave), while the E_5 Tonga 2006 tsunami is detected at the first maximum, following the leading negative wave.

As for the events E_6 Kamchatka 1997, E_7 Vanuatu 1999 and E_8 Hokkaido 2003, they are too small to be distinguished from the background noise, and missing detection is not a serious problem. As for the other two cases, i.e. the E_3 Peru 2001 and E_4 Rat Island 2003 events, some hypotheses about the missed detection can be made. A possible reason why E_4 Rat Island 2003 event is always missed can be the presence of a big oscillation, well visible in the record right before the starting of the tsunami event (see Figure 4.5). The presence of such a big wave increases the function BS and at the same time keeps the function CF at about the same level, hence masking the following tsunami waves. The E_3 Peru 2001 event is a far field tsunami and

reaches the tide gauge with a train of waves of slowly increasing amplitude. A slowly increasing signal, typical of phenomena of atmospheric origin, is not supposed to trigger a detection in TEDA because of the simultaneous increasing of the functions IS and BS. The detection of the E_5 Tonga 2006, despite its very low amplitude, is favored by the fact that before the tsunami waves arrival, the background signal is at a very low level.

4.6 TEDA security detection

The algorithm for security detection has been tested on all records. The goal of such additional algorithm of TEDA is that long waves exceeding a certain amplitude should trigger a warning, no matter if they are due to a tsunami or to seiches, since they can constitute a danger for the harbour. The goal of the secure algorithm is to identify large amplitude long period waves in the record that, as discussed before, tend to correspond to the main typical eigenmodes of the basins complex where the tide gauge is installed.

The secure detection is based on the function $M(t)$, an estimation of the detided sea level amplitudes (see section 2.4). The main issue is to set the time constant t_{sec}, whose optimal value can be searched for by considering the average spectra of the signals in Adak. In order to set the value of t_{sec}, the secure detection was applied to all records with different t_{sec} values, ranging from 1 to 60 min ($t_{sec} = 1, 2, \ldots, 29, 30, 32, 34, \ldots, 60$ min) and the maximum and the minimum value of the function $M(t)$ have been computed. The values of t_{sec} that gives the highest of the maximum value or the lowest of the minimum value are good candidate for being selected as optimal parameters.

Figure 4.12 shows the maximum values and the module of the minimum values of $M_{t_{sec}}$ for all the events and it can be seen that such functions exhibit peaks corresponding to 7-8 min, 20-21 min, 32-34 min and so on. The periodicity of these maxima is evident. Recalling that the main typical period of Adak is of 13-14 min, the t_{sec} value that evidences best such eigenmode is expectedly half of such a period, i.e. $t_{sec} = P/2$. Therefore, for Adak, it is convenient to set $t_{sec} = 8$ min.

It is important to notice that this way of estimating the wave amplitude do not reconstruct exactly the detided sea level. Oscillations of shorter and larger periods than $P = 2 \cdot t_{sec}$ will be damped, and the waves amplitude

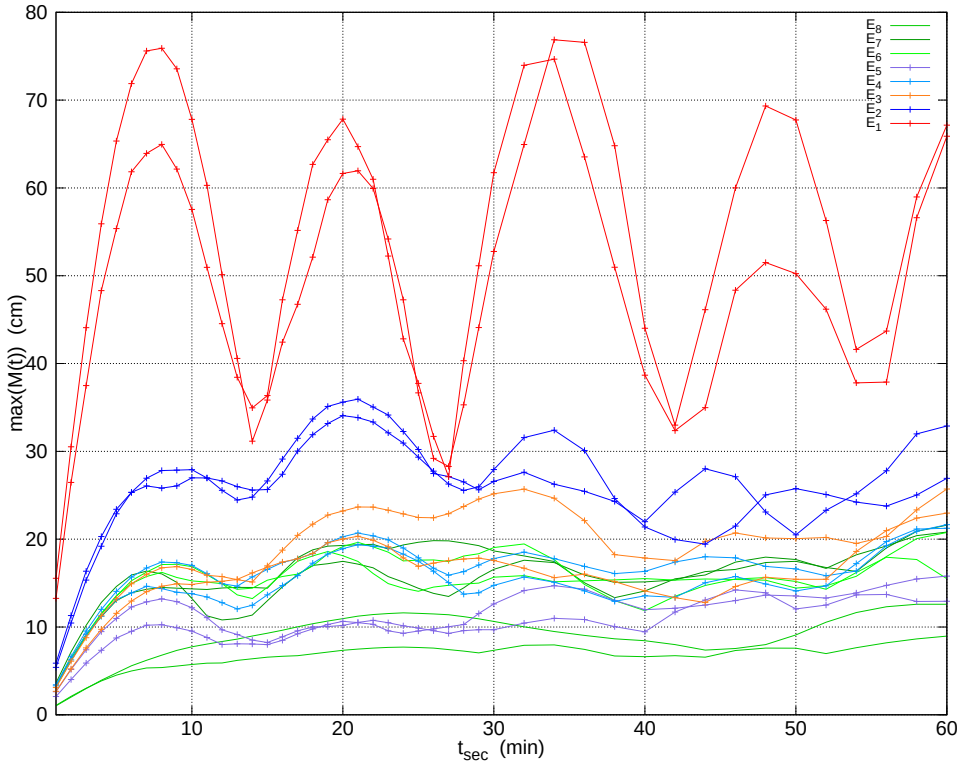

Figure 4.12: Setting t_{sec}: the maximum and minimum absolute values of $M(t)$ are shown for every record as a function of t_{sec}.

$M(t)$ varies its elevation according with t_{sec}.

The threshold λ_M for Adak can be set accordingly to the need of the harbour, by estimating the sea level height that could be dangerous, and taking into account tides and additional sea level oscillations (for example storm surges). In Figure 1.1, the function $M(t)$ is shown with the secure detection algorithm applied with a threshold $\lambda_M = 20$ cm.

With this setting, the secure detection gives a warning during the E_1 Andreanov 1996 and E_2 Kuril Island 2006 events, which are the most important ones and the same detected by TEDA tsunami detection. All other events do not trigger any warning because of their moderate amplitude (see Table 4.1). This method however does not indicate the arrival of high waves, as TEDA aims to do, before the waves have reached the maximum amplitudes, but can only indicate when the waves reach a certain amplitude. For this reason, the secure detection cannot be used as a single method for early warnings, but it should be supported by some other detection methods.

Since Sweeper Cove is a large basin, in order to have important currents

in the harbour (see equation 2.24), the wave height should be quite elevated. For example, setting a maximum current velocity of 1 m/s, the corresponding wave height is $H \simeq 3.5$ m, which implies $\lambda_M = 1.75$ m. Lower amplitude waves might carry some damage; the threshold λ_M should be set accordingly to the harbour needs.

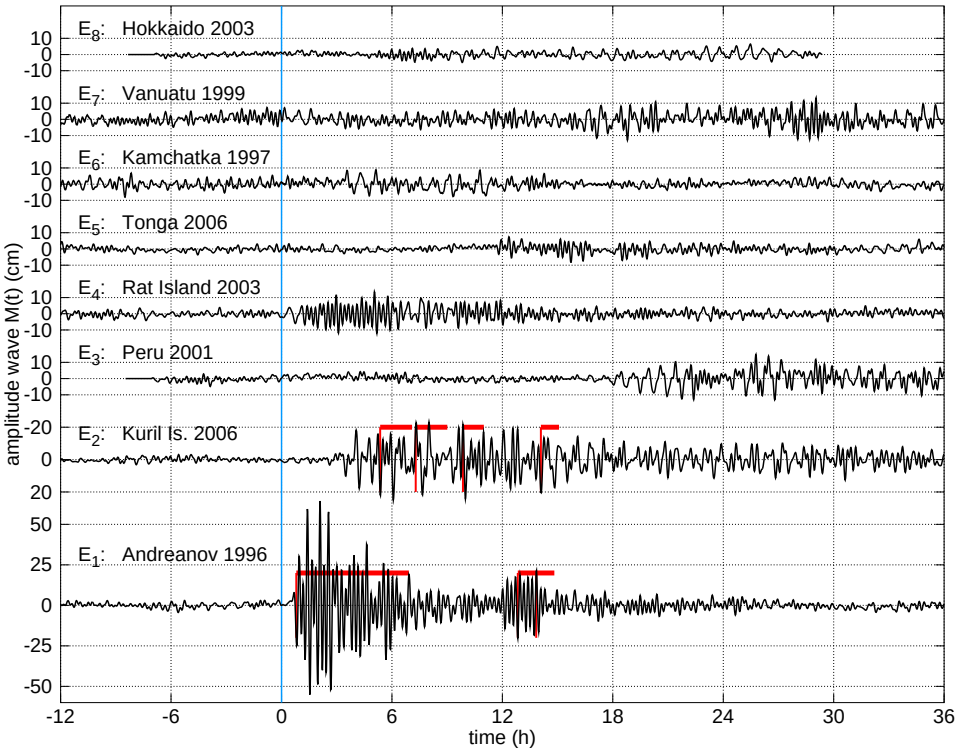

Figure 4.13: Function $M(t)$ for all the events. The blue vertical line indicates the beginning of the tsunami signal, i.e. the tsunami arrival time. Warnings for wave amplitudes bigger than $\lambda_M = 20$ cm are indicated. The security detection algorithm signals large amplitude waves for the E_1 Andreanov 1996 and for the E_2 Kuril island 2006 events.

Chapter 5

Application to DART buoys

5.1 DART: BPR offshore buoys

DART (Deep-ocean Assessment and Reporting of Tsunamis) is a real-time tsunami monitoring station, developed by PMEL/NOAA starting from 1986 and in operation in the Pacific Ocean. The DART system consists in a BPR that transmits sea level data in real time. It plays a key role in Pacific Tsunami Warning System, which issues first warnings on the base of seismic data alone, and updates them with further details or cancel them using DART data. This technology has been developed to measure tsunami far away from the coast, in order to have time to give warnings. Offshore sea level measurements have the additional advantage to be able to see the tsunami signal unmasked and not influenced by coastal inlets and basins that can modify the tsunami signal, as in coastal tide gauges. DART stations are positioned at strategic locations along the Pacific plate margins, in order to measure a tsunami wave right after its generation. At the same time, this array allows to monitor tsunami waves approaching the Pacific coasts from far away. Since the first generation DART I, DART buoys were provided by an automatic detection algorithm, by Mofjeld ("Tsunami detection algorithm"). This algorithm predicts the tidal oscillations with a polynomial of degree 3 and is based on the Newton's formula for forward extrapolation. The residuals are checked over a threshold of 1 to 3 cm. When the wave amplitude due to the residuals passes the threshold, DART gives a warning and starts a tsunami mode, which consists in transmitting data in real time with 15 s sampling interval for the first few minutes and later with 60 s sampling interval. When the tsunami mode is off, DART buoys transmit 15

min data every hour. Data are transmitted to the Tsunami Warning Center, which processes the information and is responsible to give further warnings or cancellations, with a more precise estimation of the hazard as data come available. The tsunami mode of sending data at higher sampling rate can be also triggered manually from the Tsunami Warning Center. This assures the measurement of tsunamis with amplitude below the threshold of the automatic tsunami mode.

Some event records of DART buoys have been analyzed here. A big group of these records comes from buoys located off Alaska, off the USA coasts of Washington and one off California, and a couple from the middle of the Pacific Ocean, one at Hawaii, near Hilo.

Tsunami detection for sea level data from open sea is complicated. The calibration made for the coastal tide gauge of Adak Island, based on the condition of no false detections, is impracticable, because of the different characteristics of sea level in the open sea, where usually tsunami waves have very small amplitude. Another strategy has been therefore adopted: the algorithm is activated only in a particular window in order to check if a tsunami wave is present or not; outside this window, no detection is indicated even if there are the conditions for a detection.

5.2 Event records and strategy of detection

The test for the DART has been carried out with the use of records of different buoys of six real events, Andreanov 1996, Kamchatka 1997, Vanuatu 1999, Peru 2001, Hokkaido 2003, Rat Island 2003 events, numbered and denoted as in the previous chapter, with E_n as in Table 4.1. The sampling interval of the data is 15 s. The 15 s data become available only after a buoy is recovered from the bottom of the ocean. All records have a length from 12 to 17 days. Except the DART D125, deployed in the South Pacific, the HI76 near Hawaii and the D171 in the North Pacific Ocean, most of the DART here considered are deployed either off the Alaskan coast (namely the buoys D157, D165 and SN17 and those denoted with AK), or off the coast of the Washington and California States, (namely the DART denoted with WC, NEMO, D128 and D123). In Figure 5.1 the sources of the events are shown together with the buoy locations. There are two different events, i.e. the E_4 Rat Island 2003 and E_8 Hokkaido 2003, that were recorded by the

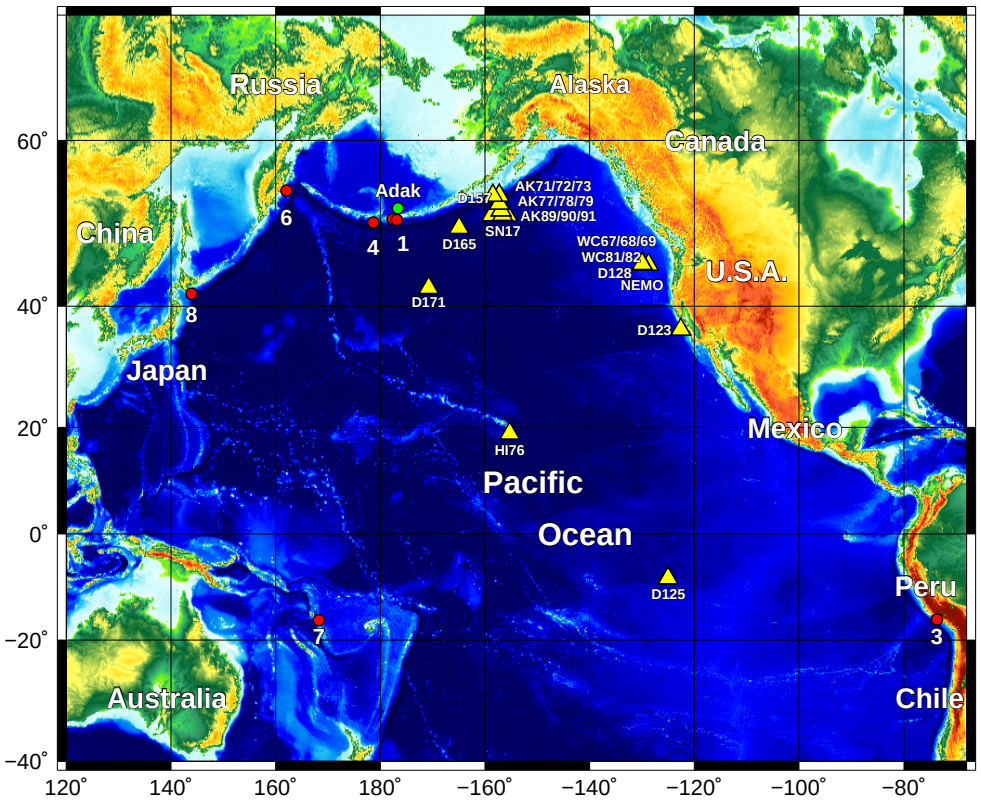

Figure 5.1: Map of the Pacific Ocean with the DART stations location (yellow triangles) and the epicenters of the tsunamigenic earthquakes (red circles). The tsunami events are the following: E_1 Andreanov 1996, E_3 Peru 2001, E_4 Rat Island 2003, E_6 Kamchatka 1997, E_7 Vanuatu 1999, E_8 Hokkaido 2003.

same buoys, i.e. the DART D125, D171 and D157.

The main signal of sea level in the open sea is the tide, that can be of mainly semi-diurnal, mainly diurnal or mixed main components and can reach a maximum height of 2 m. In the records analyzed here, no major tsunami event is present, and at the same time, some events are recorded very far from the source. In Figures 5.3, 5.4, 5.5, 5.6, 5.7 all detided records are shown. In about half of the records, it is difficult to distinguish the tsunami signal from the background oscillations. In the other half, only the first tsunami wave is easily recognizable, while, right after, the tsunami oscillations damp to almost the background level, making it impossible to

recognize the whole tsunami signal. With the exception of the HI76 buoy (see Figure 5.4), which is characterized by waves of more than 1 cm, all other records are characterized by a very low background signal, of amplitudes smaller than 0.5 cm. Since the record from the HI76 buoy is quite noisy, it has not been used in the calibration of TEDA. Only the results of the analysis of the record are presented here.

For the records where the first tsunami wave is recognizable, the maximum and minimum peak of the first wave is given in the Table 5.1, together with the coordinates of the buoy location, depth and corresponding event. The maximum wave amplitude measured by the DART buoys in the selected data set is of 2.5 cm and regards the buoy D171 recording the E_8 Hokkaido 2003 event, while for all other event the first wave amplitude hardly reaches 1 cm. These amplitudes are quite small: waves of similar amplitudes and shape are present in the records even when there is no tsunami signal, and emerge clearly from very low background level. A very evident example is a wave in the record AK90 of the E_7 Vanuatu 1999 event, nine hours after the expected arrival time, in Figure 5.3. This wave has an amplitude of about 1 cm, similar to the first tsunami wave amplitude of many records, and rises from a much lower background, of maximum amplitude of about 0.3 cm. In addition, this wave is not measured by the DART AK89 and AK91, located nearby; this gives a further proof that the wave considered is not a tsunami wave. This wave can easily trigger a detection in the tsunami detection of TEDA, because of the sudden change from the previous background signal. Similar waves are not rare and make the tsunami detection problematic. Because of the limited magnitude of tsunami waves in the record, a careful analysis of the sea level records is needed.

In two records, of DART WC81 and WC82, it is visible the passage of an atmospheric disturbance, which increases the level of the background to a maximum amplitude of the waves of about 2 cm, differing from the calm sea background maximum wave amplitude that is of about 1 cm (see Figure 5.2). In a few records, the seismic signal is present with amplitudes far above the real sea level signal. The seismic signal is due to the vertical acceleration that seismic waves induce in the BRP, which is recorded as pressure change, and converted in water wave amplitude. The seismic signal is very likely to trigger a detection, due to its very sudden large amplitudes. For this reason, it is impossible to distinguish a tsunami wave during the

seismic signal. TEDA is therefore inactivated when the TEDA seismic waves detection identifies a seismic signal.

Another issue that creates problems is the fact that tides and tsunamis may have similar sea level slope. Indeed, lets consider the functions IS_T, TF and IS, which represent respectively the average sea level slope, the tidal sea level slope and the detided sea level slope. The tidal slope and the average sea level slope, considering a tidal range of 2 m in 24 h, can reach values of 0.15 cm/min, much higher than the detided sea level slope, and comparable of those of a tsunami wave (for example, with a tsunami wave of 2 cm and a period of 30 min, the maximum IS would be of the order of $2/15 = 0.13$ cm/min). For this reason, the detiding of the function IS_T has to be very accurate in order to properly report the variations of the detided sea level slope. TEDA applies a second order polynomial to fit the tide and to obtain the detided signal for offshore buoys, which probably has to be improved. The consequence of the above two points, i.e. the presence of waves with shape similar to tsunamis and of insufficient detiding, is that it is unpractical to use the criterion of no false detection to calibrate TEDA. Indeed, imposing such criterion would imply that the thresholds of TEDA would be so large that only very large amplitude tsunami will be identified.

The assumption made here is that TEDA cannot be applied alone, independently from any other information, but must be applied on a limited time window where the tsunami is expected to come, basing on some additional source of information: typically, this information comes from a seismic network that has located a potential tsunamigenic earthquake and from numerical models, which can compute the expected arrival time of the tsunami at the buoy. It is supposed that the expected tsunami arrival time ETA is known in very short time, in order to identify a window where the arrival of tsunami waves has to be searched, after the earthquake. The strategy is to narrow the window where TEDA can trigger a detection to the tsunami window $TsuW$, defined here like for the coastal tide gauges as a 3 h window starting from 30 min before the expected tsunami arrival time. The tsunami arrival time has been calculated by means of the code WebSIFT, with the aid of synthetic marigram in the location of the buoys, for all records (Gica et al., 2008).

With this strategy, only the records within the selected window is analyzed and what happens outside has no influence for the calibration of

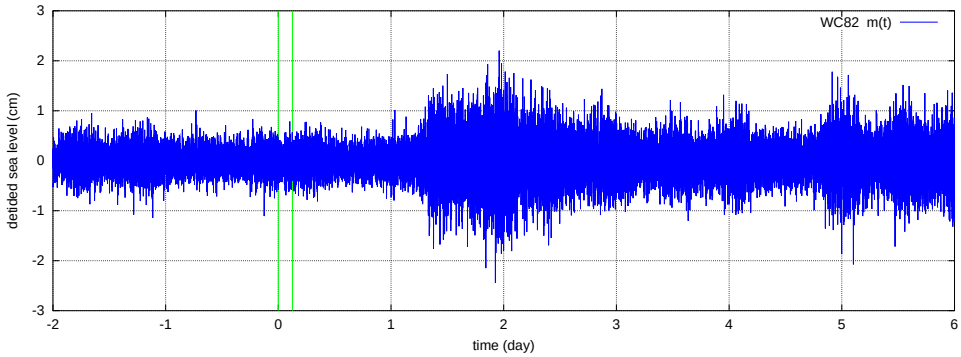

Figure 5.2: Detided sea level record of DART WC82 for the event E_6 Kamchatka 1997. Notice an atmospheric disturbance that increases the level of the background waves. The green vertical lines indicate the tsunami window $TsuW$ where the arrival of the tsunami waves is expected.

TEDA. The method adopted here is therefore very different from the method applied for Adak Island, since all detections occurring outside $TsuW$ are not considered. In case of records with the first tsunami wave identified, the window to count for acceptable detections NAD is narrowed to the first wave. The method that detects more events during the first wave is to prefer to methods and configurations that trigger detections before or after, when the sea level is back to the background level.

The way of evaluating TEDA is the following: TEDA detections are active only during the $TsuW$ window, in absence of a seismic signal. In case of first tsunami wave evident in the record, an additional window, containing the first tsunami wave, is defined. Detections falling in the first tsunami wave are counted in the NAD indicator, i.e. the acceptable tsunami detections. Detections falling outside are counted in the NF indicator, since the goal is to have detections only at the tsunami wave and not when the tsunami oscillations are similar to the background. In case of not identifiable tsunami waves, the detections that fall inside $TsuW$ are counted in the NITD indicator, i.e. the number of detections of the tsunami. The number of events detected at the first wave is counted for every method and configuration, and this is a first criterion to select the best method, followed by the comparison of the tsunami delay time TD.

Table 5.1: DART buoys and tsunami events analyzed. The coordinated and depth of the BPR deployment is indicated. A_1 and A_2 are the positive and negative peak values of the first wave. An asterisk indicates that the first tsunami wave occurs during the seismic signal.

Long	Lat	depth	DART	event	A_1 (cm)	A_2 (cm)
52.0181	-155.7235	4575	AK73	E_1 Andreanov 1996	0.8*	-0.5*
53.423	-157.278	4540	AK71	E_1 Andreanov 1996	0.6*	-0.4*
52.039	-158.751	4636	AK72	E_1 Andreanov 1996	0.9*	-0.6*
45.962	-129.967	1543	WC67	E_1 Andreanov 1996	0.9	-0.6
45.9567	-130	1550	WC68	E_1 Andreanov 1996	0.9	-0.5
45.9333	-129.9805	1535	WC69	E_1 Andreanov 1996	1.0	-0.5
45.9306	-129.9832	1520	WC82	E_6 Kamchatka 1997	-	-
54.2897	-157.2775	1704	AK77	E_6 Kamchatka 1997	-	-
53.4248	-157.2775	4608	AK78	E_6 Kamchatka 1997	-	-
52.0385	-158.7522	4683	AK79	E_6 Kamchatka 1997	-	-
18.924	-155.2596	956	HI76	E_6 Kamchatka 1997	-	-
45.957	-130.0006	1520	WC81	E_6 Kamchatka 1997	-	-
52.0347	-158.7508	4757	AK89	E_7 Vanuatu 1999	-	-
54.2907	-158.5498	1712	AK90	E_7 Vanuatu 1999	-	-
53.4253	-157.276	4646	AK91	E_7 Vanuatu 1999	-	-
36.4767	-122.6093	3190	D123	E_7 Vanuatu 1999	0.6	-0.4
50.531	-164.9415	4918	D165	E_7 Vanuatu 1999	-	-
52.0865	-156.6615	4697	SN17	E_7 Vanuatu 1999	-	-
45.861	-128.772		D128	E_3 Peru 2001	0.5	-0.3
45.861	-130		NEMO	E_3 Peru 2001	0.6	-0.5
52.6503	-156.9405	4484	D157	E_4 Rat Island 2003	0.4	-0.4
42.6368	-170.7977	5550	D171	E_4 Rat Island 2003	0.8	-0.5
-8.487	-125.0178		D125	E_4 Rat Island 2003	0.8	-1.0
-8.487	-125.0178		D125	E_8 Hokkaido 2003	0.5	-0.6
52.6503	-156.9405	4484	D157	E_8 Hokkaido 2003	-*	-*
42.6368	-170.7977	5550	D171	E_8 Hokkaido 2003	2.5 *	-2.4*

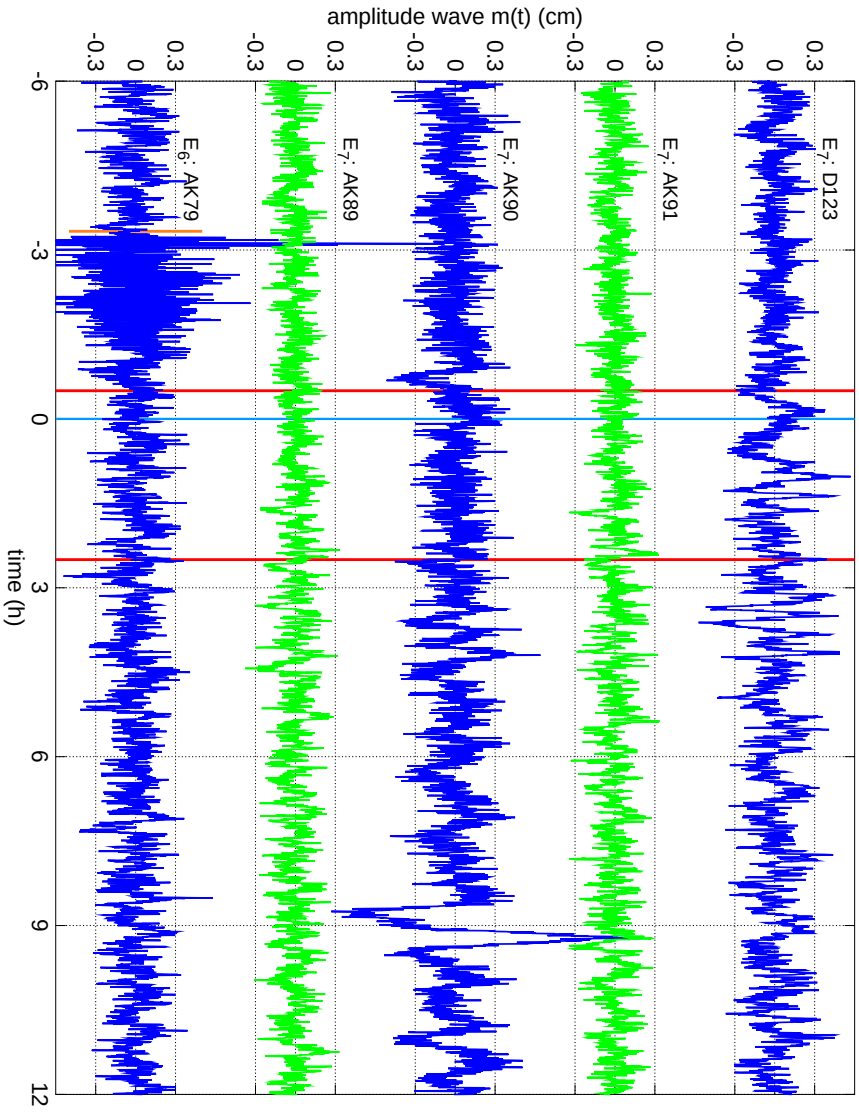

Figure 5.3: Detided event records of DART D123, AK91, AK90, AK89 for the E_7 Vanuatu 1999 event and of DART AK79 for E_6 Kamchatka 1997. The red vertical lines delimit the window $TsuW$ where TEDA detection is activated, while the blue vertical line is in correspondence of the expected arrival time. The orange vertical line for each record indicate the time of the earthquake event. Notice the wave at 9 h in the record of AK90. Notice further that the seismic signal in the record AK79 has an amplitude corresponding to a wave of about 2 cm.

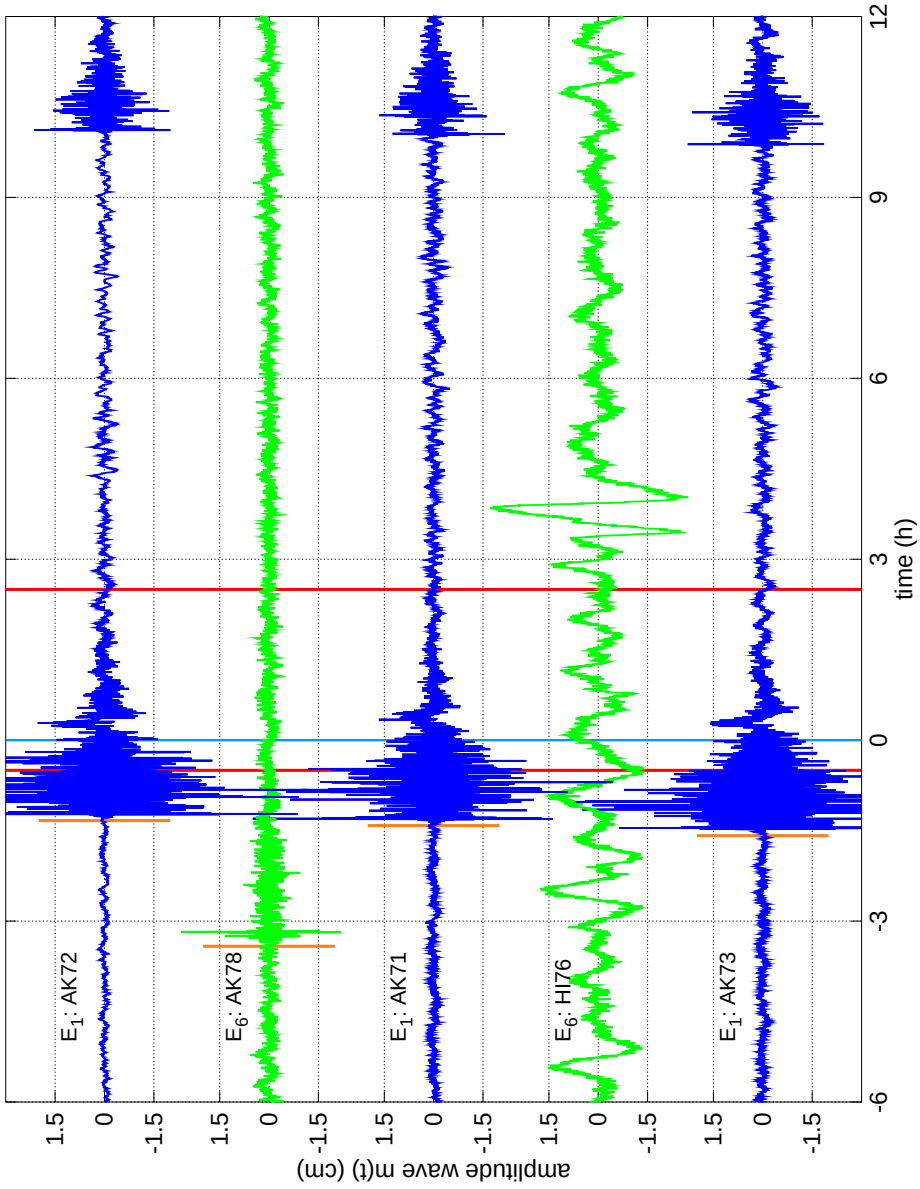

Figure 5.4: Detided event records of DART AK72, AK71, AK73 for E_1 Andreanov 1996 and of AK78 and HI76 for E_6 Kamchatka 1997 event. Notice for the E_1 records, the seismic signal of the two Andreanov earthquakes and the first tsunami wave towards the end of seismic signal. Notice further the peculiarity of the HI76 record.

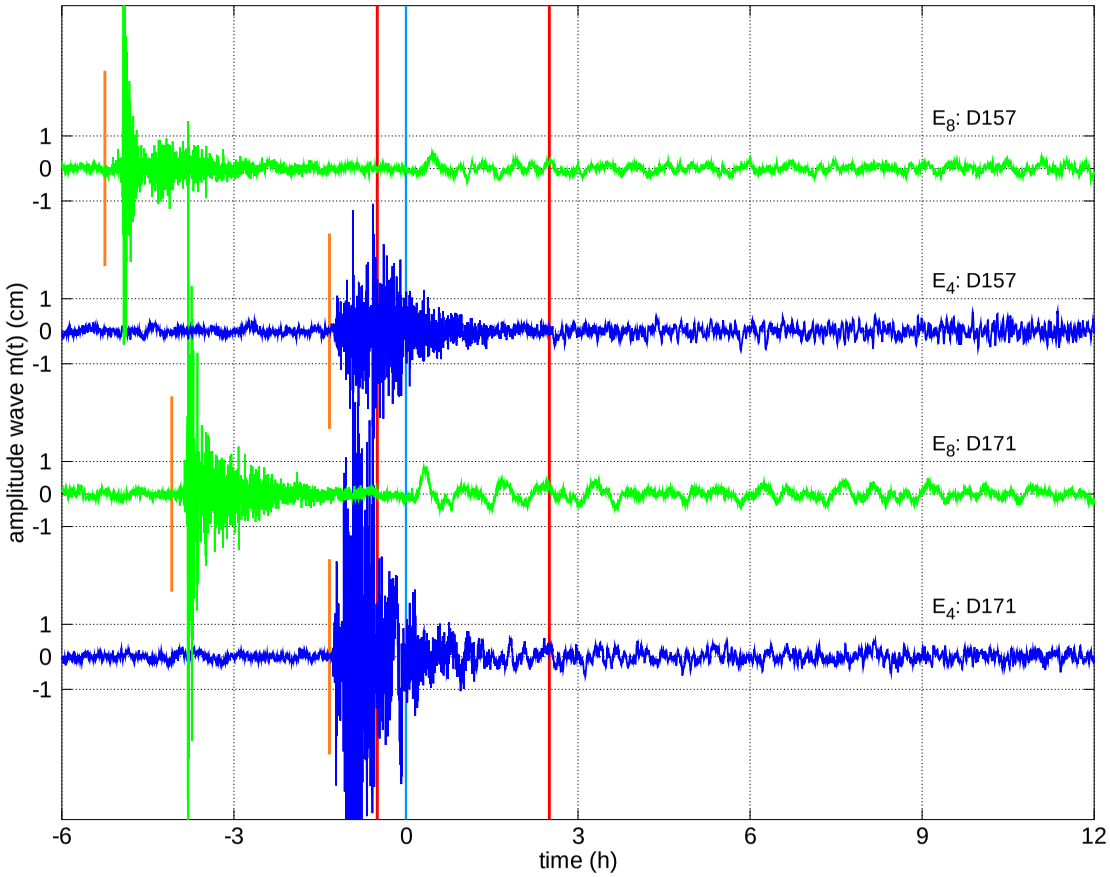

Figure 5.5: Detided event records of DART D154 and D171 for E_4 Rat Island 2003 and E_6 Kamchatka 1997 events. Notice that in the E_4 D171 record, the first tsunami wave is embedded in the tsunami signal. Notice further that the expected arrival time ETA is posticipated respect to the arrival of the first tsunami wave, therefore the anticipation of 30 min of the tsunami window $TsuW$ is considered in order to avoid few precision in ETA estimations from simulations.

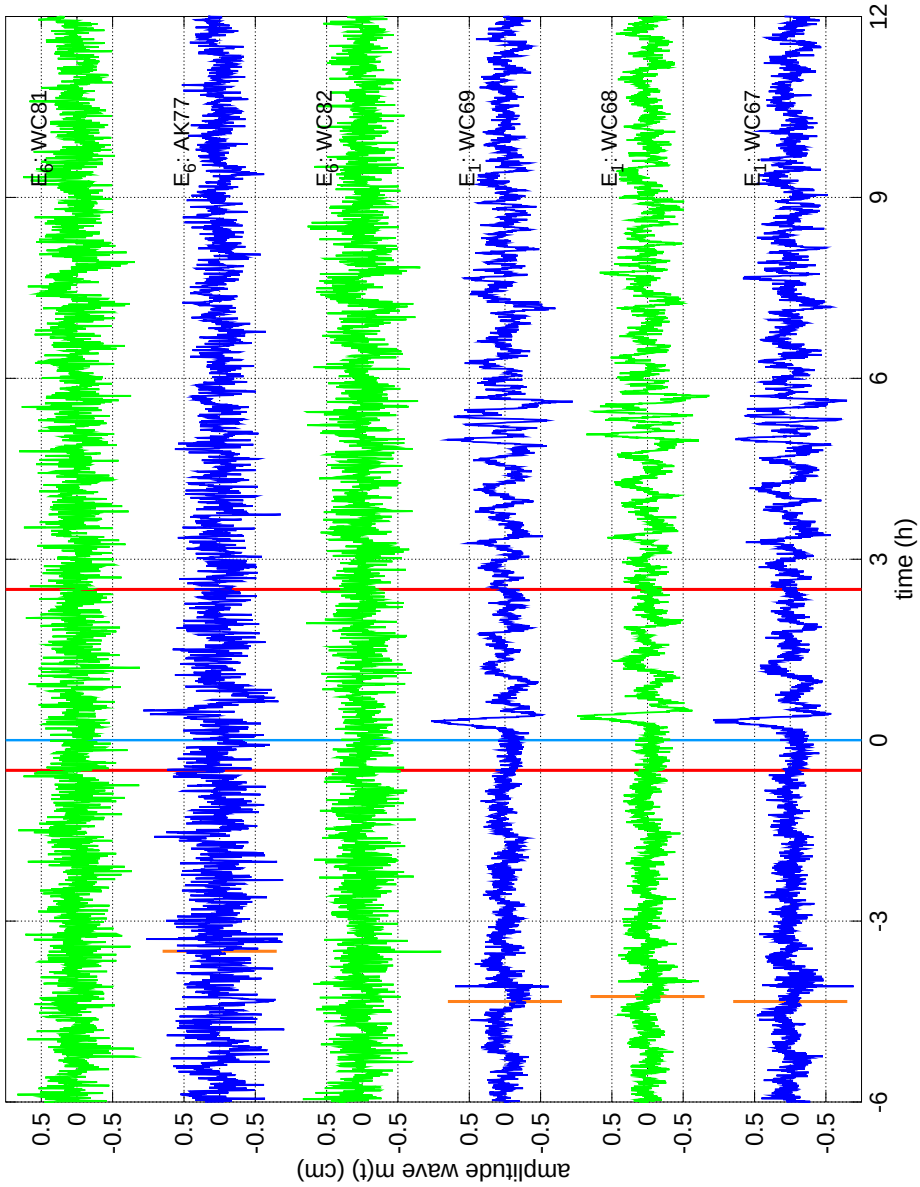

Figure 5.6: Detided event records of DART WC81, AK77, WC82 for E_6 Kamchatka 1997 and of DART WC69, WC68, WC67 for E_1 Andreanov 1996 event.

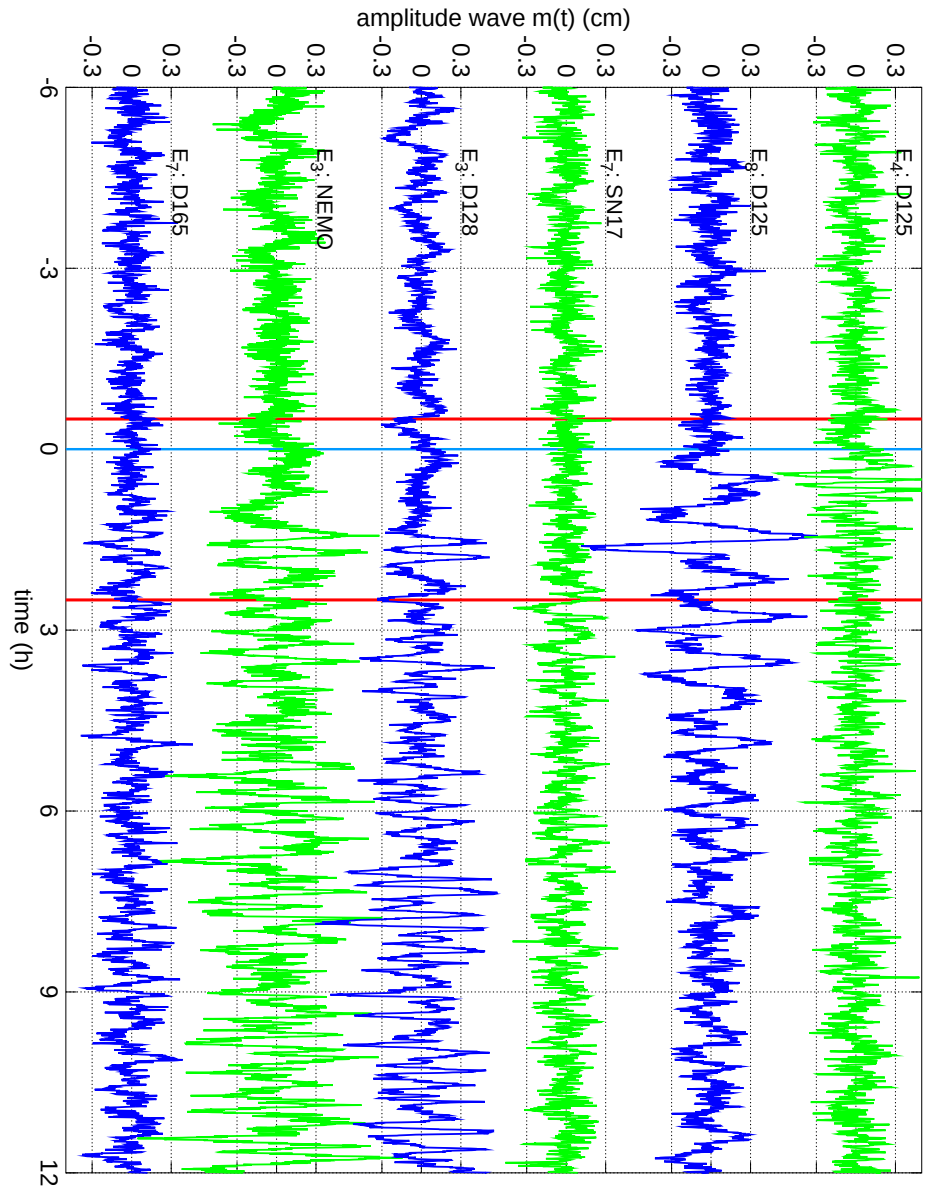

Figure 5.7: Detided event records of DART D175, SN17 for E_7 Vanuatu 1999, of DART D125 for E_4 Rat Island 2003 and E_8 Hokkaido 2003, of DART D128 and NEMO for E_3 Peru 2001 event.

5.3 The spectral analysis

The records have been studied with the spectral analysis, using FFT on 10.5 h mobile windows, with relative shifting of 30 min, on the detided records. The procedure is the same as for the Adak Island records, i.e. the spectra have been averaged in order to decrease the noise level and the spectra of the tsunami are computed when the mobile window overlap with the tsunami signal; in this case about ten windows centered over the tsunami signal $TsuW$ have been considered. Particular attention has been given to avoid the seismic signal, both in the computation of the background spectrum and in the computation of the seismic spectrum.

In general, the shape of the spectrum of all DART records is very similar: it is characterized by a very low intensity in the high frequency range, corresponding to periods shorter than about 1 min and by a zone with the same intensity in the long wave range, from about 1 min to about 10 min periods. For longer periods, the spectrum intensity increases till a maximum of 1 to 2 h. In the long wave spectrum, from periods of about 1 min to 10 min, the spectrum is characterized by almost white noise. The level of the noise varies, but there are indeed DART records that share the same noise level and some that share exactly the same spectrum. In Figure 5.8, the spectrum of the background signal of all DART buoys is shown. The spectra have been grouped in order to make it evident that some DART buoys share the same spectrum. One spectrum of every group is then plotted in Figure 5.9 to better compare them. With the exception of HI76 spectrum, all spectra differ mainly in the level of the white longwave noise and in its limits. In general, the longwave noise is restricted to periods from about 1-2 min to periods of about 10 min. For example, looking at the top panel of Figure 5.9, referring to buoys located in the North of Pacific Ocean offshore Alaska, the limits of the longwave noise are from 1-2 min to 10 min for all spectra except those of DART AK71, AK72, AK73, from 2 to 5 min. All spectra share almost the same level of longwave noise, with the exception of the DART WC81 and WC82, whose level is an order of magnitude bigger and is comparable to that of the spectrum peak of 1-2 h period, and of the DART AK71, AK72 and AK73, with longwave noise of one order of magnitude lower. The high level of the longwave noise in the DART WC81 and WC82 is caused by an atmospheric perturbation recorded in the sea level series, shown in Figure 5.2.

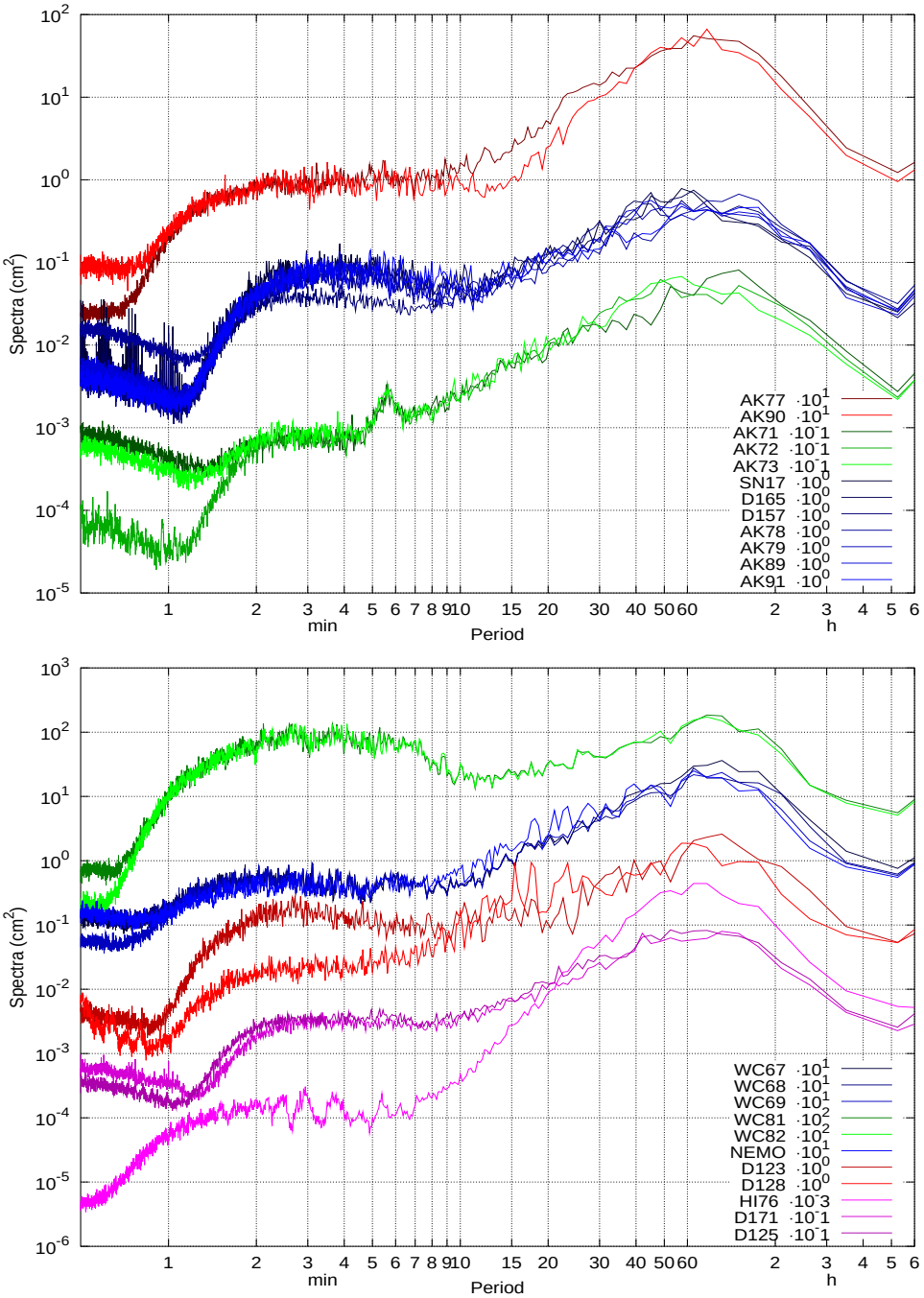

Figure 5.8: Spectral analysis of the background signal. Spectra have been grouped in order to stress the similarity of the spectra. Spectra are shifted vertically to make the figure more clear. In the top panel, spectra relative to DART buoys located in the Pacific Ocean offshore Alaska are shown, while in the bottom figure all remaining spectra are shown. The peaks in the high frequency range of buoy D157 (top panel in blue) are due to instrumental noise. Notice in the bottom panel the intensity of the DART HI76, which is much more elevated than those of all the other buoys, by about two order of magnitude.

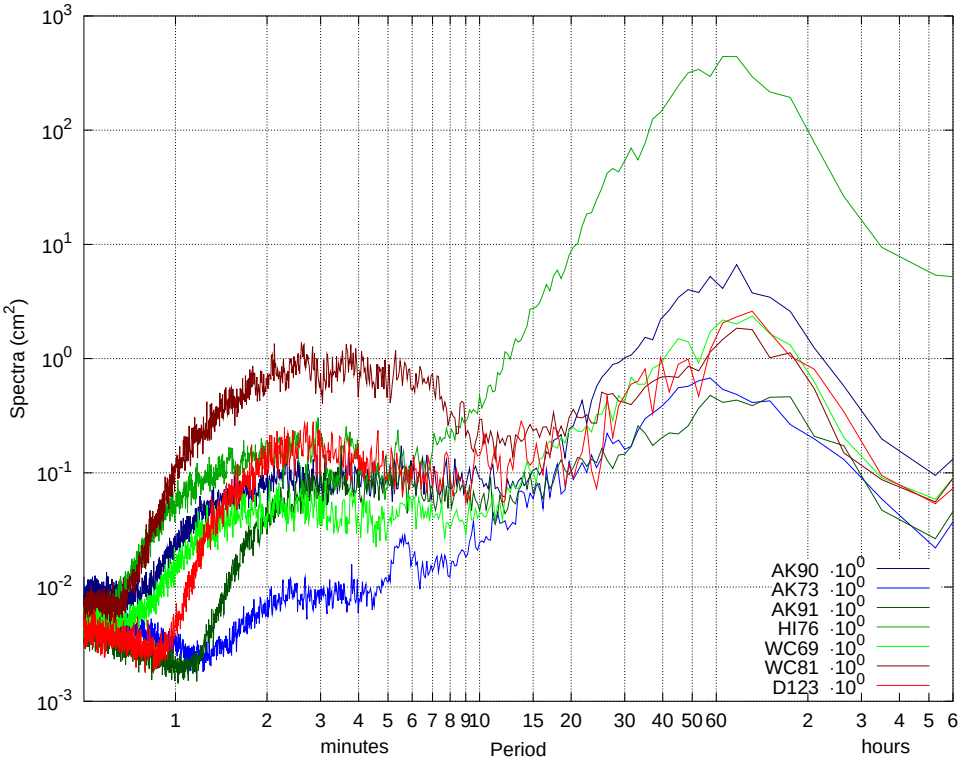

Figure 5.9: Spectral analysis of the background signal.

The DART AK71, AK72 and AK73 present an additional peak around 5-6 min. The HI76 spectrum has the typical shape of all other DART buoys with a maximum at about 1-2 h, a longwave noise and high frequency waves filtered, but it differs as regards the intensity of the peak of the 1-2 h min period, which is by two orders of magnitude bigger than those of all the other buoys.

Since tsunamis in the open ocean are characterized by long periods, usually longer than 10 min, the tsunami signal is visible in the range 10-30 min. In the record analyzed, not all tsunami spectra are different from the background spectrum. Three examples of tsunami spectrum and seismic spectrum are shown in Figures 5.10 and 5.11. In Figure 5.10 the tsunami spectrum for the DART WC67 is different from the typical shape of the background spectrum, while for the DART WC82 it is coincident, even if more noisy. In this case, the tsunami signal cannot be separated from the background signal and this is equivalent to claim that the there is no tsunami. The tsunami identification in such cases is therefore impossible, since any

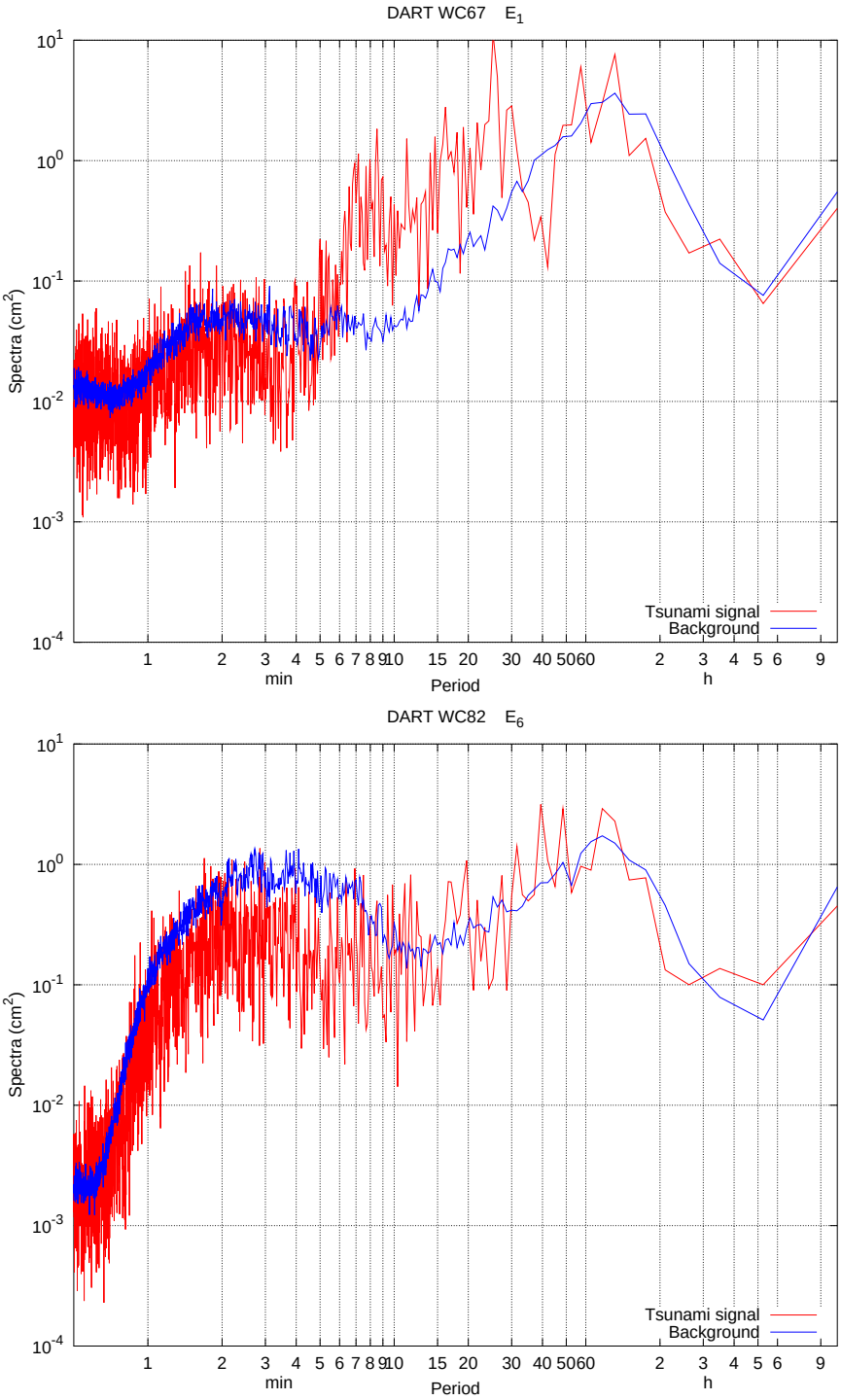

Figure 5.10: Examples of spectra of tsunami signal and seismic signals for DART WC67 and WC82.

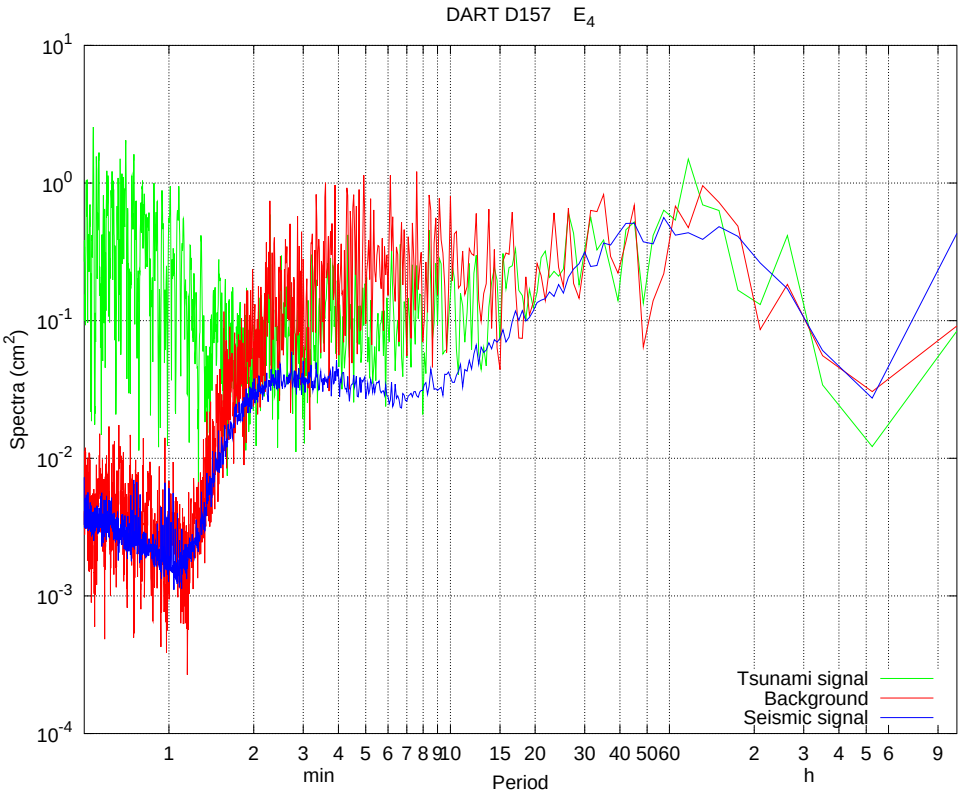

Figure 5.11: Examples of spectra of tsunami signal and seismic signals for DART D171.

algorithm would detect the tsunami and also the background noise. The same reasoning is valid for all other cases when the tsunami spectrum is not different from the background spectrum, i.e. for DART AK77, AK78, AK79, AK89, AK90, AK91, WC81, HI76, D171 and D125 for the E_8 Hokkaido 2003 record, D157 for both records and for WC82. The records that present a tsunami spectrum not different from the background, do not have a clear signal of the first tsunami wave, except for few cases, such as the DART D125, D157 and D171 for the E_4 Rat Island 2003 event, for which a first tsunami wave is recognizable but the tsunami spectrum does not differ from the background.

The remaining events are characterized by a tsunami spectrum different from the background spectrum: the main differences are in the range from periods of 6-7 min to the 1-2 h peak, while for periods smaller than 6-7 min the tsunami spectrum is coincident with the background spectrum. An example is given in Figure 5.10 for DART WC67. In this example, additional peaks at about 7-9 min, at 15 min, and at 25-30 min are evident and they

mark in addition the peak relative to the 1-2 h period. Not all records with tsunami spectrum different from the background spectrum have such a well defined features, but in general their shape is different, both in the tsunami range periods, from about 5 to 30 min periods, and in the longwave range.

An example of spectrum of the seismic signal can be seen in Figure 5.11 for DART D157, concerning the E_8 Hokkaido 2003 event. The tsunami spectrum in this case has the only consequence of rising the longwave noise, so that the spectrum looks like white noise from the whole range considered, from 1 min to 2 h. The spectrum of the seismic signal instead expectedly increases the level of high frequency waves, usually not present in the record.

5.4 Preliminary analysis and test results

A preliminary analysis has been performed, in order to narrow the choice of parameters used to test TEDA. The possible configuration are listed in Table 5.2, and are $t_T = 120, 180$ min, $t_{BS} = 60$ min, $t_S = 6, 8, 10$ min with $t_G = 10, 15$ min and $t_S = 12$ min with $t_G = 15$ min. Each parameters configuration has been denoted with C_i, with i in the range $1-14$. The proof that false detections are impossible to avoid with the method here described comes from the analysis of each record with all three methods A1, A2 and A3 and all parameter combinations with the following threshold values: $\lambda_{IS} = 0, 05, 0.75, 0.1, 0.12$, $\lambda_{CF} = 1.0, 1.1, 1.2, \ldots, 10$ and $\lambda_\sigma = 0.2, 0.25, 1$.

The same temporal combinations have been used to test TEDA performance without the condition of no false detections, evaluating in a very different way the acceptable and not acceptable detections: detections are accepted only in the first wave signal, when evident, while detection falling in no clear tsunami signal are to avoid. This strategy has been used with the same temporal combinations and with the following values of thresholds: $\lambda_{IS} = 0.1$, $\lambda_{CF} = 1.0, 2.0, 3.0$ and $\lambda_\sigma = 1$.

The number of events detected for every method and configuration has been counted. The total number of events detected, represented by the gain function G, is not a significative indicator: the more sensitive method would be selected, without any proof of the correspondence of detections with the tsunami signal. For this reason, a narrower window corresponding to the first tsunami wave has been defined for such DART records that present a recognizable signal, i.e. for DART AK73, AK71, AK72, WC67, WC68,

WC69, D123, D128, NEMO, D157 for the E_4 Rat Island 2003 event and D171 and D125 for both event records.

For this reason, the number of events detected in the first tsunami wave is used as a much more significant indicator. In order to choose the best method, the indicators to maximize are the number of events detected in the first tsunami wave window, together with the maximum number of events detected. The method that detects the maximum number of events in the first tsunami wave is to be preferred to the other methods. These are then compared with the detection delay time TD.

The methods that detect most events at the first tsunami wave are $A2C_3$ and $A2C_6$, with $\lambda_{CF} = 2$. They detect in total eleven tsunami event records. Events detections are shown in Figure 5.12. Method $A2C_3$ detects records of buoys AK71, WC67, WC68 for the E_1 Andreanov 1996 event, WC82 for the E_6 Kamchatka 1997, D123 for the E_7 Vanuatu 1999, D128 and NEMO for the E_3 Peru 2001, D157, D171 and D125 for the E_8 Hokkaido 2003, and D125 for the E_4 Rat Island 2003 event. Method $A2C_6$ detects records of buoys AK71, AK72, WC68, WC69 for the E_1 Andreanov 1996 event, AK77 for the E_6 Kamchatka 1997, D123 for the E_7 Vanuatu 1999, D128 and NEMO for the E_3 Peru 2001, D171 and D125 for the E_8 Hokkaido 2003 and D125 for the E_4 Rat Island 2003 event.

Table 5.2: TEDA configuration: a configuration C_n consists of a specific combination of temporal parameters and thresholds that are used to test TEDA.

C_n	t_S $[min]$	t_T $[min]$	t_G $[min]$	t_BS $[min]$
C_1	6	120	10	60
C_2	6	120	15	60
C_3	8	120	10	60
C_4	8	120	15	60
C_5	10	120	10	60
C_6	10	120	15	60
C_7	12	120	15	60
C_8	6	180	10	60
C_9	6	180	15	60
C_10	8	180	10	60
C_11	8	180	15	60
C_12	10	180	10	60
C_13	10	180	15	60
C_14	12	180	15	60
λ_{IS}		1 $[cm/min]$		
λ_{CF}		$1.00, 1.05, 1.10, \ldots, 5.00$		

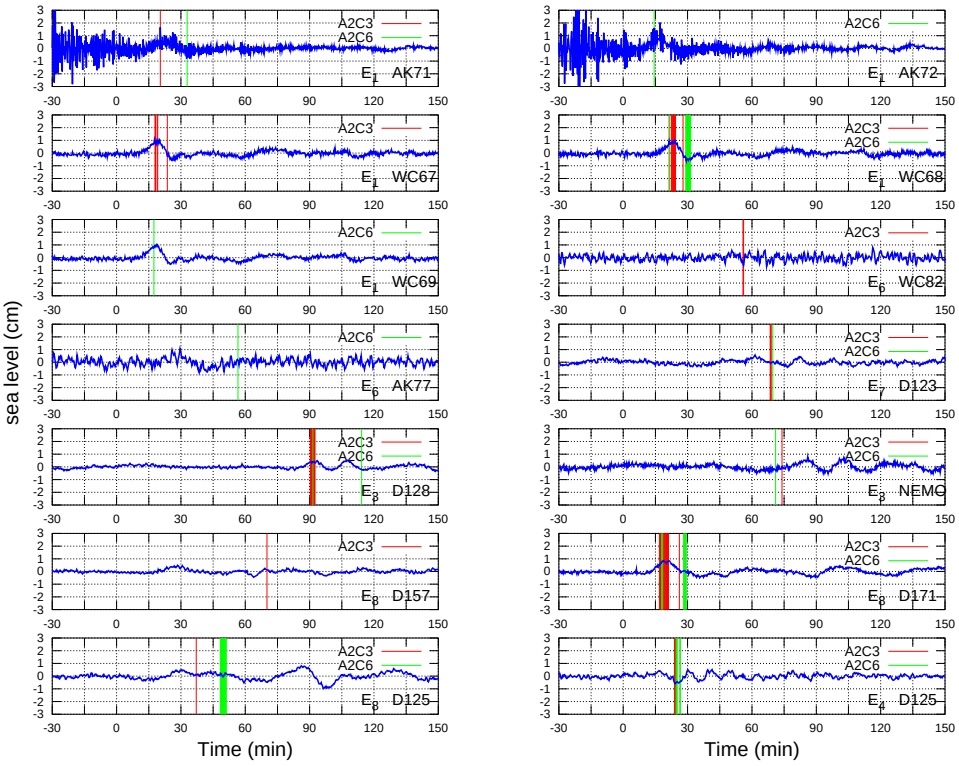

Figure 5.12: Events detections.

From the results obtained, we can make some considerations. Looking at the Figure 5.12, it is clear that in many cases the tsunami wave is detected well. However, sometimes the tsunami wave with the biggest amplitude is not detected, and in addition, there are always detections in the tsunami window $TsuW$ with no apparent tsunami signal. Therefore, the question of detection of tsunamis in offshore buoys record needs further study and cannot be considered solved satisfactorily.

Conclusions

The TEDA algorithm for tsunami detection has been developed in the frame of the Tsunami Research Team for coastal tide gauges and calibrated for the tide gauge station of Adak Island with eight event records. The calibration has been performed with the condition that the tsunami detection should not trigger any false detections. This strategy is important for the reliability of the algorithm itself. The results of the tests carried out to calibrate the algorithm allow to set TEDA time parameters and thresholds and to determine which method and configuration is to prefer ($A3C_6$) respect to the others. The spectral analysis of the records confirms that Adak Island is a site characterized by seiches and that the tsunamis mainly excites the typical oscillations of the basins where Adak is situated, losing their spectral signature. Since tsunamis at Adak have almost the same spectral content of background oscillations, the condition of no false detections has as a consequence that small amplitude tsunamis are not detected. The results of TEDA calibration are positive: the test of TEDA tsunami detection for the Adak Island tide gauge proved that the tsunamis of large amplitude waves here considered are detected within the first wave. TEDA secure detection is an algorithm that issues warnings for large amplitude waves of long period. This method has been calibrated and tested with the event records of Adak, and it is valid to warn for high amplitude waves.

The application of TEDA to offshore buoys gives interesting information about the characteristics of the background sea level signal in the open sea, and it evidences all the problematics that have to be solved in order to perform a tsunami detection. The analysis showed that sea level records by offshore buoys have many common characteristics independently from the location of the buoys, which allow a calibration of TEDA for more offshore locations: the signal is dominated by the tide, with the absence of high frequency waves and a characteristic area of white noise in the long wave

range. The tsunami waves of the records analyzed are characterized by very low amplitude: in many cases, the only tsunami wave evident in the record is the first, with a maximum amplitude in the records analyzed of about 2.5 cm, and the tsunami oscillations are not identifiable in about half of the records. In addition, the principle on which TEDA is based, i.e. that tsunami waves introduce a sudden change in sea level, is valid also for other kinds of waves present in the record that carries no threat to harbours and people. For all these reasons, the condition of avoiding false detections seems impracticable, therefore the strategy to solve the problem of false detections is to limit the window where the detection of TEDA is active, and selecting the method that detects the most events. This strategy proved not to be satisfactory, therefore tsunami detection in the open sea needs further studies, which might imply more records to test, an improved tidal corrections and higher thresholds.

List of Figures

List of Tables

Bibliography

Adak tide gauge home page, NOS/NOAA: (http://tidesandcurrents.noaa.gov/geo.shtml?location=9461380).

Bellotti, G., M. Di Risio, and P. De Girolamo (2009). "Feasibility of Tsunami Early Warning Systems for small volcanic islands". In: *Nat. Hazards Earth Syst. Sci.*

Beltrami, G.M. (2008). "An ANN algorithm for automatic, real-time tsunami detection in deep-sea level measurements". In: *Ocean Engineering.*

Bernard, E. N. (2005). "The US National Tsunami Hazard Mitigation Program: a successful statefederal partnership". In: *Nat. Hazards.*

Bernard, E. N., H. O. Mofjeld, V. Titov, C. E. Synolakis, and F. I. González (2006). "Tsunami: scientific frontiers, mitigation,forecasting and policy implications". In: *Phil. Trans. R. Soc. A.*

Chew, S. and K. Kuenza (2009). "Detecting tsunamigenesis from undersea earthquake signals". In: *Journal of Asian Earth Sciences.*

Cox, D. C. (1979). "Economic justification of tsunami research: A specific example based on reduction of false alarms in Hawaii". In: *Marine Geodesy.*

DeMets, C. (1992). "Oblique convergence and deformation along the Kurile and Japan trenches". In: *Journal Geophysical Research.*

DeMets, C., R.G. Gordon, D.F. Argus, and S. Stein (1994). "Effects of recent revisions to the geomagnetic reversal time scale on estimates of current plate motions". In: *Geophys. Res. Lett.*

Developing tsunami-resilient communities: the National Tsunami Hazard Mitigation Program (2005). Springer.

Eble, M. C., J. Newman, J. Wendland, B. Kilonsky, D. Luther, Y. Tanioka, M. Okada, and F. I. Gonzalez (1997). *The 10 June 1996 Andreanov tsunami database.* NOAA Data Report ERL PMEL. PMEL/NOAA.

Falck, C., M. Ramatschi, C. Subarya, M. Bartsch, A. Merx, J. Hoeberechts, and Schmidt G. (2010). "Near real-time GPS applications for tsunami early warning systems". In: *Nat. Hazards Earth Syst. Sci.*

Gica, E., M. Spillane, V.V. Titov, C.D. Chamberlin, and J.C. Newman (2008). *Development of the forecast propagation database for NOAA's Short-term Inundation Forecast for Tsunamis (SIFT)*. Tech. rep. NOAA.

González, F. I., E. N. Bernard, C. Meinig, M. C. Eble, H. O. Mofjeld, and S. Stalin (2005). "The NTHMP Tsunameter Network". In: *Natural Hazards*.

Henson, J.I., F. Muller-Karger, D. Wilson, S. L. Morey, G.A. Maul, M. Luther, and C. Kranenburg (2006). "Strategic Geographic Positioning Of Sea Level Gauges To Aid In Early Detection Of Tsunamis In The Intra-Americas Sea". In: *Science of Tsunami Hazards*.

Honda, K., T. Terada, Y. Yoshida, and D. Isitani (1908). "An investigation on the secondary undulations of oceanic tides". In: *J. College Sci.*

Illigner, J. and T. Schöne (2009). *TRANSFER Project: TRANSFER Project: GFZ software, (2009), Software for Automatic Detection, Analysis and Quality Control of high-frequency and low-latency sea level signals*. Tech. rep. TRANSFER Project.

Johnston, D., J. Becker, C. Gregg, B. Houghton, D. Paton, G. Leonard, and R. Garside (2007). "Developing warning and disaster response capacity in the tourism sector in coastal Washington, USA". In: *Disaster Prevention and Management*.

Kato, T., Y. Terada, M. Kinoshita, H. Kakimoto, H. Isshiki, T. Moriguchi, M. Takada, T. Tanno, M. Kanzaki, and J. Johnson. "A new tsunami monitoring system using RTK-GPS". In: *ITS 2001 Proceedings*.

Kato, T., Y. Terada, M. Kinoshita, H. Kakimoto, H. Isshiki, M. Matsuishi, A. Yokoyama, and T. Tanno (2000). "Real-time observation of tsunami by RTK-GPS". In: *Earth Planets Space*.

Komen, G. and N. Smith (1999). "Wave and sea level monitoring and prediction in the service module of the Global Ocean Observing System (GOOS)". In: *Journal of Marine Systems*.

Kulikov, E.A., A.B. Rabinovich, and A.I. Spirin (1983). "Measurements of Tsunamis in the Open Ocean". In: *Marine Geodesy*.

Leonard, G.S., D.M. Johnston, D. Paton, A. Christianson, J. Becker, and H. Keys (2008). "Developing effective warning systems: Ongoing research

at Ruapehu volcano, New Zealand". In: *Journal of Volcanology and Geothermal Research.*

Liu, P.L., X. Wang, and A.J. Salisbury (2009). "Tsunami hazard and early warning system in South China Sea". In: *Journal of Asian Earth Sciences.*

Maramai, L. and S. Tinti (1996). "Study for a Pilot Monitoring and Alarm System for the Calabrian Sicilian Tsunamis". In: *Phys. Chem. Earth.*

Martin-Neira, M. and C. Buck. "Tsunami detection using the PARIS concept". In: *Progress in Electromagnetics Research Symposium.*

Mero, T.N. "NOAA/National Ocean Service Application of Real-Time Water Levels". In: *Proceedings.*

Miller, G. R. (1972). "Relative spectra of tsunamis". In:

Miller, G. R. and F. E. Snodgrass (1962). "Long-period waves over Californias continental borderland, II, Tsunamis". In: *J. Mar. Res.*

Mofjeld, H.O. "Tsunami detection algorithm".

Munger, S. and K.F. Cheung (2008). "Resonance in Hawaii waters from the 2006 Kuril Islands Tsunami". In: *Geophysical Research Letters.*

Omira, R., M. A. Baptista, L. Matias, J.M. Miranda, C. Catita, F. Carrilho, and E. E. Toto (2009). "Design of a Sea-level Tsunami Detection Network for the Gulf of Cadiz". In: *Nat. Hazards Earth Syst. Sci.*

Rabinovich, A. B. (1997). "Spectral analysis of tsunami waves: separation of source and topography effects". In: *J. Geophys. Res.*

Rabinovich, A. B. and F.E. Stephenson (2004). "Longwave Measurements for the Coast of British Columbia and Improvements to the Tsunami Warning Capability". In: *Natural Hazards.*

Rabinovich, A. B., R. E. Thomson, and F. E. Stephenson (2006). "The Sumatra tsunami of 26 December 2004 as observed in the North Pacific and North Atlantic oceans". In: *Surv Geophys.*

Reymond, D., S. Robert, Y. Thomas, and F. Schindelé (1996). "An Automatic Tsunami Warning System: TREMORS Application in Europe". In: *Phys. Chem. Earth.*

Ruppert, N.A., J. M. Lees, and N. P. Kozyreva (2007). "Seismicity, Earthquakes and Structure Along the Alaska-Aleutian and Kamchatka-Kurile Subduction Zones: A Review". In: *Volcanism and Subduction: The Kamchatka Region.*

Sahal, A., J. Roger, S. Allgeyer, B. Lemaire, H. Hébert, F. Schindelé, and F. Lavigne (2009). "The tsunami triggered by the 21 May 2003 Boumerdés-Zemmouri (Algeria) earthquake: field investigations on the French Mediterranean coast and tsunami modelling". In: *Nat. Hazards Earth Syst. Sci.*

Sanchez, A. J. and S. F. Farreras (1983). "Maximum entropy spectral analysis of tsunamis along the Mexican coast, 1957–1979". In: *Tsunamis: their science and engineering*. Ed. by K. Iida and T. Iwasaki.

Satake, K., M. Okada, and K. Abe (1988). "Tide gauge response to tsunamis: Measurements at 40 tide gauge stations in Japan". In: *Journal of Marine Research*.

Schindelé, F., A. Loevenbruck, and H. Hébert (2008). "Strategy to design the sea-level monitoring networks for small tsunamigenic oceanic basins: the Western Mediterranean case". In: *Nat. Hazards Earth Syst. Sci.*

Schroeter, J., D. Sein, E. Taguchi, D. Sidorenko, S. Danilov, and S. Braune (2006). "The modelling concept of the German-Indonesian Tsunami Early Warning System GI TEWS". In:

Schwartz, J. (2004). "Sounding the Alarm on a Tsunami Is Complex and Expensive". In: *Science*.

Synolakis, C.E. and E.N. Bernard (2006). "Tsunami science before and after Boxing Day 2004". In: *Phil. Trans. R. Soc.*

Taguchi, E., J. Schroeter, D.V. Sein, D.V. Sidorenko, and S. Harig (2006). "On data assimilation within German Indonesian tsunami early warning systems (GI-TEWS)". In:

Thomson, R.E., A.B. Rabinovich, and M.V. Krassovski (2007). "Double jeopardy: Concurrent arrival of the 2004 Sumatra tsunami and storm-generated waves on the Atlantic coast of the United States and Canada". In: *Geophysical Research Letters*.

Tinti, S., L. Bressan, and F. Zaniboni (2009). *TRANSFER Project: Report on algorithms for detection and warning methods for the Messina Straits, Italy, tsunami monitoring system*. Tech. rep. TRANSFER Project.

Tinti, S., A. Manucci, G. Pagnoni, A. Armigliato, and F. Zaniboni (2005). "The 30th December 2002 landslide-induced tsunamis in Stromboli: sequence of the events reconstructed from the eyewitness accounts". In: *Natural Hazards and Earth System Sciences*.

Titov, V. V., F. I. González, E. N. Bernard, M. C. Eble, H. O. Mofjeld, J. C. Newman, and A. J. Venturato (2005). "Real-Time Tsunami Forecasting: Challenges and Solutions". In: *Natural Hazards*.

Van Dorn, W. G. (1984). "Some Tsunami Characteristics Deducible From Tide Records". In: *American Meteorological Society*.

— (1987). "Tide Gage Response To Tsunamis. Part II: OtherOceansAnd Smaller Seas". In: *American Meteorological Society*.

Vela, J. and B. Pérez (2009). *TRANSFER Project: TRANSFER Project: Puertos del Estado (OPPE) software, (2009), Software for Automatic Detection, Analysis and Quality Control of high-frequency and low-latency sea level signals*. Tech. rep. TRANSFER Project.

Šepić, J., L. Denis, and I. Vilibić (2009). "Real-time procedure for detection of a meteotsunami within an early tsunami warning system". In: *Physics and Chemistry of the Earth*.

Wang, X. and P. L. Liu (2006). "Numerical Simulation of Nov15 2006 Central Kuril Islands Tsunami".

Whitmore, P., H. Benz, M. Bolton, G. Crawford, L. Dengler, G. Fryer, J. Goltz, R. Hansen, K. Kryzanowski, S. Malone, D. Oppenheimer, E. Petty, G. Rogers, and J. Wilson (2008). "NOAA/West Coast And Alaska Tsunami Warning Center Pacific Ocean Response Criteria". In: *Science of Tsunami Hazards*.

Wijeratne, E.M.S. and P.L. Woodworth (2009). *TRANSFER Project: NERC (POL) software, (2009), Software for Automatic Detection, Analysis and Quality Control of high-frequency and low-latency sea level signals*. Tech. rep. TRANSFER Project.

Zhang, D.H., T.L. Yip, and C. Ng (2009). "Predicting tsunami arrivals: Estimates and policy implications". In: *Marine Policy*.